Neural assemblies as core elements for modeling neural networks in the brain

THÈSE N^{O} 8228 (2017)

PRÉSENTÉE LE 30 NOVEMBRE 2017
À LA FACULTÉ INFORMATIQUE ET COMMUNICATIONS
LABORATOIRE DE CALCUL NEUROMIMÉTIQUE (IC/SV)
PROGRAMME DOCTORAL EN INFORMATIQUE ET COMMUNICATIONS

ÉCOLE POLYTECHNIQUE FÉDÉRALE DE LAUSANNE

POUR L'OBTENTION DU GRADE DE DOCTEUR ÈS SCIENCES

PAR

Hesam SETAREH

acceptée sur proposition du jury:

Prof. M. C. Gastpar, président du jury
Prof. W. Gerstner, directeur de thèse
Prof. M. Diesmann, rapporteur
Prof. G. La Camera, rapporteur
Prof. C. Petersen, rapporteur

ÉCOLE POLYTECHNIQUE
FÉDÉRALE DE LAUSANNE
Suisse
2017

To my father and my mother, for their patiences, their kindness and their advices
To my brother and his wife, for their supports and continues care

Acknowledgments

When it comes to appreciation, tons of names come to my mind! First of all, I would like to thank my advisor Prof. Wulfram Gerstner who provided me freedom to identify my research topics and projects. My calm during the thesis writing and preparation for the thesis defense, which surprised my friends and colleagues, came from a simple sentence he told me: "I'm not worried about your thesis". I also want to appreciate Prof. Carl Petersen who suggested great ideas for my researches and provided very useful feedbacks on the results of my projects. I thank Prof. Mehdi Tafti and Dr. Sohrab Saberi Moghadam for sharing their experimental datasets with me. I would like to thank Dr. Moritz Deger who supported me during my PhD studies.

Next, I would like to thank my colleagues in the laboratory of computational neuroscience and the laboratory of sensory processing for their friendship and useful discussions.

I am very thankful to my thesis committee members: Prof. Markus Diesmann, Prof. Michael Gastpar, Prof. Giancarlo La Camera and Prof. Carl Petersen for accepting to assess my thesis and for their constructive comments.

I would like to express my sincere gratitude and respect to my family, my father, my mother, my brother and my sister in law who keep supporting me during my entire life. I could not come this far without their helps.

I express my appreciation to my closest friends in Lausanne, Mohammad Dashti, Faeze Karimipanah and their beloved children Daniel and Benjamin, Nooshin Mirzadeh, Ashkan Norouzi Fard and Aida Mousavifar.

Finally, I would like to thank my friends in Chalet group who proved we can have unlimited joy in a limited time interval. I want to thank Abolfazl Soltani, Aida Mousavifar, AmirHossein Ghadimi, AmirHossein Khalilzadeh, Ashkan Norouzi Fard, Atena Fadaei, Bahar Haghighat, Bahareh Ghadiani, Ehsan Mansouri, Farnaz Eslami, Farnood Salehi, Fatemeh Navaee, Hossein Sekhavatmanesh, Homa Mohammadi, Mehdi Tamizifar, Mohammad Yaghini, Mohammadjafar Bereyhi, Morteza Hassani, Morteza Toopchi, Nastaran Asadi, Niloufar Pouyan, Omid Talebi, Parima Ahmadipour, Reza Ghanaatian, Sattar Nakhjavani, Shakiba Fadaei and Zhaleh Hosseini.

Abstract

How does the brain process and memorize information? We all know that the neuron (also known as nerve cell) is the processing unit in the brain. But how do neurons work together in networks? The connectivity structure of neural networks plays an important role in information processing. Therefore, it is worthwhile to investigate modeling of neural networks.

Experiments extract different kinds of datasets (ranging from pair-wise connectivity to membrane potential of individual neurons) and provide an understanding of neuronal activity. However, due to technical limitations of experiments, and complexity and variety of neural architectures, the experimental datasets do not yield a model of neural networks on their own. Roughly speaking, the experimental datasets are not enough for modeling neural networks. Therefore, in addition to these datasets, we have to utilize assumptions, hand-tuned features, parameter tuning and heuristic methods for modeling networks.

In this thesis, we present different models of neural networks that are able to produce several behaviors observed in mammalian brain and cell cultures, e.g., up-state/down-state oscillations, different stimulus-evoked responses of cortical layers, activity propagation with tunable speed and several activity patterns of mice barrel cortex. An element which is embedded in all of these models is a network feature called neural assembly. A neural assembly is a group (also called population) of neurons with dense recurrent connectivity and strong internal synaptic weights. We study the dynamics of neural assemblies using analytical approaches and computer simulations. We show that network models containing assemblies exhibit dynamics similar to activity observed in the brain.

Keywords: Cortical neural network, microcircuits of brain, neural assembly, neural oscillations, spiking activity propagation, excitation chain, cell culture.

Zusammenfassung

Wie verarbeitet und speichert das Gehirn Informationen? Wir wissen, dass Neuronen, auch Nervenzellen genannt, ein elementarer Baustein der Informationsverarbeitung sind. Aber wie arbeiten Neuronen in Netzwerken zusammen? Von zentraler Bedeutung für die Funktionalität eines Netzwerkes sind dessen Verbindungsstrukturen, welche wir in dieser Arbeit modellieren und untersuchen.

In Experimenten werden Daten unterschiedlicher Natur (von Spannungspotentialen an den Membranen einzelner Neuronen zu paarweisen Verbindungen zwischen mehreren Neuronen) erhoben und verbessern unser Verständnis der neuronalen Aktivität. Aufgrund technischer Grenzen der Experimente sowie der Komplexität und Vielfältigkeit neuronaler Netzwerke, liefern die experimentell erhobenen Daten jedoch noch kein Modell für die neuronale Architektur. Stattdessen treffen wir zusätzliche Annahmen über mögliche Netzwerkarchitekturen und benutzen heuristische Methoden um biologisch plausible Modelle zu konstruieren welche dann mit den experimentell erhobenen Netzwerkaktivitäten verglichen und validiert werden.

In der vorliegenden Arbeit stellen wir Modelle neuronaler Netzwerke vor, welche in der Lage sind verschiedene im Säugetiergehirn sowie in Zellkulturen beobachtete Aktivitätsmuster zu reproduzieren. Dazu gehören Oszillationen zwischen Phasen hoher und niedriger Aktivität, Stimulus getriebene Aktivitäten kortikaler Schichten, Aktivitätsausbreitung mit kontrollierbarer Geschwindigkeit sowie mehrere Aktivitätsmuster wie sie im Kortex von Mäusen beobachtet wurden.

In allen unseren Modellen verwenden wir neuronale Netzwerke mit einer charakteristischen Struktur: ein kleiner Teil der Neuronen bilden (mindestens) eine Subpopulation mit einer hohen Anzahl starker gegenseitiger Verbindungen. Mit Simulationen und analytischen Methoden untersuchen wir das dynamische Verhalten solcher Neuronengruppen und zeigen, dass unsere Netzwerkmodelle Aktivitätsmuster produzieren welche experimentell bestimmten Gehirnaktivitäten ähnlich sind.

Stichwörter: kortikales neuronales Netzwerk, Mikroschaltkreise des Gehirns, Subpopulation, neuronale Oszillation, Ausbreitung gepulster Aktivität, Erregungsleitung, Zellkultur

Contents

[1] Text copied from Setareh H, Deger M, Petersen CCH and Gerstner W, Front. Comput. Neurosci. 2017 (full citation in the Reference).

[2] Text copied from Setareh H, Deger M, and Gerstner W, manuscript is under review in PLOS Comput. Biol.

[3]Text copied from Saberi-Moghadam S, Simi A*, Setareh H*, Mikhail M and Tafti M, manuscript is under review in Int. J. Neural Sys. (* contributed equally to this work).

List of Figures

List of Tables

Chapter 1

Introduction

Our brain is a wonderful machine. It is able to perform different information processing tasks ranging from recalling memories to processing visual and audio inputs on the time scale of seconds or even milliseconds. Nerve cells or neurons are known as the main processing elements in the brain. Neurons can connect together through junctions called synapses and form neural networks. These networks act like processor systems, and are capable of receiving input and generating desired outputs.

In this thesis, we try to study the effect of embedding a network feature (neural assembly) in neural networks and formulate the behavior resulting from this feature. We will show that neural networks containing assemblies are able to reproduce different phenomena observed in the brain as well as in cell cultures.

1.1 Processing information in neocortex

Neocortex is a part of the brain involved in sensory perception, cognitive behaviors and generating commands for movements (Figure 1.1A). In terms of functions, the neocortex can be divided into different regions, while each region processes a special type of sensory input or handles motor commands (Figure 1.1B). Visual, auditory, olfactory and somatosensory cortices are examples of sensory cortices. Thalamus (a centrally-located brain structure) relays sensory inputs between sensory organs (e.g. eyes, ears, ...) to the cortices. Then, each sensory signal is processed in its related region. Anatomically, the neocortex is divided to six horizontal layers, labelled from the outermost inwards, layer 1 to 6. Layers differ from each other in terms of number and type of neurons, connectivity pattern between neurons and dynamic of neurons (Figure 1.1C).

In most parts of this work, we have used datasets extracted from barrel cortex. Barrel cortex is a region of rodent somatosensory cortex which processes tactile information from whiskers (Petersen, 2007). However, suggested structures and methods are independent of the region and can be potentially applied to neural networks of different areas.

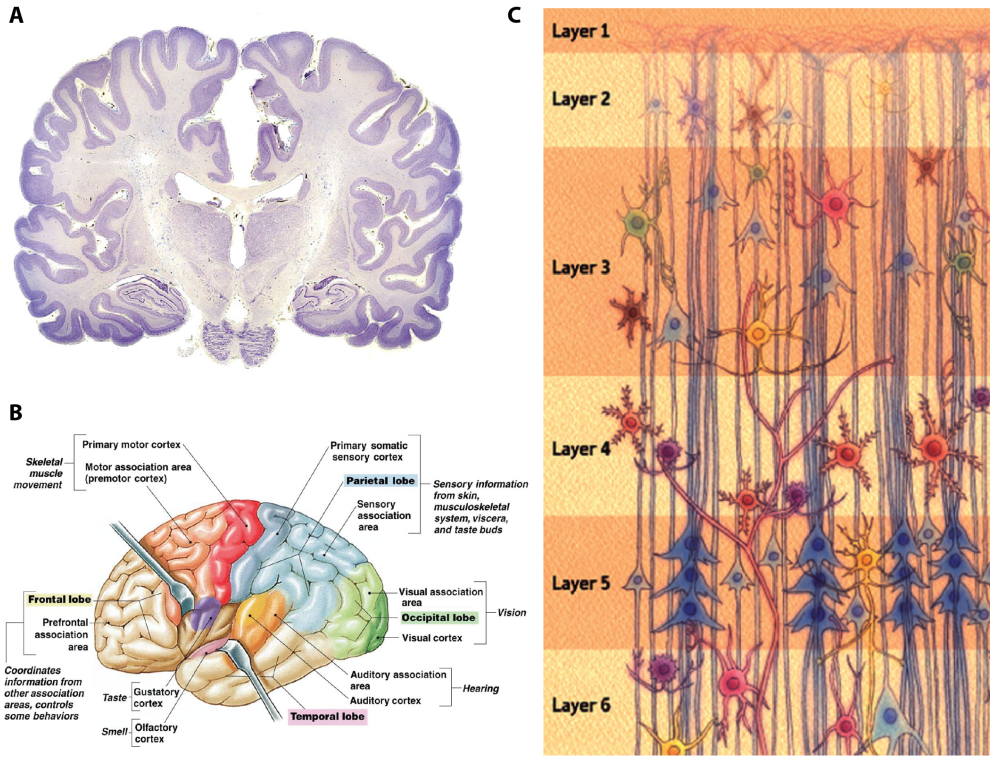

Figure 1.1: Neocortex is the outer layer of cerebrum (**A**) which is involved in higher-order brain functions. It contains different regions with distinct functions (**B**). Each region processes (or generates) signals from (for) an organ. Anatomically, neocortex can be divided into six horizontal layer with different neural structures (**C**). Images A, B and C are respectively taken from www.neurosciencelibrary.org, www.chronopause.com and www.monardo.info.

1.2 Modeling neural networks

Finding the structure and architecture of cortical neural networks is the key to understand how neocortex processes information. In order to model the neocortical networks, we need experimental datasets that characterize behavior of neurons and express some aspects of network dynamics.

Beside modeling the connectivity structure between neurons, we need to model dynamics of single neurons. The behavior of single neurons can be described by neuron models. We consider spiking neuron models in this research. Spiking neuron models range from simple leaky integrate-and-fire which consider a neuron as a resistor-capacitance circuit to detailed Hodgkin-Huxley model (Hodgkin and Huxley, 1952) which exhibit different ion channels of neuron. Each model has its own advantages and limits (Naud and Gerstner, 2012b; Gerstner et al., 2014). Despite the differences, spiking neuron models share key concepts. They keep an internal variable for the membrane potential or voltage of the neuron. Whenever the membrane potential reaches firing threshold, the neuron emits a short-lasting pulse of large amplitude called spike

or action potential (Several neuron models do not have explicit firing threshold). Every neuron model has a set of parameters that should be valued for each neuron. These neural parameters can by fitting the neuron model to experimental data. In this research, we use a Generalized integrate-and-fire (GIF) model (Mensi et al., 2012; Pozzorini et al., 2015) that is able to capture with high accuracy both subthreshold dynamics of membrane potential and the spiking activity recorded from neurons during current injection (Mensi et al., 2012; Pozzorini et al., 2013). We will review the model in section 2.2.

In the following sections, we describe several types of experimental data that are used in the modeling. Then, we explain the general approach of modeling networks and different tools that we used in this research.

1.2.1 Structural data

There are certain data types that allow us to characterize neurons and the connections between them. We refer to them as structural data.

We need neural parameters for each cell type. Data are extracted by fitting the neuron model to experimental data. In other words, a current is injected to a neuron in a slice of cortex. Using patch clamp recording, the membrane potential and spikes of the neuron are measured. This set of input/output is used to optimize parameters for that neuron. Then, using the parameters for broad range of different time-dependent current, the neuron model is able to generate output, i.e., membrane potential and spikes (Lefort et al., 2009; Avermann et al., 2012; Mensi et al., 2012; Pozzorini et al., 2015). The match between experimentally measured output and generated output indicates wether the parameter extraction was successful. Figure 1.2A summarizes this process.

In order to collect data on network connectivity, intracellular recordings are performed (Markram et al., 1997; Feldmeyer et al., 1999; Lefort et al., 2009; Avermann et al., 2012; Chapeton et al., 2012). In each experiment, one neuron is injected by a current pulse until it fires a spike. In parallel the membrane potential of one or several other neurons are measured. If a measured neuron shows a peak with a short temporal delay after injection of the pulse, we can conclude that there is connection from the injected neuron to the measured neuron. Besides, the amplitude of the peak is considered as the weight of synapse between those neurons. Repeating this experiment yields a bunch of synaptic weights. We can illustrate their distribution (Figure 1.2B) and use parameters of the distribution for building the network model. The fraction of connected neurons over the whole tested neuron pairs is another important quantity which is called connection probability.

Finally, the number of neurons based on neuron types in each cortical layer is a very useful dataset extracted from experiments (Lefort et al., 2009; Avermann et al., 2012).

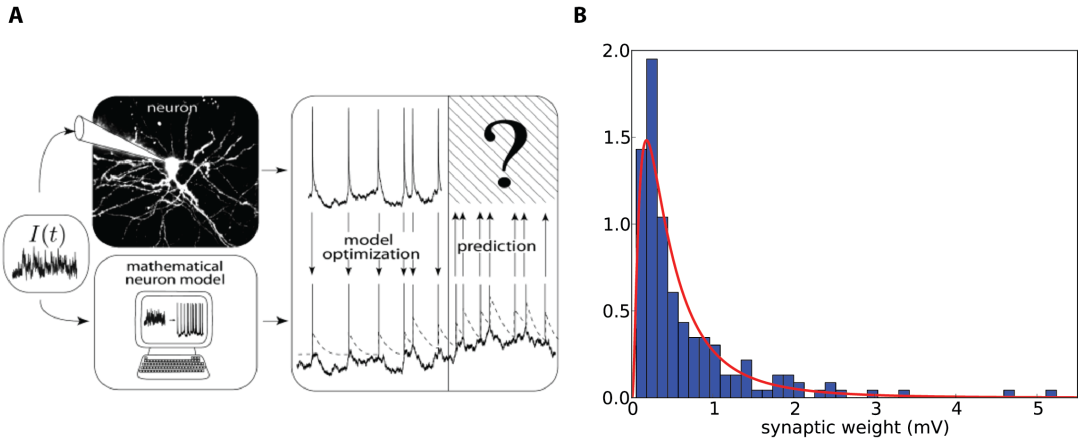

Figure 1.2: **A**) Neuron model is able to capture the dynamic of biological neuron after we drive its parameters. Image from Gerstner et al. (2014). **B**) Distribution of synaptic weights in cortical neural network. Blue bars show the histogram of experimentally observed synaptic weights in excitatory neurons of layer 5 of mice barrel cortex (Lefort et al., 2009). Red line indicates a lognormal distribution fitted by the experimental data. We will use the fitted distribution in order to construct models of neural networks.

1.2.2 Dynamical data

Dynamical data types describe behaviors and activities of neurons. They may express dynamics at the level of a single neuron or a population of neurons.

Intracellular recordings provide the membrane potential and spikes of single neurons, while extracellular recordings only extract spikes. Recording with multielectrode arrays is a technique that allows us to extract spikes of many neurons simultaneously.

For observing the behavior of neurons at larger scales, calcium or voltage sensitive dye imaging is used (Grinvald et al., 1984; Smetters et al., 1999; Petersen et al., 2003b,a). Transient change of calcium concentration in a cell indicates existence of spike. Therefore, calcium imaging (Smetters et al., 1999) visualizes spiking activity of neural network over a big area. Voltage sensitive dye imaging (Grinvald et al., 1984) displays the evolution of membrane potential of a group of neurons on a large scale.

The dynamics of neurons are recorded using the above techniques during both spontaneous regime and in response to external stimulations. Both regimes provide useful information about the behavior of neural networks. In this thesis, we different kinds of dynamical datasets (Sanchez-Vives and McCormick, 2000; Sanchez-Vives et al., 2000; Cossart et al., 2003; Petersen et al., 2003b,a; Hromádka et al., 2008; Vijayan et al., 2010; Beltramo et al., 2013).

1.2.3 Our modeling approach

We start building neural networks using structural data. We create neural populations with the same number of neurons as those found in experiments. Then, we establish random connections

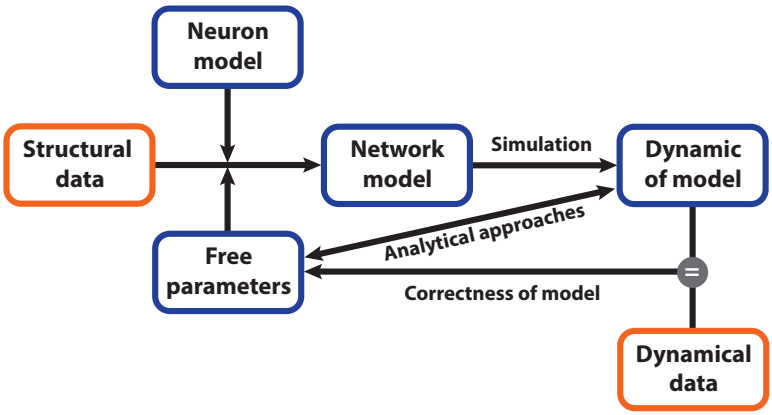

Figure 1.3: Framework of neural network modeling in our research. Using structural data and neuron models, we build a network model. Each network model has a set of free parameters that should be tuned in order to achieve biologically plausible results. After building the model, its dynamics can be obtained using computer simulations. The match between dynamical data and model's dynamics indicates the correctness of model. Based on this measurements, we are able to find a correct set of free parameters. Analytical methods provide a shortcut for finding value of free parameters.

between neurons based on experimentally observed connection probabilities. Synaptic weights of the model are drawn from weight distributions extracted by experiments. Beside network parameters whose values are found from experiments, there are free parameters that need to be tuned. We will present more details of network creation and related parameters in following chapters.

After building the model, we have to obtain its behavior. Computer simulators are powerful tools to generate network behavior given its structure. If the model produces dynamics similar to the dynamical data, we can claim that the model is biologically plausible. Otherwise, we have to change the free parameters to obtain behaviors more similar to the dynamical data. In case of a small number of free parameters, we are able to search in the parameters space and find a parameter set which yields the best match with experiments. In some cases, we can relate the model dynamics and its parameters using analytical approaches. Therefore, we can directly extract suitable values of free parameters without simulation and search. Analytical methods are also used to explain and clarify the reasons of model's behaviors. Figure 1.3 summarizes the process of modeling.

In this research we used two different computer simulators, Brian (Goodman and Brette, 2008) and NEST (Gewaltig and Diesmann, 2007). Brian provides more flexibility for recording different variables of the models (membrane potentials, currents, adaptation variables, plasticity variables, ...). However, NEST is able to scale up models and is more efficient for simulating big networks. We will mention in each chapter which simulator is used.

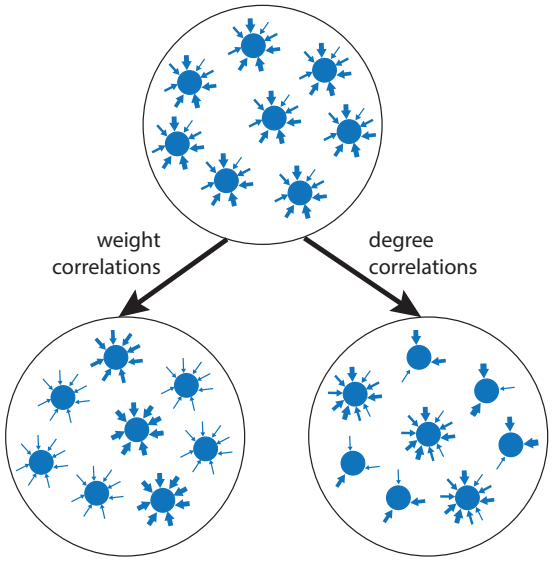

Figure 1.4: In a random network with a random distribution of synaptic weights (**Top**) each neuron receives a combination of weak and strong weights. Furthermore, number of connections of all neurons is close to each other. In case of adding weight correlations (**Left**), a few neurons receive strong weights, while the rest receive weak weights. In case of adding degree correlations (**Right**), a few neurons receive large number of connections, while the remaining neurons receive small number of connections.

1.3 Neural assembly

The simplest network architecture that can be used for modeling is a random model (Erdös and Rényi, 1959). In this model, the probability of having connection between every arbitrary pair of neurons is constant and equals p. The parameter p is the same as the connection probability extracted from experiments. Despite the simplicity and ease of creation, this model is not able to reproduce dynamical phenomena observed in the cortex (Koulakov et al., 2009; Tomm, 2011; Tomm et al., 2014). Complex network models such as small-world (Watts and Strogatz, 1998) and scale-free (Barabási and Albert, 1999) models are used in different studies (Roxin et al., 2004; Koulakov et al., 2009; Roxin, 2011; Litwin-Kumar and Doiron, 2012; Doiron and Litwin-Kumar, 2014; Tomm et al., 2014; Mazzucato et al., 2015, 2016) to achieve more biologically plausible models and reproduce cortical dynamics with better approximations. In these models, both degree and weight distributions are manipulated to add non-randomness into models (Figure 1.4). These non-random features affect the dynamics and cause behaviors similar to experimental observations.

In this thesis, we exploit a non-random network feature called neural assembly. A neural assembly is defined as a group of neurons that are strongly connected with each other (Hebb, 1949), i.e., the connection probability inside the group is higher than the outside. Due to dense connectivity, the stimulation of a sufficient number of assembly neurons can activate the entire

assembly (Palm, 1982). We also hypothesize that synaptic weights between neurons inside an assembly are larger than other synapses. We will study the effect of embedding neural assemblies in bigger networks using both computer simulations and analytical methods. We will show that cortical activities such as slow oscillations and different stimulus-evoked response can be reproduced using a network containing neural assemblies (chapter 2). We then connect neural assemblies together in order to build an excitable media for propagating neural activities (chapter 3). We also show that assemblies can form a 2-dimensional architecture in order to build a multicolumn model for cortex and generate different dynamical patterns observed in large scale imaging (chapter 3). Then, we will study behaviors of cortical cultures grown on multielectrode arrays (cell cultures). We will illustrate that different dynamics observed in cultures can be reproduced by embedding neural assemblies with different properties in neural networks (chapter 4).

In chapter 2 we introduce the term 'weight-hub' neuron, i.e., neurons that receive large synaptic weights. We then study the role of assembly of weight-hub neurons in this chapter. In other chapters, we focus on assembly of neurons (not necessarily weight-hub neurons) and use it as the core of our network modeling.

1.4 Related works

1.4.1 Large-scale models of neocortex

In this thesis, we focus on constructing mid-size models of cortical network (all of our models contain less than 15000 neurons). Beside other mid-size cortical models (which are briefly described in sections 2.4 and 3.3), there exist several large-scale networks for modeling neocortex (Izhikevich and Edelman, 2008; Garis et al., 2010; Merolla et al., 2014; Potjans and Diesmann, 2014; Markram et al., 2015).

Potjans and Diesmann, 2014 built a model of cortical column containing ~ 80000 leaky integrate-and-fire neurons (Figure 1.5A). They reconstructed connection probabilities between different populations of neurons by combining the structural data extracted from electrophysiological experiments (Thomson et al., 2002) and anatomical approaches (Binzegger et al., 2004) in order to derive a combined connectivity map. Firing rates of populations in the simulated network (Figure 1.5B) were close to the dynamical data found in experiments (Greenberg et al., 2008; de Kock and Sakmann, 2009). In case of transient thalamic stimulation, the response (Figure 1.5C) was also similar to experimental observations (Sakata and Harris, 2009).

Izhikevich and Edelman, 2008 constructed a very large model of the thalamocortical system which contains one million multi-compartment neurons. The dynamics of each compartment was modeled by the Izhikevich neuron model (Izhikevich, 2003). They used an anatomical dataset (Binzegger et al., 2004) for the connections between neurons. Their model also features short-term plasticity and spike-timing-dependent plasticity. Excitatory and non-fast spiking inhibitory neurons showed Poissonian behavior in the model, while fast spiking inhibitory neurons exhibited

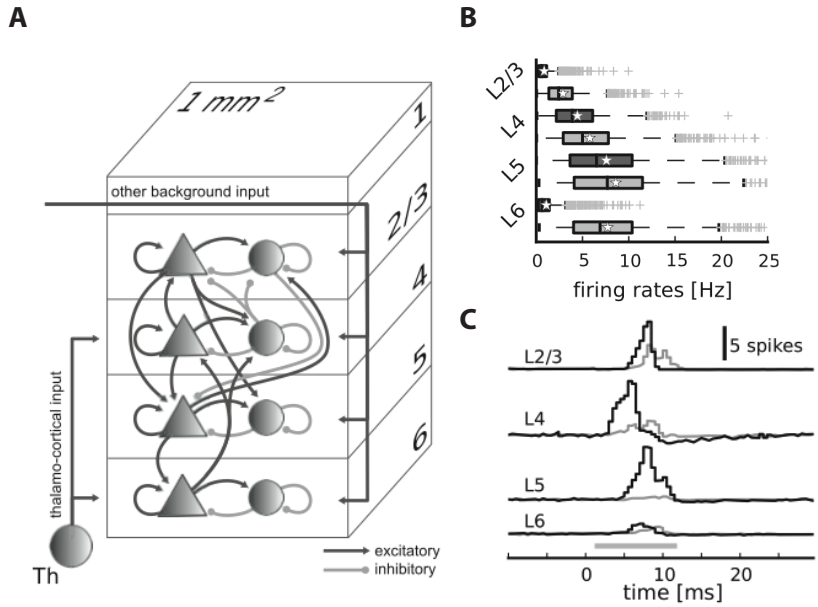

Figure 1.5: **A**) The network model contains 4 layers. Each layer includes one excitatory and one inhibitory population of neurons. The thalamus is modeled by a group of Poisson neurons. **B**) Boxplot of firing rates of 1000 neurons recorded for 60 seconds. Black bars indicate excitatory and gray bars indicate inhibitory neurons. **C**) Response of the model to a transient thalamic stimulation (gray bar). Black (gray) lines show the spike-count of excitatory (inhibitory) populations. Images are taken from Potjans and Diesmann, 2014.

higher firing rate and produced strong gamma rhythms $(40 - 50\text{Hz})$ in some layers. The model was also able to generate oscillatory behavior in the delta $(1 - 3\text{Hz})$, alpha $(\sim 10\text{Hz})$ and beta $(\sim 20\text{Hz})$ ranges.

Markram et al., 2015 used morphological and electrical properties of neurons, anatomical properties of neural microcircuits and synaptic diversities for building a virtual slice of somatosensory cortex and modeling thalamic input. Their simulations reproduced a number of in vivo and in vitro observations. For example, in the spontaneous regime their network generated slow oscillatory bursts $(\sim 1Hz)$ which was initiated in layer 5, then spread from there to to layer 6, layer 4 and layer 2/3. The oscillations were replaced by asynchronous and irregular activity in case of decreasing the concentration of Ca^{+2}. A biologically plausible response of neurons to thalamic input and balanced excitation-inhibition input to the neurons are other aspects of the model.

Merolla et al., 2014 built a chip which contains 1 million spiking neurons and 256 million configurable synapses. They programmed the chip in order to perform visual processing tasks. It is able to recognize objects in 30 frames per seconds videos in real time with low power consumption.

1.4.2 Neural assembly in previous studies

As mentioned earlier, a neural assembly is defined as a group of neurons that are strongly connected with each other (Hebb, 1949). In other words, the connection probability inside the group is higher than the outside. Neural assembly was previously investigated in experimental works and theoretical studies. Yoshimura et al., 2005 studied cross-correlation of layer 2/3 excitatory neurons in response to spike emission of other neurons. They found that there exist subgroups of excitatory neuron in cortical layer 2/3 which share common input from layer 4 and within layer 2/3. In other words, connected neurons share common input while unconnected neurons share very low (if any) common input from layer 4 and layer 2/3. We interpret each subgroup as a neural assembly.

In theoretical studies neural assemblies are used for reproducing cortical trial-to-trial variability (Litwin-Kumar and Doiron, 2012; Doiron and Litwin-Kumar, 2014; Mazzucato et al., 2015, 2016). Litwin-Kumar and Doiron, 2012 simulated the spontaneous activity of a network (which contains several assemblies) for several trials. They reported the spike count Fano factor averaged over all excitatory neurons as a measure of spiking variability. The Fano factor is defined as the ratio of trial-to-trial variance to mean of the number of spikes a neuron emits in a fixed time window. They found that the Fano factor increases as they increase the ratio of the connection probability inside assemblies over the connection probabilities between assemblies. Mazzucato et al., 2016 embedded several neural assemblies in an excitatory population which shares global inhibition among it neurons. They could generate the state sequences that observed in rats gustatory cortex. In case of external stimuli, multistability turns to bistability and leads to the reduction of trial-to-trial variability.

Neural assemblies are also used for implementing working memory models (Barak and Tsodyks, 2007; Mongillo et al., 2008; Zenke et al., 2015). Working memory is the computational ability of storing and recall information on time scales of minutes. In the models of working memory, several assemblies are embedded or formed by synaptic plasticity rules in the network (Litwin-Kumar and Brent, 2014). Each assembly is either in a low firing rate state or in a high firing rate state. From this perspective, the state of an assembly can be considered as one bit of information. Therefore, a group of assemblies in the network is able to memorize several bits and acts like a memory unit (Hopfield, 1984).

1.4.3 Models of excitable media and activity propagation in neural networks

Using abstract rate equations, Wilson and Cowan, 1973 described a neural model of excitable media for producing activity propagations. They studied the dynamics of excitatory and inhibitory activity in a synaptically coupled neuronal network using analytical approaches. Key parameters of the model are the strength of synaptic weights between and inside excitatory and inhibitory populations. Varying the parameters generates a diversity of dynamical behaviors like multistability, oscillations, traveling waves, and spatial patterns. Jirsa and Haken, 1997

extended the neural model in order to describe the interaction between functional units within the brain.

For spiking neurons, two famous models also exist for propagating activity within neural networks. The first model, which is called synfire chain model, uses several groups of neuron with feedforward structure, i.e., each neuron in a group is unidirectionally connected to the neurons of the next group (Abeles, 1982, 1991; Diesmann et al., 1999; Gewaltig, 2000; Kistler and Gerstner, 2002; Kumar et al., 2008). If we stimulate the first group and force enough number of neurons to emit spikes, the spiking activity may propagate to the last group. In some cases the activity vanishes before reaching the end of chain. Synaptic weights between groups, number of neurons in the groups, number of spikes and standard deviation of spike times in the first group are important parameters for obtaining a reliable propagation. The synfire chain propagates the activity on the time scale of synaptic delay (order of milliseconds) plus the rise time of the postsynaptic potential (Kistler and Gerstner, 2002). Therefore, to cover a time window of one second, about $200 - 500$ groups of neurons are needed, each contains ~ 100 neurons.

Second, rate propagation models (van Rossum et al., 2002; Vogels and Abbott, 2005) use a similar feedforward architecture, but instead of spikes they propagate fluctuations of the firing rate. Similar to the synfire chain, the number of neurons and connections between groups should be adjusted for avoiding vanishment of activity. The propagation speed in this model is slower comparing to the synfire chain and is on the scale of the synaptic time constant (order of ten milliseconds). Consequently, we need about $100 - 200$ groups of neurons to cover a time window of one second.

1.5 Overview and contributions

This thesis collects the main results I obtained during my PhD studies between 2012 and 2017 under the supervision of Prof. Wulfram Gerstner at EPFL. The main goal of my research was suggesting models for cortical neural networks and reproducing their observed behaviors (dynamical data). I found that by embedding neural assemblies in models, we are able to produce biologically plausible dynamics while the parameters and elements of the model remain in the experimentally observed range (structural data). Beside modeling cortical networks, I used neural assemblies to model dynamics of networks in cell culture. This study is performed in collaboration with Prof. Mehdi Tafti and Dr. Sohrab Saberi Moghadam at university of Lausanne (UNIL). The thesis is divided into four chapters.

In **chapter 2**, I build a model of Layer 5 of one barrel column. The model is able to produce up-state/down-state oscillations observed in anesthetized cortex. I show that different dynamical phenomena of the model, e.g. firing rate distribution, irregularity of oscillations, correlation between neurons' dynamics, are similar to dynamical data previously observed in experiments. I state that neural assemblies are crucial elements and the model is unable to produce biologically plausible results without them.

I designed and implemented the model. I also performed the analysis of the model's results.

Moritz Deger (MD) helped me during design and data analysis. I wrote the text in collaboration with MD, Wulfram Gerstner (WG) and Carl Petersen (CP). Ideas and comments of CP were very constructive for polishing the model. This chapter is published in Frontiers in Computational Neuroscience (doi: 10.3389/fncom.2017.00052).

In **chapter 3**, I developed a model (excitation chain) for propagating spiking activity on a time scale comparable with animals behaviors. Again neural assemblies are the key elements in the model. I show that properties of neural assemblies eliminate the need for feedforward structure in the chain. Then, I extend the chain to a 2-dimensional grid and use it as the skeleton for a multicolumn model of cortex. The multicolumn model reproduces different patterns of activity propagation observed in barrel cortex.

I designed and implemented the models. I also developed the theoretical framework for analysis and prediction of the models dynamics. MD and WG helped me in developing the framework and presentation of results. I wrote the text in collaboration with MD and WG. I also used useful comments of CP for constructing models.

In **chapter 4**, I focus on the behavior of cortical networks grown on multielectrode arrays. The results show that in mature cultures, neural networks exhibit slow oscillations. In case of stimulation, the oscillations cease. However, networks are able to recover from the stimulus-evoked state in a stimulus-dependent homeostatic response. I also illustrate that different oscillations observed in networks can be reproduced by models containing neural assemblies (neural assembly is called neural cluster is this chapter). I also argue that the difference between dynamics before and after stimulation can be interpreted by changing the number and size of neural assemblies embedded in networks.

Mehdi Tafti and Sohrab Saberi Moghadam (SSM) conceived the study, analyzed the experimental data and wrote the manuscript. SSM, Alessandro Simi, and Cyril Mikhail performed the experiments and analyzed the data. I performed the simulations, analyzed the experimental and simulated data and wrote the text related to the simulations.

In **appendix A**, I build a model for reproducing monkey's scribbling using the excitation chain introduce in chapter 3. I show that the speed of drawing can be regulated by modifying synaptic weights in the chain. I designed and implemented the model.

Chapter 2

Cortical dynamics in presence of assemblies of densely connected weight-hub neurons[1]

Abstract

Experimental measurements of pairwise connection probability of pyramidal neurons together with the distribution of synaptic weights have been used to construct randomly connected model networks. However, several experimental studies suggest that both wiring and synaptic weight structure between neurons show statistics that differ from random networks. Here we study a network containing a subset of neurons which we call weight-hub neurons, that are characterized by strong inward synapses. We propose a connectivity structure for excitatory neurons that contains assemblies of densely connected weight-hub neurons, while the pairwise connection probability and synaptic weight distribution remain consistent with experimental data. Simulations of such a network with generalized integrate-and-fire neurons display regular and irregular slow oscillations akin to experimentally observed up/down state transitions in the activity of cortical neurons with a broad distribution of pairwise spike correlations. Moreover, stimulation of a model network in the presence or absence of assembly structure exhibits responses similar to light-evoked responses of cortical layers in optogenetically modified animals. We conclude that a high connection probability into and within assemblies of excitatory weight-hub neurons, as it likely is present in some but not all cortical layers, changes the dynamics of a layer of cortical microcircuitry significantly.

[1]Text copied from Setareh H, Deger M, Petersen CCH and Gerstner W, Front. Comput. Neurosci. 2017 (full citation in the Reference).

2.1 Introduction

Is it possible to uniquely constrain a model network of point neurons with experimental data? First, suppose that we have access to experimental measurements of electrophysiological properties of single neurons. Indeed a wealth of single-neuron data exists (Markram et al., 2004, 2015) and methods have been developed that enable a rapid and reliable extraction of parameters of generalized integrate-and-fire neuron models from such experimental data (Jolivet et al., 2006; Pillow et al., 2008; Mensi et al., 2012; Pozzorini et al., 2013, 2015). Thus, parameters of neuron models, including spread of parameters caused by heterogeneity, can be completely constrained by experiments. Second, suppose that we have access to experimental measurements of the distribution of synaptic weights. Indeed, experimental data suggests a unimodal, possibly log-normal, distribution of EPSP amplitudes (Feldmeyer et al., 1999, 2002; Song et al., 2005; Feldmeyer et al., 2006; Frick et al., 2008; Lefort et al., 2009). Thus, we can constrain the distribution of synaptic weights in a network model with the data collected over many pairs of neurons. Third, suppose that we know the probability that two neurons (say, of types A and B located in layers n and m of the same cortical column) make a short-range connection from A to B. Again, such data exists (Lefort et al., 2009; Avermann et al., 2012) and should be used to constrain a network model. But is data collected on single neurons and pairs of neurons sufficient to constrain the parameters of a network model?

The answer is negative. There are at least two reasons: (i) The distribution of synaptic weights does not indicate whether a single neuron is driven by a random combination of strong and weak synapses, or whether one neuron receives all the strong input synapses and another one all the weak ones. Similarly, (ii) an average connection probability of say, 20 percent, is consistent with a network of a 1000 neurons where each neuron receives exactly 200 connections, but also equally consistent with a network where half the neurons receive 100 inputs and the other half 300. In this paper, we systematically explore network variants that implement the variations indicated under (i) and (ii) while keeping all single-neuron parameters, number of neurons, as well as pair-wise connection probabilities and synaptic weight distributions fixed. To keep the arguments as transparent, consistent, and precise as possible, we focus on a single cortical layer of mouse barrel cortex and use data from a single lab (Lefort et al., 2009; Avermann et al., 2012).

The hypothetical variations (i) and (ii) make our networks different from a classical Erdős–Rényi random network. Indeed, experimental data from various labs indicate non-random features in network connectivity (Song et al., 2005; Yoshimura et al., 2005; Kampa et al., 2006; Perin et al., 2011). The influence of some of these features on activity patterns in neuronal networks has already been studied in a set of modeling papers (Koulakov et al., 2009; Roxin, 2011; Litwin-Kumar and Doiron, 2012; Pernice et al., 2013; Vasquez et al., 2013; Hu et al., 2013, 2014; Jahnke et al., 2014; Luccioli et al., 2014; McDonnell and Ward, 2014; Mazzucato et al., 2015, 2016). We focus on two features of network connectivity which we call degree-hub and weight-hub. For example, if a few neurons receive more synaptic input connections than others (Roxin, 2011; Pernice et al., 2013; Tomm et al., 2014), we will refer to these neurons as degree-hubs. On the other hand, even in a network where there are no degree-hubs, there can still be a few neurons

(which we will call weight-hubs) that receive all the strong connections while others receive all the weak connections (Koulakov et al., 2009; Tomm et al., 2014), but chosen such that the total distribution of synaptic weights across the network remains consistent with experimental data. More generally, such non-random features can be described as "correlations" in the connectivity matrix or synaptic weight distribution. For example, the input connectivity in a network with weight-hubs is correlated: It is more likely to find a second strong input connection in a neuron in which you have already found a strong synapse than in a neuron for which you have found a weak synapse.

Several experiments studied the existence of both degree-hub and weight-hub neurons in different regions of the brain. In the hippocampus GABAergic neurons that receive more synapses than average were detected (Bonifazi et al., 2009). Excitatory neurons which receive many synapses from inhibitory neurons were found in mouse frontal cortex (Fino and Yuste, 2011). Recently, Okun et al. (2015) found that neurons that are strongly correlated to the population-averaged firing rate receive larger numbers of synapses from their neighbors. Neurons receiving stronger connections than others were also observed in experiments (Song et al., 2005; Perin et al., 2011). Yassin et al. 2010 and Cossart et al. (2003) investigated neocortical excitatory neurons that systematically fire more than other neurons. Such a high firing rate can be due to different intrinsic neuronal properties or more frequent or stronger excitatory synapses onto the neurons. In the latter case, the receiving neurons can be considered as candidates of degree- or weight-hubs. Even though experimental evidence for the existence of weight-hubs within pyramidal neurons is not yet convincing, we explore here signatures of hypothetical weight-hub neurons in neuronal activity.

Another experiment unravels a related but different phenomenon in the cortex. Yoshimura et al. (2005) suggest that excitatory neurons in the cortex can form assemblies and that neurons inside each assembly share common synaptic input. Here we explore a hypothetical network where connectivity between weight-hub neurons is higher than average. We show that such an elevated connection probability *between* weight-hub neurons significantly changes the dynamics of the network. Note that a subnetwork of densely connected weight-hub neurons can be interpreted as a neuronal assembly (Hebb, 1949).

We build a neuronal network which models layer 5A (L5) of a mouse barrel cortex column that generates up-state/down-state oscillations. Neuron numbers, pairwise connection probabilities and distribution of synaptic weights are matched to experimental data (Lefort et al., 2009; Avermann et al., 2012). Parameters of the neuron model such as membrane time constants, firing threshold and adaptation have been extracted from experimental data (Mensi et al., 2012). We show that in our network of adaptive integrate-and-fire neurons, the existence of weight-hub neurons is not sufficient for producing metastable up- and down-states. For oscillations to appear, weight-hub neurons need to form assemblies with dense internal connectivity. Another phenomenon that we address here is the different light-evoked responses of cortical supra-granular and infra-granular layers. Experiments (Beltramo et al., 2013) show that optogenetic stimulation in L5 leads to a large depolarization and a notable number of emitted spikes in non-stimulated neurons. In contrast after stimulation of a group of neurons in layer 2/3 (L2/3), non-stimulated neurons do not show significant responses. We show that such a

difference can be explained by the presence or absence of an assembly of hub neurons. We hypothesize that in L5 weight-hub neurons are connected together densely and form assemblies while in L2/3 their connections are sparse. This may explain experimental observations (Sakata and Harris, 2009; Chauvette et al., 2010; Beltramo et al., 2013) which indicate that up-states are initiated in L5, and that L2/3 largely follows the oscillation passively.

2.2 Materials and Methods

Neuron model and population parameters

In each simulation we model one cortical layer, either layer 5A (L5) or layer 2/3 (L2/3) from mouse somatosensory cortex. Based on experimental data (Lefort et al., 2009), our model of a L5 barrel column contains 454 excitatory and 90 inhibitory neurons while L2/3 contains 1691 excitatory and 230 inhibitory neurons. The two layers are studied separately and are not connected to each other.

As a neuron model, we use a current-based Generalized Integrate-and-Fire (GIF) model (Mensi et al., 2012) that features both an adaptation current and a dynamic threshold for spike-frequency adaptation. The GIF model parameters that we use in our simulations have been previously extracted from experimental data (Mensi et al., 2012). Importantly, the GIF model has been shown to capture with high accuracy both the subthreshold dynamics of the membrane potential and the spiking activity recorded from neurons in mouse barrel cortex slices during current injection (Mensi et al., 2012; Pozzorini et al., 2013). In this model, the subthreshold membrane potential $V(t)$ is described by the differential equation:

$$C\frac{dV(t)}{dt} = -g_{\mathrm{L}}(V(t) - E_{\mathrm{L}}) - \sum_{\hat{t}_j<t} \eta(t - \hat{t}_j) + I(t) \tag{2.1}$$

where the parameters C, g_{L} and E_{L} define the passive properties of the neuron (for parameter values see Table 2.1), $I(t)$ is the input current and $\{\hat{t}_j\}$ are the spike times. Each time a spike is emitted, an intrinsic current with stereotypical shape $\eta(t)$ is triggered (see Table 2.1). Currents triggered by different spikes accumulate and produce spike-frequency adaptation. Immediately after firing, the membrane potential is reset to V_{reset}, integration of Eq. 2.1 restarts and the neuron goes through an absolute refractory period of duration τ_{ref}.

Spikes are produced stochastically according to a point process with the firing intensity

$$\lambda(t) = \lambda_0 \exp\left(\frac{V(t) - V_{\mathrm{T}}(t)}{\Delta V}\right) \tag{2.2}$$

where λ_0 is the stochastic intensity at the firing threshold V_{T}, ΔV is a constant which defines the level of stochasticity and V_{T} is a time-dependent firing threshold:

Parameter	Excitatory	Inhibitory
C (pF)	83.1	46.1
g_L (nS)	3.7	6.6
E_L (mV)	-67.0	-71.2
τ_{ref} (ms)	4.0	4.0
V_{reset} (mV)	-36.7	-48.4
$\eta(t)$	$\eta_1(t) + \eta_2(t)$	$\eta_1(t) + \eta_2(t)$
$\eta_1(t)$ (pA)	$56.7e^{-t/57.8\text{ms}}$	$31.8e^{-t/11.5\text{ms}}$
$\eta_2(t)$ (pA)	$-6.9e^{-t/218.2\text{ms}}$	$1.6e^{-t/500.1\text{ms}}$
$\gamma(t)$	$\gamma_1(t) + \gamma_2(t)$	$\gamma_1(t) + \gamma_2(t)$
$\gamma_1(t)$ (mV)	$11.7e^{-t/53.8\text{ms}}$	$5.6e^{-t/11.5\text{ms}}$
$\gamma_2(t)$ (mV)	$1.8e^{-t/640.0\text{ms}}$	$0.6e^{-t/473.7\text{ms}}$
λ_0 (kHz)	10	10
ΔV (mV)	1.4	0.6
V_T^* (mV)	-39.6	-41.2

Table 2.1: The mean of GIF neuron model parameters extracted from Mensi et al. (2012).

$$V_{\text{T}}(t) = V_T^* + \sum_{\hat{t}_j < t} \gamma(t - \hat{t}_j) \tag{2.3}$$

where V_T^* is a constant and $\gamma(t)$ describes the stereotypical time course of the firing threshold after the emission of an action potential (see Table 2.1).

For all neuronal parameters, we use the values given in Table 2.1 with $\pm 15\%$ uniformly distributed variations in all simulations, except for Figure 2.3A. For comparison in Figure 2.3A all neuron parameters are as in Table 2.1 without any variation. The values of Table 2.1 are extracted from experimental data from mouse barrel cortex (Mensi et al., 2012) and no parameter tuning of neuronal parameters was done for the network simulations reported here.

In the network, the input current $I_i(t)$ in Eq. 2.1 is generated by synaptic current pulses into a specific neuron i

$$I_i(t) = \sum_j w_{ij} \sum_f \alpha(t - t_j^f) = \sum_j w_{ij} \int_0^\infty \alpha(s) S_j(t - s) ds \tag{2.4}$$

where t_j^f is the f^{th} spike of a presynaptic neuron j and $S_j = \sum_f \delta(t - t_j^f)$ is the spike train of neuron j where δ denotes the Dirac δ-function. We choose an exponential shape for post-synaptic currents (PSC) α with a time constant τ_{syn}: $\alpha(t) = e^{-(t-\Delta)/\tau_{\text{syn}}}$ for $t \geq \Delta$. The transmission delay (Δ) of synaptic connections in all our simulations is 1ms. The symbol w_{ij} denotes the synaptic weight from neuron j to neuron i. The term synaptic weight is commonly used for either of two different quantities, either the amplitude of the PSC or the amplitude of

	Connection probability	τ_{syn} (ms)	Synaptic weight			
			PSP amplitude(mV)		w_{ij} (pA)	
			Mean	Std	Mean	Std
exc→exc	19%	16.3	0.66	0.76	7.9	9.1
exc→inh	37%	6.9	0.55	0.51	9.9	9.2
inh→exc	50%	1.3	0.48	0.44	36.5	33.5
inh→inh	35%	6.9	0.48	0.49	8.7	8.9

Table 2.2: Network parameters as extracted from mouse barrel cortex (Lefort et al., 2009; Avermann et al., 2012).

	r_{Poisson} (Hz)	τ_{syn} (ms)	Synaptic weight
			w_{ij} (pA)
Poisson→assembly1	100	16.3	30
Poisson→assembly2	100	16.3	30
Poisson→assembly3	100	16.3	30
Poisson→non-hubs	100	16.3	10
Poisson→inhibitory	100	6.9	80

Table 2.3: Each neuron receives input from an independent Poisson process with a rate of r_{Poisson} and a synaptic weight w_{ij}.

the post-synaptic potential (PSP). In this study we take the first definition, i.e. w_{ij} denotes the PSC amplitude; see Eq. 2.4. However, the experimental datasets we used report the synaptic weight based on the second definition (PSP amplitude). Given the neuronal parameters, one can easily relate the two quantities. We report the synaptic weight we used in our simulations according to both of the definitions in Table 2.2.

All network parameters (Table 2.2), e.g. connection probabilities, the distribution of synaptic weights and number of neurons are chosen based on previously published data extracted from mouse barrel cortex (Lefort et al., 2009; Avermann et al., 2012). At present there is no comparable dataset for L5 inhibitory neurons. Therefore, for inhibitory neurons, we use neuronal and network parameters similar to those of L2/3 inhibitory neurons (Avermann et al., 2012). Since these neurons do not play a crucial role in initiating the up/down oscillations and stimulus-evoked responses, the exact choice of their parameters does not strongly affect the results. Moreover, the study of Pfeffer et al. (2013) explored some aspects of connectivity pattern between different subsets of inhibitory neurons and highlighted more similarities than differences between L2/3 and L5 inhibitory network. In the model, all neurons receive external Poisson noise whose properties are described in Table 2.3.

In order to reproduce the light-evoked stimulation (Figure 2.4), we randomly select 15% of the neurons and inject a step current with amplitude 100 pA for 300 ms. For simulating the light-evoked response in L2/3, the connection probability and the mean synaptic weights inside excitatory population are 16.8% and 0.37 mV, respectively (Avermann et al., 2012). The other

network parameters are the same as L5. For simulating the active cortical state (Figure 2.4), during the active period each neuron receives synaptic input from 70 Poisson process neurons firing with a rate of 5 Hz. The synaptic weights of synapses from Poisson neurons to assemblies, non-hubs and inhibitory neurons are 25, 5, and -25 pA, respectively.

All simulations were run using the Brian simulator (Goodman and Brette, 2008).

Partitioning the Excitatory Population into Weight-Hubs and Non-hubs Subpopulations

In order to distinguish between weight-hub and other neurons ("non-hubs"), and to capture the properties of weight-hub neuron subpopulations (assemblies), we use two methods explained in the following. The first method (heterogeneity approach) maintains the heterogeneity of synaptic weights in the population. The experimentally obtained probability density function of synaptic weights $p(w)$ is well-approximated by a lognormal distribution (Lefort et al., 2009):

$$p(w) = \frac{1}{w\sigma\sqrt{2\pi}} e^{-\frac{(\ln\frac{w}{w_\mathrm{m}}-\mu)^2}{2\sigma^2}} \tag{2.5}$$

where μ and σ are the two parameters of the distribution and w_m is the median of synaptic weights (Figure 2.1).

Following Tomm et al. (2014), we first change the synaptic weight matrix in order to have local inward weight correlations, as described in the following. We start by generating an initial random connectivity matrix (connection probability $p = 19\%$, see Table 2.2) with weights drawn from Eq. 2.5. Let $\hat{W} = [\hat{w}_{ij}]_{N\times N}$ be the initial weight matrix, where N is the total number of excitatory neurons. We continue by generating a vector $A = [a_i]_{N\times 1}$ using another lognormal distribution. Now, we define a new weight matrix W by

$$w_{ij} = \hat{w}_{ij} a_i \,. \tag{2.6}$$

A high value of a_i increases the weight of all synapses received by the i-th neuron. Therefore, a high value of a_i tends to convert the neuron to a weight-hub neuron, because it will have many large inward weights. Moreover, since multiplication of two lognormal variables yields a lognormal variable, we can be sure that new weights w_{ij} are drawn from a lognormal distribution. We choose the parameters of the two lognormal distributions ($\mu = 0.141$, $\sigma = 0.924$ and $w_\mathrm{m} = 0.372$mV for the distribution of $\hat{w}_{ij}$, and $\mu = 1.4 \cdot 10^{-4}$, $\sigma = 0.15$ and $a_\mathrm{m} = 1$ (median) for the distribution of a_i) to set the mean and variance of the final weights equal to the values found in the experimental data (Lefort et al., 2009) ($\mu = 0.005$, $\sigma = 0.936$ and $w_\mathrm{m} = 0.419$mV). The mean weight is then 0.66mV and the standard deviation is 0.76mV with the above choice of parameters. $N_\mathrm{h} = 95$ neurons out of $N_\mathrm{e} = 454$ excitatory neurons (20.9%) were labeled as "weight-hubs", by choosing those with the highest sum of inward weights (Figure 2.1A). Note that other values may have been used for the distribution parameters of $\hat{w}_{ij}$ and a_i, as long as the distribution of w_{ij} matches the experimental data (Lefort et al., 2009). We chose the mentioned parameters to achieve biologically plausible network dynamics (skewed firing rate

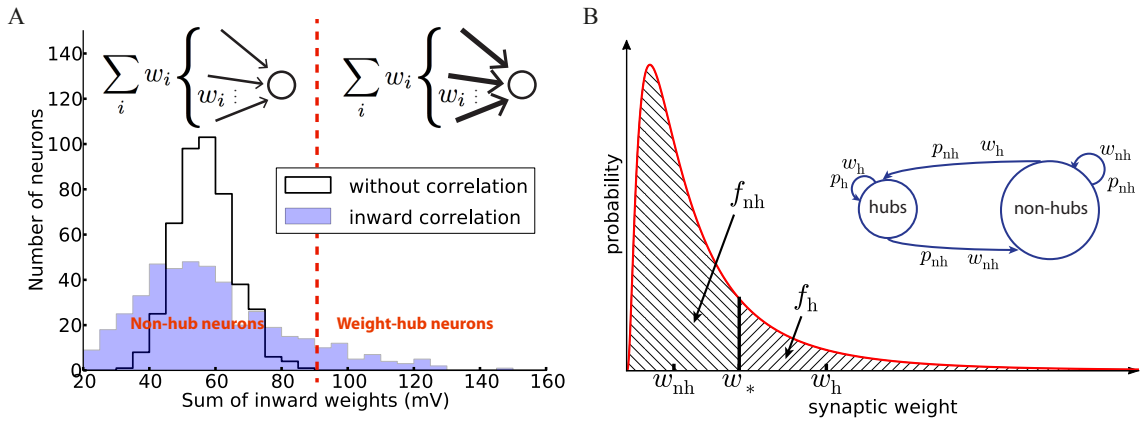

Figure 2.1: Networks with weight-hub neurons. **A**) Histogram of the sum of inward weights for a random (solid line, network without weight-hubs) and inward correlated (filled, network with weight-hubs) network topology. While the random topology (without weight-hubs) shows an approximately normal distribution, the inward-correlated topology has a broader, lognormal-like distribution. Weight-hub neurons form the tail of this distribution. Both networks, without and with weight-hubs, have the same lognormal distribution of individual weights shown in (**B**) (red line). Inset: In a heterogeneous network with inward correlations, most neurons receive many weak (thin arrows) connections (left) whereas weight-hub neurons (right) receive many strong connections. (**B**) Fitting the experimental distribution (red line) of synaptic weights (EPSP amplitudes) by a two-element "homogeneous" distribution (dashed areas). The lognormal distribution (solid line) was fitted to experimental data (Lefort et al., 2009) and is used to find the values of weak and strong weights, w_{nh} and w_{h}, respectively. Inset: Splitting the excitatory population into two subpopulations. Weight-hub neurons receive strong synaptic weights (w_{h}) and non-hub neurons receive weak synaptic weights (w_{nh}). All connection probabilities are low (p_{nh}; nh: non-hub) except for the hub-to-hub connections (p_{h}).

distribution and low correlations between neurons). Note that if we only consider weight matrix $\hat{W}$ (without multiplying by a_i), then our network does not contain weight-hub neurons. We used this approach in Figure 2.4C.

In a second step we rewire the network to increase the number of connections between weight-hub neurons in the assembly (such that connection probability between weight-hub neurons increases from $\bar{p} = 19\%$ to $p_{\mathrm{h}} = 50\%$), while keeping the total number of connections fixed. To do so, we randomly select two unconnected weight-hub neurons and add a connection between them. The weight of this new synapse is again drawn from the lognormal distribution described earlier. Then we randomly select a connected neuron pair which contains at least one non-hub neuron and remove the synapse connecting them. This procedure is repeated until we reach the desired connection probability between weight-hubs. An issue here is that, since we remove a weak weight and add a strong one, the overall average weight increases slightly. However, the number of replaced synapses is very small compared to the overall number of synapses: The number of synapses between weight-hub neurons before the rewiring is $S_{\mathrm{h}}^{\mathrm{intial}} = N_{\mathrm{h}}^2 \bar{p} = (20.9\% \cdot N_{\mathrm{e}})^2 \bar{p}$ and after that it should be $S_{\mathrm{h}}^{\mathrm{final}} = N_{\mathrm{h}}^2 p_{\mathrm{h}} = (20.9\% \cdot N_{\mathrm{e}})^2 p_{\mathrm{h}}$. Therefore the fraction of replaced

synapses equals:

$$\frac{S_{\mathrm{h}}^{\mathrm{final}} - S_{\mathrm{h}}^{\mathrm{initial}}}{S_{\mathrm{e}}} = (20.9\%)^2(\frac{p_{\mathrm{h}}}{\bar{p}} - 1) = 0.071 \tag{2.7}$$

where $S_{\mathrm{e}} = N_{\mathrm{e}}^2\bar{p}$ is the total number of synapses between excitatory neurons. That means the rewiring concerns only 7.1% of all excitatory synapses, and therefore causes only a small increase of the average weight (average exc. weight is 0.659mV before and is 0.666mV after rewiring). Note that choosing a higher fraction of assembly neurons in the network increases the fraction of replaced synapses. For example, if assembly neurons form 35% of all excitatory neurons, 20% of all excitatory synapses will be affected. Clearly, it leads to a significant change in the average of excitatory weighs (0.659mV before and 0.701mV after rewiring).

The rewiring procedure can be modified in order to make several connected weight-hub assemblies instead of just one. To this end, we randomly assign weight-hub neurons into several groups. Then new synapses are added inside the groups and the same number of existing synapses between the groups or between a pair of non-hub neurons are removed. Using this procedure, each group becomes an assembly of densely connected weight-hub neurons.

As we observed in the previous method, we could choose different levels of heterogeneity in synaptic weight structure by choosing different values for the distribution parameters of $\hat{w}_{ij}$ and a_i. However, this heterogeneity does not affect the main outcome of the model, which is oscillation. We support this idea by showing that a model with homogenous weight structure is able to generate oscillations. Here we explain the second method for building weight-hub neurons in the excitatory population. This method produces homogenous synaptic weights within each subpopulation. Hence, we call it homogenous approach. We use it for the analytical results and for Figure 2.3A. The method splits the excitatory population into two subpopulations. The first one (the assembly of densely connected weight-hubs) contains N_{h} weight-hub neurons, the second one contains N_{nh} non-hub neurons. Weight-hubs are those neurons that receive strong synapses from other weight-hubs and from other excitatory neurons; all input weights onto weight-hubs have the same value w_{h}. Non-hubs receive weak synapses, all with identical input weights w_{nh}. Let us assume that all connection probabilities between and inside subpopulations are the same (p_{nh}) except for the weight-hub to weight-hub connection probability (p_{h}) which is larger. Figure 2.1A summarizes the parameters of this network structure.

The experimental data (Lefort et al., 2009) do not distinguish between weight-hubs and non-hubs but reports an overall synaptic weight distribution ($p(w)$) and an average connection probability ($\bar{p}$). We adjust the network parameters of the two homogeneous subpopulations using these data. The average connection probability ($\bar{p}$) should be maintained, despite the split of the population into weight-hubs and non-hubs. Computing the average connection probability in this model yields the equation:

$$\bar{p} = \frac{N_{\mathrm{h}}^2 p_{\mathrm{h}} + N_{\mathrm{nh}}^2 p_{\mathrm{nh}} + 2N_{\mathrm{h}}N_{\mathrm{nh}}p_{\mathrm{nh}}}{(N_{\mathrm{h}} + N_{\mathrm{nh}})^2} \tag{2.8}$$

We approximate the synaptic weight distribution $p(w)$ obtained by experiments (Lefort et al., 2009) with a two-element distribution formed by w_{h} and w_{nh} (Figure 2.1A). The strategy is

simple: a classification boundary (w_*) divides the synaptic weights into two disjoint sets, i.e., synaptic weights lower than w_* and synaptic weights higher than w_*. All weights lower than w_* are set to w_{nh} and the others to w_{h}.

In order to obtain the value of w_*, we introduce the fraction of weak connections f_{nh} as a parameter:

$$f_{\mathrm{nh}} = \frac{N_{\mathrm{nh}}^2 p_{\mathrm{nh}} + N_{\mathrm{h}} N_{\mathrm{nh}} p_{\mathrm{nh}}}{(N_{\mathrm{h}} + N_{\mathrm{nh}})^2 \bar{p}} \tag{2.9}$$

The classification boundary w_* follows from the condition that the probability mass of weak connections must account for the fraction of weak connections:

$$\int_0^{w_*} p(w) dw \; = f_{\mathrm{nh}}. \tag{2.10}$$

Because $p(w)$ is positive there is a unique solution for w_* which we determine numerically. Once the boundary w_* is fixed, averaging w over the respective support yields the synaptic weights of weight-hubs w_{h} and non-hubs w_{nh}:

$$w_{\mathrm{nh}} = \frac{1}{f_{\mathrm{nh}}} \int_0^{w_*} w\, p(w)\, dw \tag{2.11}$$

$$w_{\mathrm{h}} = \frac{1}{f_{\mathrm{h}}} \int_{w_*}^{\infty} w\, p(w)\, dw\,, \tag{2.12}$$

where $f_{\mathrm{h}} = 1 - f_{\mathrm{nh}}$. A similar procedure may be applied in the case of several connected weight-hub neurons subpopulations. Choosing $p_{\mathrm{h}} = 50\%$ and $N_{\mathrm{h}} = 95$, we obtain the remaining parameter values: $w_{\mathrm{h}} = 1.42$ mV, $w_{\mathrm{nh}} = 0.34$ mV for PSP amplitudes, and $p_{\mathrm{nh}} = 18\%$. The PSC amplitudes can be calculated using the PSP amplitudes: $w_{\mathrm{h}} = 16.9$ pA and $w_{\mathrm{nh}} = 4.0$ pA.

Rate-current relations

Consider a population or a subpopulation of neurons. We can obtain a relation between the average firing rate of all neurons and the average synaptic input current using two different approaches. The first approach employs the neurons' gain function, a generalization of the frequency-current ($f-I$) curve (the terms firing frequency and firing rate are used interchangeably here). Injecting a weakly fluctuating current I_{syn} into a neuron causes an average firing rate of

$$r \;\; = \;\; g(\langle I_{\mathrm{syn}} \rangle,\; \sigma_{\mathrm{I}})\,, \tag{2.13}$$

where g is the gain function and $\langle I_{\mathrm{syn}} \rangle$ and σ_{I} are the average and standard deviation of synaptic current over time, respectively. Although there are ways to compute the firing rate of adaptive integrate-and-fire neuron models in closed-form (Fourcaud-Trocmé et al., 2003; Hertäg et al., 2014) or by using a self-consistent numerical approach (La Camera et al., 2004; Richardson,

2007, 2009), we obtain it here by numerical simulations, using a certain amount of fluctuations in the input:

$$I(t) = \langle I_{\text{syn}} \rangle + \frac{\sigma_{\text{I}}}{\sqrt{q_2}} \int_0^\infty \alpha(s)\xi(t-s)ds \tag{2.14}$$

where $\alpha(t)$ is the shape of an elementary postsynaptic current (PSC) defined in Eq. 2.4, $\xi(t)$ is white noise of unit standard deviation and $q_2 = \int_0^\infty \alpha^2(t)dt$. If the current is injected for short episodes of 10ms or less, we can estimate the firing rate in the non-adapted state by averaging over several trials. If it is injected for a longer time, we can divide the time into intervals of 10ms and extract the frequency-current relation in the different, progressively more adapted states.

The second relation between the average firing rate and the average synaptic current follows from the network activity; see Amit and Brunel (1997) and Gerstner et al. (2014). Each neuron i receives the synaptic current produced by the input spike train:

$$I_{i,\text{syn}}(t) = \sum_j w_{ij} \left(\int_0^\infty \alpha(s) S_j(t-s)ds \right) \tag{2.15}$$

where $S_j(t)$ is the spike train of j-th neuron, and w_{ij} is the synaptic weight of this input onto the receiving neuron. By averaging both sides over time and input neurons we obtain the average input current (also known as the mean field) $\langle I_{\text{syn}} \rangle = Npq\bar{w}r$, where N and p are the number of neurons in the population and the connection probability between them, respectively. Here $q = \int_0^\infty \alpha(t)dt$ is the total charge of one PSC pulse, $\bar{w}$ is the average synaptic weight and r is the average firing rate of neurons in this population. Rearranging this equation yields the network feedback relation:

$$r = \frac{\langle I_{\text{syn}} \rangle}{Npq\bar{w}} \tag{2.16}$$

which is a linear relation of $\langle I_{\text{syn}} \rangle$ and r with slope $1/(Npq\bar{w})$. We refer to the denominator as the network feedback (C_{fb}) of the population:

$$C_{\text{fb}} = Npq\bar{w} \tag{2.17}$$

Eq. 2.13 and 2.17 will be used in the "Results" section to get insight into the network dynamics.

K-Means Clustering Method

K-means is a machine learning method for assigning data samples of a dataset to K clusters. In this method, each data sample is represented by a vector of numbers.

The algorithm works as follows. It initializes the center vectors of the K clusters randomly. Then, K clusters are created by assigning each data sample to the nearest center vector (using Euclidean distance). Afterward, the new center of each cluster is calculated by averaging over

all data samples to the cluster. The algorithm repeats the assignment and averaging steps until it converges (i.e., until no change happens to the clusters by repeating these steps).

An important issue is how to determine the number of clusters (K) to begin with. This has generally to be done with the task in mind. Here we use the algorithm for two tasks. The first one is distinguishing weight-hubs from non-hubs. Clearly, in this task K = 2, because we are looking for two different classes of neurons. The second task is assigning weight-hubs to different clusters. Here, we use the so-called elbow method for choosing the value of K: We run the algorithm for different values of K (2, 3, ...). Generally, the error of clustering (sum of squared distances between each data sample and the center of its cluster) decreases with increasing K. However, we choose the K at which the error decreases abruptly and a greater K does not decrease the error that much. This method leads us to K = 3 for the second task.

2.3 Results

2.3.1 Layer 5-model network produces irregular oscillations

Both during anesthesia and slow-wave sleep cortical neurons show slow oscillations ($\sim$ 1Hz) between two states (Steriade et al., 1993b; Cowan and Wilson, 1994; Lampl et al., 1999; Sanchez-Vives et al., 2000; Sanchez-Vives and McCormick, 2000; Petersen et al., 2003b), the active up-state and the quiescent down-state. The underlying mechanism of this phenomenon is not fully understood, but several neuronal network models have been suggested, mostly based on short-term plasticity (Holcman and Tsodyks, 2006; Melamed et al., 2008; Ghorbani et al., 2012).

Here we model cortical L5 with neuron model parameters and network parameters extracted from experimental data of a single column of somatosensory cortex in mice (see Materials and Methods and Table 2.1 and 2.2). An important feature of our model is that its excitatory population (which consists of 454 neurons) contains three assemblies of densely ($p = 50\%$) connected weight-hubs which consist of 45, 30 and 20 weight-hub neurons, respectively. A weight-hub neuron, or simply weight-hub, is defined here as a neuron receiving many strong synapses so that the sum of incoming synaptic weights across all connections from other neurons in the network is large compared to that of other neurons (Figure 2.1A).

Figure 2.2A shows the membrane potential and spike raster of several sample neurons. Simulations show that the model exhibits irregular up/down state transitions reminiscent of irregular slow oscillations in anesthetized cortex (Stern et al., 1997; Lampl et al., 1999). In order to compare the up-state durations in the model with experimental data (Stern et al., 1997; Cossart et al., 2003), we quantify the variability of the duration T of the up-state by the coefficient of variation, defined as std(T)/mean(T), where the up-state duration T is measured as the duration for which the membrane potential of a neuron stays at least 10mV above the resting potential (E_L). To this end, the membrane potential is smoothed by filtering with a Gaussian filter kernel (of width 20ms) in order to remove rapid fluctuations. The coefficient of variation of this presumed up-state duration, averaged over all neurons that have not been classified

as weight-hub, is 0.42, which shows that their up-state duration is rather irregular (Figure 2.2C). Similarly, if we repeatedly select 10 excitatory neurons (choosing randomly from both weight-hubs and other neurons) and measure the average coefficient of variation of the up-state duration, we find a coefficient of variation of 0.40 ± 0.06.

The L5-network model produces a skewed and long tailed distribution of firing rates in the whole population (Figure 2.2B) that is approximately lognormal (Figure 2.2B, inset). Weight-hub neurons have a high firing rate and form the tail of the distribution, whereas non-hubs have a low firing rate. The overall shape of the firing rate distribution is consistent with observations in *in-vivo* experiments (Hromádka et al., 2008; Vijayan et al., 2010).

We investigated the correlations of transition times from down- to up-state and vice versa (Figure 2.2D-F). Transitions inside subpopulations are highly correlated. The mean correlation coefficient for transition from down- to up-state is 0.84, 0.82, 0.69 for neurons within assemblies 1, 2 and 3, respectively, 0.77 for non-hub neurons and 0.78 for inhibitory neurons (Student's t test for difference in mean: all p-values are smaller than 10^{-10}). The mean cross-correlation for all pairs of neurons is 0.58, indicating a high correlation between randomly chosen pairs of neurons. The corresponding values for transition from up- to down-state are 0.68, 0.64, 0.56 for assemblies 1, 2 and 3, respectively, 0.83 for non-hub neurons, 0.84 for inhibitory neurons and 0.60 for all pairs of neurons (Student's t test for difference in mean: all p-values are smaller than 10^{-10}). These results indicate that an overall synchrony between neurons in the up-/down state oscillations are maintained, consistent with recordings from multiple extracellular electrodes (Petersen et al., 2003b; Fucke et al., 2011). Note that assemblies oscillate out of phase, but not in anti-phase, because they do not strongly compete with each other, as opposed to a network in a winner-takes-all mode. Therefore occasionally more than one assembly is active at a time (see raster plot in Figure 2.2A). Competitive neurons with anti-phase oscillations would instead lead to reduced correlation of up/down state transitions, averaged across all neuron pairs in the network. High correlations inside each subpopulation also increase the overall correlation. The peak of the overall correlation distribution mostly belongs to correlations of pairs inside subpopulations (Figure 2.2B). Another noteworthy point is that since the size of assembly 3 is small (20 neurons), its properties differ from other assemblies. In particular, the firing rate of assembly 3 neurons is less than that of the two other assemblies, and even less than several non-hub neurons (Figure 2.2B). Also, the correlation of up/down transitions is less than other assemblies and non-hub neurons.

To investigate whether the heterogeneity of the network structure, the broad distribution of synaptic weights, and the variation of neural parameters values are important for these dynamics, we built a similar model in which all synaptic weights inside a given subpopulation (i.e. weight-hubs, non-hubs and inhibitory) are identical (See Materials and Methods) and values of neural parameters inside each subpopulation are identical (Table 2.1). The model still produces the irregular up/down state oscillations (Figure 2.3A).

On the other hand, the reduction of the connection probability inside the assemblies of weight-hub neurons from 50% to 20% (while maintaining the overall connection probability such that it agrees with experimental data) causes the dynamics to change significantly, and the irregular

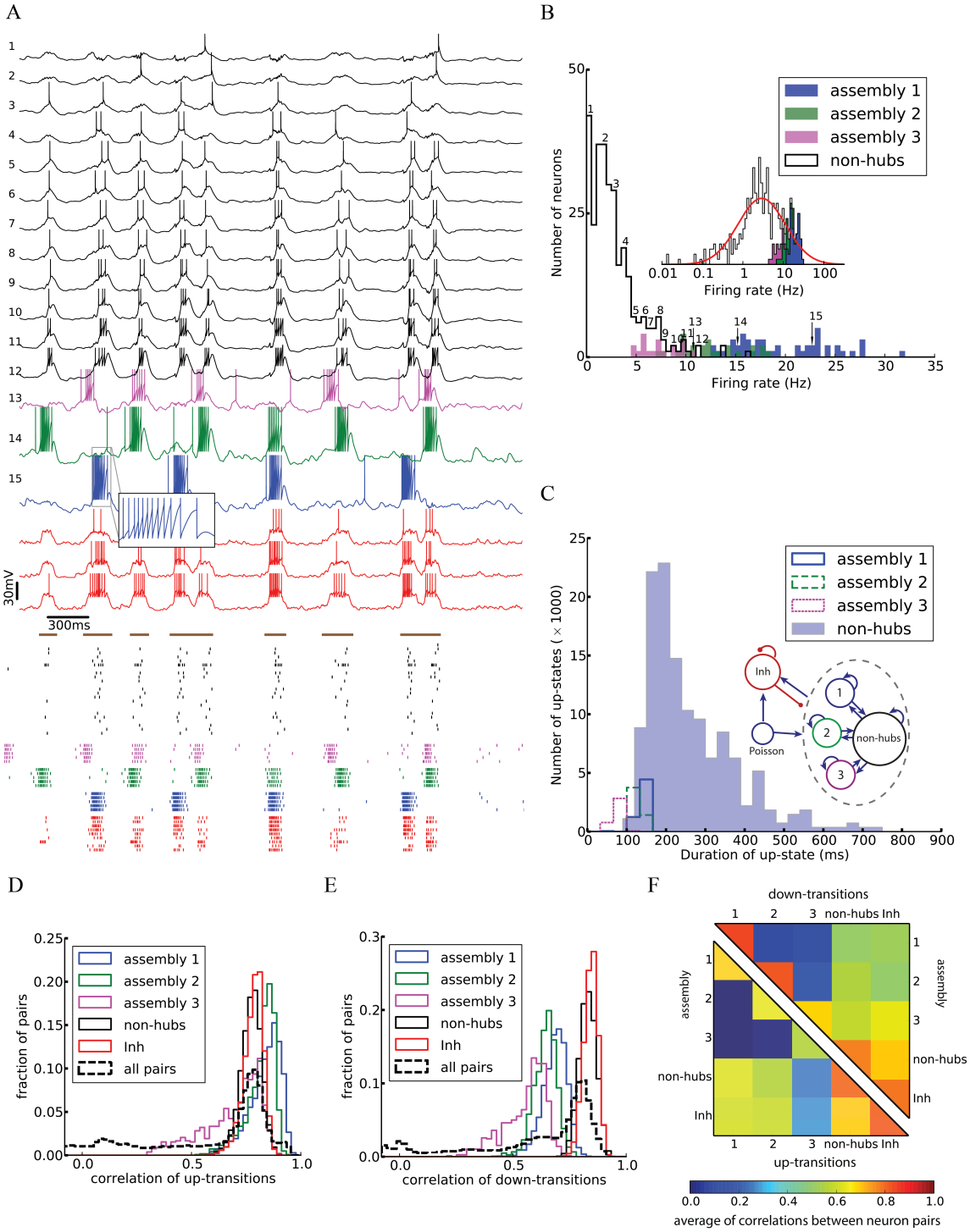

Figure 2.2: Irregular up- and down-state transitions in a network with three assemblies of densely connected

Figure 2.2: ***(Continued)*** weight-hubs. **A-Top**) Membrane potential of sample non-hub (black, labeled 1-12) and weight-hub (labeled 13-15) and inhibitory neurons (red, without label). Inside each group neurons have been sorted by their firing rate. Brown bars indicate time intervals which are considered as up-states for bottommost inhibitory neuron. **A-Bottom)** Raster plot of several neurons of each population (same color). **B)** Rate distribution of excitatory neurons. Numbered labels indicate the firing rate of neurons whose membrane potential traces are shown in A. Inset: The distribution of firing rates is close to a normal distribution (red curve) on a (semi-) logarithmic scale. **C)** Histograms of the up-state duration for each group of excitatory neurons. The coefficients of variation for the assemblies are 0.06, 0.10 and 0.16, which signifies regular durations. The non-hub neurons (filled histogram) exhibit a broad distribution of up-state durations with coefficient of variation of 0.42. Inset: The Excitatory population contains three assemblies of weight-hubs and a large population of non-hubs. **D**, **E)** Distribution of pairwise Pearson correlation coefficients of transition times from down- to up-state (**D**) and from up- to down-state (**E**) inside each subpopulation (solid lines) and over all 145530 pairs of neurons (dashed lines). Transitions of two neurons are counted as coincident if they happen in the same time bin of 20ms. **F)** Averaged Pearson correlation coefficients of transitions from down- to up-state (upper triangle) and up- to down-state (lower triangle).

oscillations vanish (Figure 2.3B) even though network and neuronal parameters are heterogeneous. Thus the connection probability inside weight-hub neurons assemblies plays an important role in the model dynamics. This is consistent with the model of Litwin-Kumar and Doiron (2012), in which clusters of neurons were predefined. Decreasing the connection probability inside the neuronal clusters causes the transitions of clusters between active and inactive states to cease. In a related model (Mazzucato et al., 2015), in which inter- and intracluster connection probabilities are equal, decreasing the synaptic weights inside the clusters leads to a loss of oscillations.

Finally, we also simulate a network with a single assembly of densely connected weight-hubs (Figure 2.3C). While transitions between up and down states occur, the oscillations in non-hub neurons (and therefore the majority of neurons) are much more regular than in the full model of Figure 2.2 (the coefficient of variation of up-state duration for non-hub neurons in Figure 2.3C is 0.08 for, while it is 0.42 for Figure 2.2).

Simulation of optogenetic stimulation. Here, we explore the light-evoked response of our model of barrel cortex networks. Mimicking a recent experiment (Beltramo et al., 2013), a small subset of model neurons is stimulated to fire. Then, the activity of several non-stimulated neurons is recorded to investigate the relation and effect of the stimulated subset on the other neurons in the network. In our framework, an increased connection probability between weight-hub neurons can potentially explain the observation of the experiment: Optogenetic stimulation of a group of L5 neurons causes a long-lasting depolarization in non-stimulated L5 excitatory neurons, while the same experiment shows different results in L2/3 (Beltramo et al., 2013). Non-stimulated neurons in L2/3 show little depolarization and a smaller number of emitted spikes upon optogenetic stimulation of L2/3. These results imply that the L5 excitatory population is able to spread the optically induced activation more than the L2/3 one. In principle, this difference could be due to neuron parameters, neuronal morphology or the structure of neuronal networks. Here we argue that the presence or absence of densely connected weight-hubs assemblies, which is a property of the network structure, can explain the difference in the spread of activation within each layer. We propose that weight-hubs may be densely connected

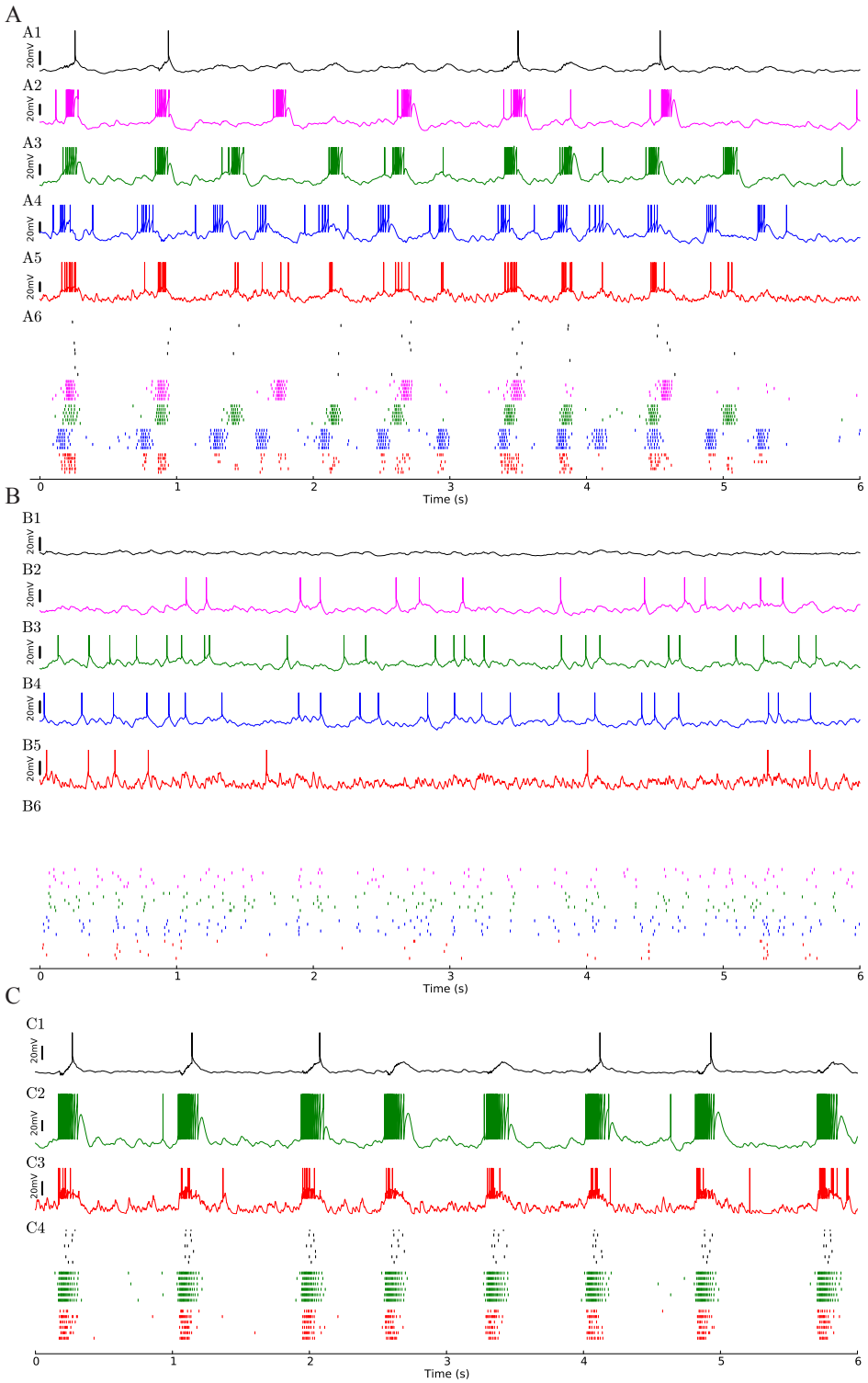

Figure 2.3: **A)** Network of 454 excitatory and 90 inhibitory neurons with identical neuron parameters, organized

Figure 2.3: ***(Continued)*** into homogenous subpopulations with dense connectivity within each assembly and non-hubs. Membrane potential traces of a non-hub neuron (**A1**), neurons from each of the three weight-hub assemblies (**A2**, **A3**, **A4**) and an inhibitory neuron (Inh) (**A5**). **A6**) Raster plot of several neurons of each population (same colors). Oscillations of the assemblies are different in terms of the up-state and down-state durations. Non-hub and inhibitory neurons receive input from the three oscillating assemblies and exhibit irregular oscillations. Note that there are 359 non-hub neurons in the network, which is the majority of cells. **B)** Heterogeneous network as in Figure 2.2, but sparse connectivity ($p = 20\%$) inside assemblies. Membrane potential of non-hub (**B1**), three weight-hub neurons (**B2**, **B3**, **B4**) and inhibitory neurons (**B5**) and the raster plot of several neurons of each population (**B6**). The Up-state/down-state oscillation vanishes. Weight-hubs (**B2**-**B4**) occasionally emit spikes since they receive stronger synapses from Poisson neurons, while non-hub neurons (**B1**) do not spike at all. **C)** Oscillations in a network with a single assembly of densely connected weight-hubs are more regular than in Figure 2.2. Membrane potential of a non-hub (**C1**), a weight-hub (**C2**) and an inhibitory neuron (**C3**). **C4**) Raster plot of randomly selected neurons of each population. While weight-hub neurons (green ticks) exhibit a high firing rate in the up-state, non-hub neurons (black ticks) show only a small number of spikes. Inhibitory neurons (Inh) are shown in red.

in L5, but their connectivity may be sparse in L2/3. This difference can be considered as one of several possible ways for interpretation of different light-evoked response in L2/3 and L5. Another noteworthy point is that although both connection probability and average synaptic weights in L2/3 are lower than L5 (see Section Materials and Methods), the number of neurons in L2/3 is much larger than L5 in our framework (1691 vs. 454). Therefore, the number and total strength of inward synapses into L2/3 neurons are not lower than L5 neurons.

We examined whether the experiments in L2/3 and L5 can be explained by our cortical network model. Figures 2.4A,B respectively show the responses of L2/3 and L5 excitatory population models to a transient direct current stimulus, which we used to model optogenetic stimulation (Beltramo et al., 2013). The stimulus is received by a random subset (15%) of excitatory neurons, to account for the fact that about 15% of experimentally observed neurons express the light-sensitive ion channel. In the L2/3 population model, the connections within the weight-hubs assembly are sparse, whereas in the L5 model they are dense. Non-stimulated model neurons in L2/3 show little depolarization while L5 ones show a high depolarization and a substantial number of spikes, in agreement with experiments in mouse visual cortex (Beltramo et al., 2013). Therefore, we conclude that dense connectivity between weight-hub neurons in L5 and sparse weight-hub connectivity in L2/3 can generate biologically plausible light-evoked responses.

In the simulations of Figures 2.2, 2.3, we observed that densely connected weight-hubs produce up-state/down-state oscillations while sparsely connected ones do not. Taken together with the simulation of Figure 2.4 these results suggest that L5 is the main source of the up/down oscillations in the cortex, while L2/3 is subsidiary. Experimental studies (Sakata and Harris, 2009; Chauvette et al., 2010; Beltramo et al., 2013) provide further support of this conclusion.

To assess whether the concept of weight-hubs is necessary to explain the light-evoked responses, we modified the structure of L5 network and repeated the simulation. In the new structure, we did not use weight-hub neurons (neurons that receive strong synaptic weights from all other neurons) but we instead implemented an assembly with high connection probability and strong

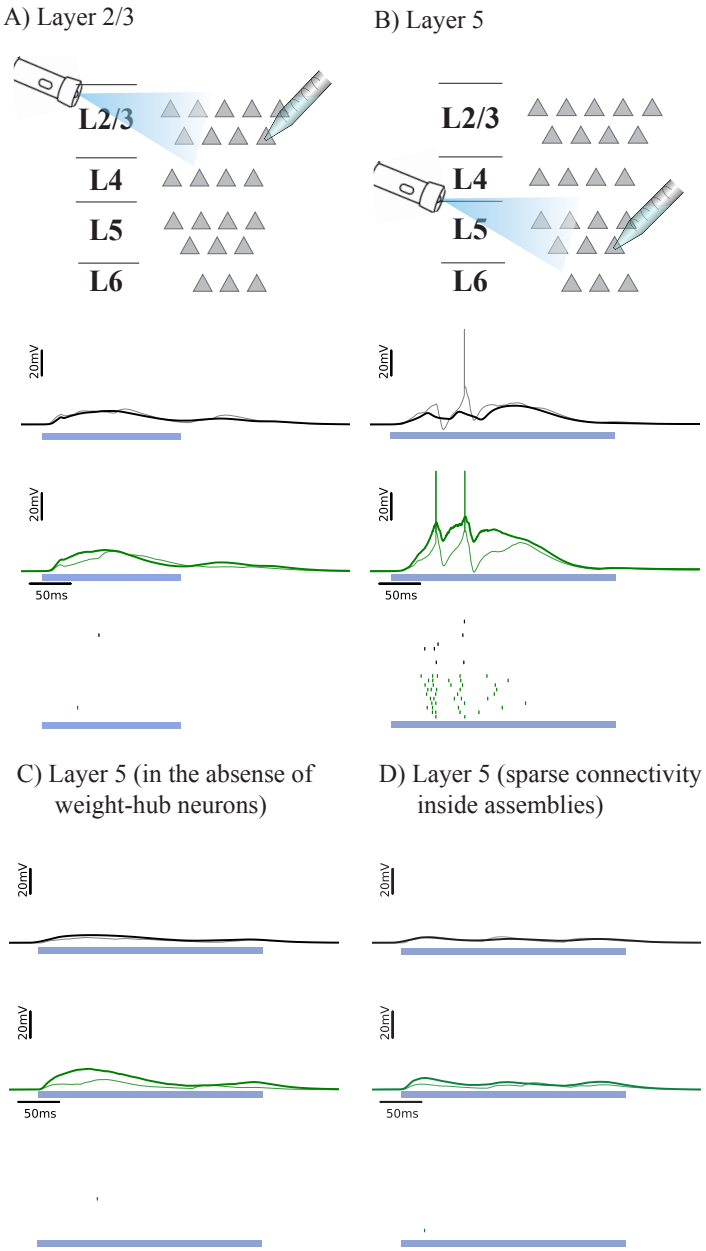

Figure 2.4: Simulated response to light-evoked stimulation of non-stimulated excitatory neurons in cortical L2/3 (**A**) and in L5 (**B**). Approximately 15% of all neurons (weight-hubs, non-hubs and inhibitory) are stimulated in each layer for a time period of 300 ms (blue bar). Membrane potentials (lines) and spikes (ticks) of weight-hubs (green) and non-hubs (black). L2/3 neurons (**A**) show little depolarization due to sparse connectivity between weight-hubs, while L5 neurons (**B**) display a long-lasting depolarization and a significant number of spikes. This effect is due to the dense connectivity between weight-hubs in the L5 network model, but not in the L2/3 model. (**C**) Simulation of L5 in case of a modified assembly model that only has strong internal synaptic weights but is not innervated as strongly from other neurons as the weight-hub assembly in (**B**), see main text for details. In the absence of weight-hub neurons, L5 does not generate long-lasting depolarization in response to the stimulation. (**D**) Simulation of L5 in case of having sparse connectivity ($p = 20\%$) inside assemblies. The network is unable to produce long-lasting depolarization.

synaptic weights internally. In other words, in the new structure the neurons of the assembly receive strong synaptic weights from each other while they receive normal weights (broadly distributed weak and strong weights, as shown in Figure 2.1B) from the neurons outside the assembly. Our simulation shows that this structure is unable to produce a long-lasting depolarization and a notable number of spikes (Figure 2.4C), indicating that the weight-hub property is important to explain the light-evoked response of L5. We also simulated light-evoked response of another variant of L5 model (Figure 2.4D). We showed that L5 in presence of sparsely connected weight-hub neurons cannot generate long-lasting depolarization.

Correlations. A characteristic of weight-hub assemblies in the model (Figure 2.2) is that the activity of hub neurons is strongly correlated. We quantified correlations by computing the correlation coefficients of pairs of neurons, both of the subthreshold membrane potentials and the spike trains, binned into a 10ms time window (Figure 2.5A). In the heterogeneous network of Figure 2.2 the subthreshold membrane potentials of neurons inside each subpopulation are strongly correlated (Figure 2.5B and 2.5D; mean correlation coefficient 0.80, 0.79, 0.75 for assemblies 1, 2 and 3, respectively and 0.94 for inhibitory neurons) and significantly smaller (Student's t test for difference in mean: all p-values are smaller than 10^{-10}) for non-hubs (mean correlation coefficient 0.65). In contrast, correlations between neurons of different weight-hub assemblies are small, because their oscillations are not synchronized (Figure 2.5D). The correlation analysis of the spikes generated in the heterogenous network of Figure 2.2 also shows correlated behavior inside subpopulations except for non-hubs (Figure 2.5C and 2.5D). The mean correlation coefficients for the spike trains of the non-hubs is 0.06, smaller (Student's t test for difference in mean: all p-values are smaller than 10^{-10}) than that of other subpopulations (mean correlation coefficient 0.79, 0.65, 0.42 for assemblies and 0.52 for inhibitory neurons). If we randomly select two neurons in the network, we find a broad distribution of pairwise spike correlations (Figure 2.5C, dashed line) with a peak close to zero, consistent with experimental data (Reich et al., 2001) and previous model of metastable dynamics (Mazzucato et al., 2016). Heterogeneous (Figure 2.5D) and homogeneous (Figure 2.5E) variants of the model show very similar correlation structure, but in the network with sparsely connected weight-hub neurons (Figure 2.5F), the correlations disappear, because assemblies are mainly driven by external noise and do not show any joint transitions to the up-state (Figure 2.3B).

Active cortical state. Our network model can switch from the oscillatory state (which resembles slow-wave sleep or anesthesia) to an active state and vice versa without any change of network properties. In particular, the assemblies of weight-hub neurons, which are responsible for producing the up-down state oscillations, are always embedded in the network. In the active state, cortical neurons receive sensory input predominantly from layer 4 and layer 6 neurons which relay the sensory signals between thalamus and other cortical layers (Binzegger et al., 2004; Poulet et al., 2012). Here we simulate the active state by injecting an external stimulus (homogenous Poisson process to generate excitatory spike trains) to all neurons of the model. Figure 2.6A shows that the network stops oscillating immediately after receiving the stimulus, and switches back to the up-down state oscillations when the stimulation stops.

The effect of the external input can be explained as follows. When there is no strong external input, the network is driven by the dynamics of the weight-hub assemblies. Since they show

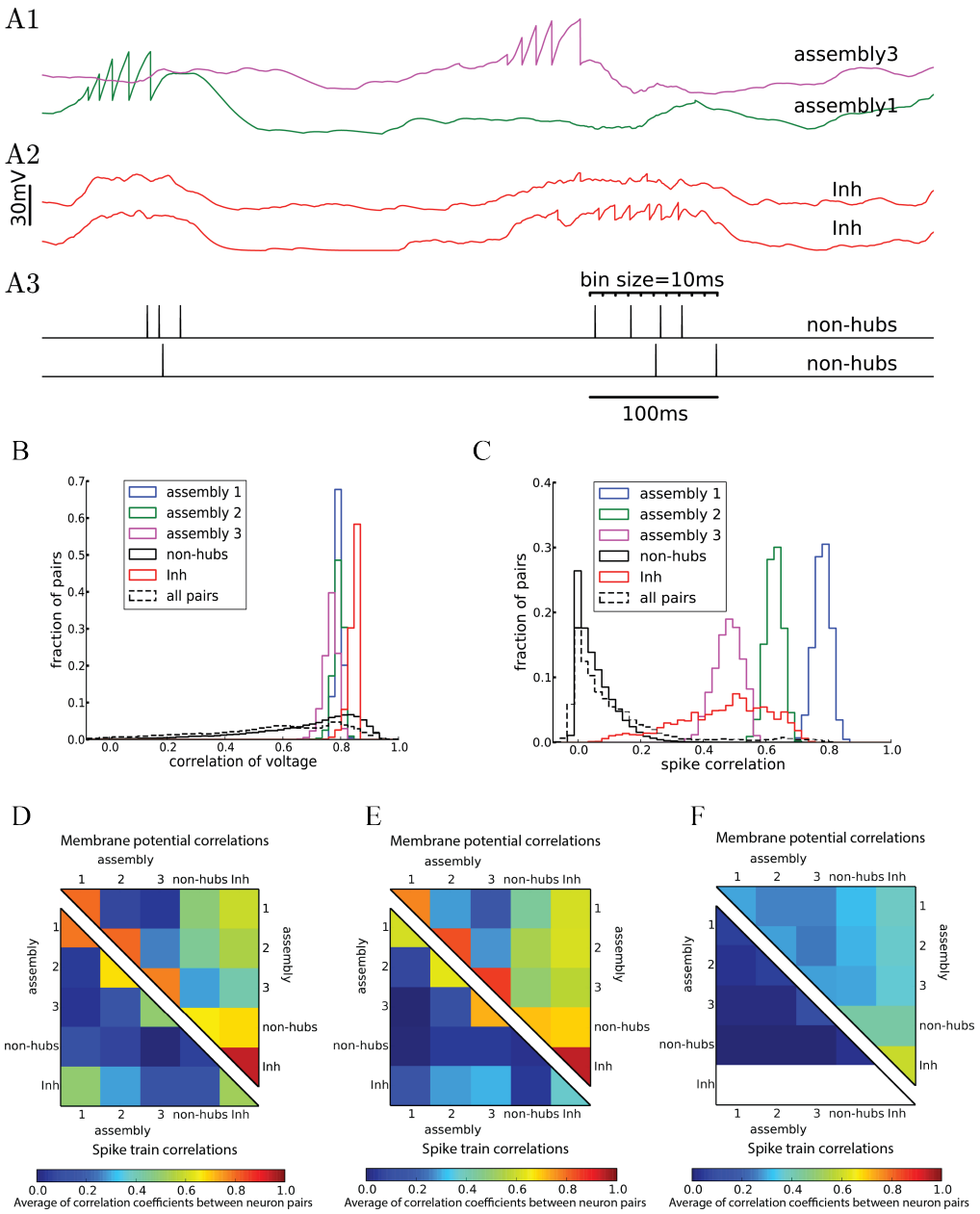

Figure 2.5: Cross-correlations of neuronal activity. **A**) Two pairs of subthreshold membrane potentials (spikes have been removed) with low (**A1**) and high (**A2**) correlation and a pair of spike trains (**A3**). Spikes are counted as coincident if they fall within the same bin of 10ms. **B**, **C**) Distribution of Pearson correlation coefficients of subthreshold membrane potentials (**B**) and spike trains (**C**) of pairs of neurons inside each subpopulation (solid lines) and over all 145530 pairs of neurons (dashed lines). **D**, **E**, **F**) Averaged Pearson correlation coefficients between the membrane potentials (upper triangle) and the spike trains (lower triangle). Correlations are computed for pairs of neurons in the respective subpopulations of (**A-D**) the heterogeneous network of Figure 2.2, (**E**) the homogeneous network of Figure 2.3A and (**F**) the sparsely connected weight-hubs network of Figure 2.3B. Because inhibitory neurons do not fire any spikes in the sparsely connected weight-hubs network (**F**), the spike train correlations of them are not defined (white area).

self-sustained oscillations, the whole network is affected by the oscillations and follows them. In case the external input is present, however, the network is driven mainly by the input (even if the input is stationary, as in the case driving our stimulus with a homogenous Poisson process) and not the assembly dynamics. Therefore all neurons, including the weight-hub neuron assemblies, are governed by the input and stop oscillating. During the input-driven active state, the firing rate distribution is narrow (Figure 2.6B) and the correlation between neurons is very low (Figure 2.6C). The average correlation coefficients for the active state (0.15, 0.14, 0.12 for assemblies 1, 2 and 3, respectively and 0.25 for inhibitory neurons) are smaller than in the oscillatory state (Figure 2.5C) (Student's t test for difference in mean: all p-values are smaller than 10^{-10}). The very low average correlations between (over all neuron pairs, 0.04 ± 0.05, Figure 2.6C, dashed line) and inside excitatory neurons (Figure 2.6C, black line) are consistent with recent experimental observations (Ecker et al., 2010). Therefore, the network preserves important aspects of biologically plausibility (such as skewed firing rate distribution and low value of pairwise correlations) also in the active cortical state.

2.3.2 The role of the weight-hub neurons assembly in the slow oscillations

In order to understand why the assembly of densely connected weight-hub neurons generates oscillations, we use methods from network analysis (Amit and Brunel, 1997; Laing and Chow, 2002; Giugliano et al., 2004; Moreno-Bote et al., 2007; Giugliano et al., 2008; Shpiro et al., 2009; Gerstner et al., 2014; Mazzucato et al., 2015). We relate the mean firing rate of neurons of the assembly to the mean synaptic current received by them. The first relation is given by the neuronal gain function (Eq. 2.13, curve in Figure 2.7A), i.e., the firing rate that each neuron produces when it is driven by a certain input current. The second relation is given by the feedback of the network (Eq. 2.16, lines in Figure 2.7A), i.e., how much synaptic current is produced by the activity of the neurons. In the absence of adaptation, intersection points between the two curves form candidates of fixed points of network activity. We define the "network feedback" (C_{fb}, Eq. 2.17) as the strength of synaptic feedback within the assembly. This quantity is the inverse of the slope of the feedback line (lines in Figure 2.7A). A high (low) value of C_{fb} leads to a strong (weak) response of the assembly to synaptic currents.

In the framework of up- and down-state oscillations, an assembly (or any subpopulation of neurons) with low value of C_{fb} is not able to oscillate and remains in a low firing rate fixed point. This can be explained as follows: A low value of C_{fb} implies that the feedback line has a large slope (solid line in Figure 2.7A). Therefore, the two curves have only one intersection point whose rate is close to zero. We refer to this fixed point as "low-point". In the case of a high value of C_{fb}, the slope of the feedback line is low (dashed lines in Figure 2.7A) and there are two additional fixed points of the system. The middle fixed point is unstable and is called the "switch point", and the upper one is typically stable (neglecting adaptation and oscillatory instabilities (Brunel, 2000; Gerstner, 2000)) and is called the "high point". Let us refer to their positions with symbols (I_{s},r_{s}) and (I_{h},r_{h}) with indices s and h for "switch" and "high", respectively. I_{s} acts as a threshold for the behavior of the assembly. In case of driving neurons with a current lower

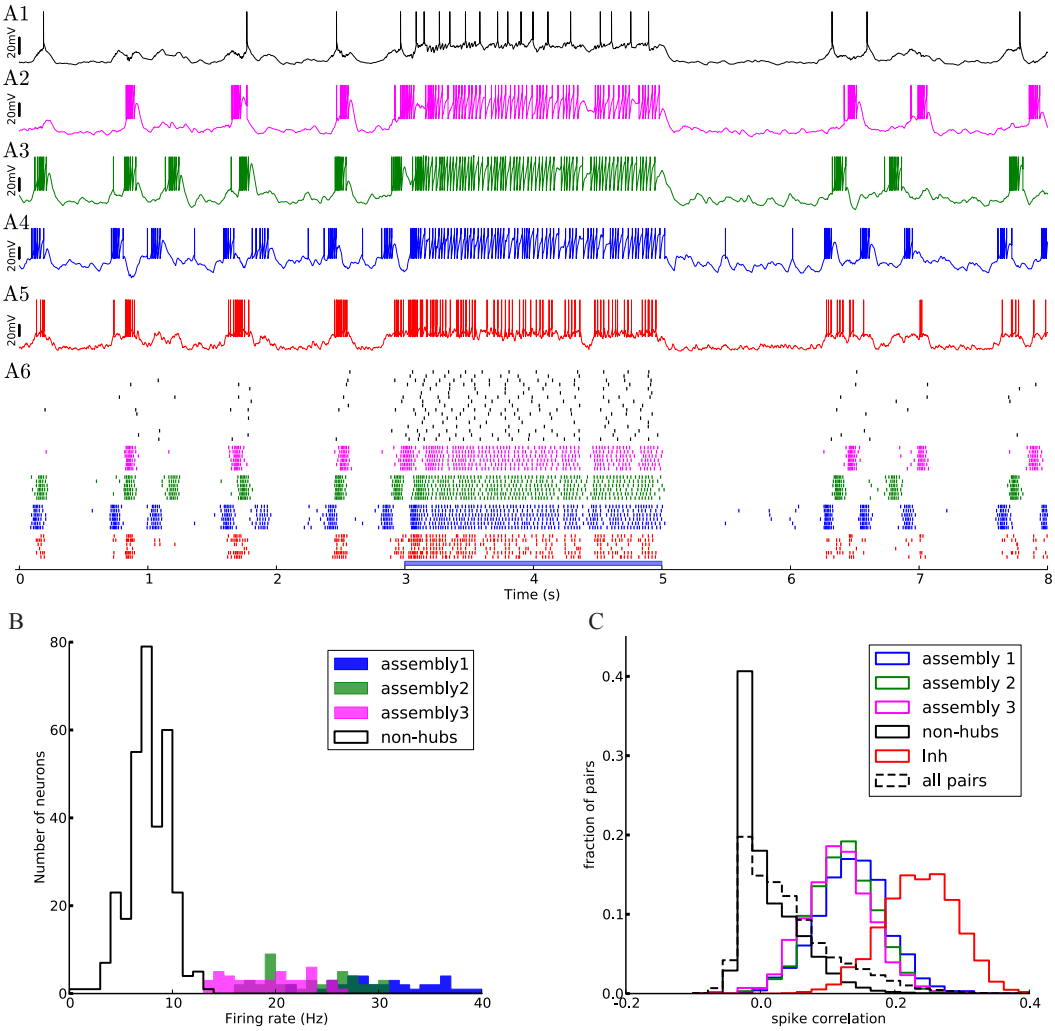

Figure 2.6: Transition from up-down-state oscillations to "active" state. **A1-A6)** Network of Figure 2.2 receiving external Poisson process stimulus from $t = 3s$ to $t = 5$s (blue bar). Neurons show up-down state oscillation before and after the stimulus, while they exhibit higher firing rate (20.9Hz for inhibitory neurons and 12.4Hz for excitatory neurons, split into 37.4Hz, 33.6Hz, 33.0Hz, 6.4Hz for assemblies 1, 2, 3 and non-hubs neurons respectively) during the stimulation period. **B)** Distribution of firing rates across neurons in the network during stimulation interval (blue bar in A). **C)** Distribution of Pearson pairwise correlation coefficients (bin size = 10ms) of spike trains of pairs of neurons inside each subpopulation (solid lines) and over all pairs of neurons (dashed lines) during stimulation interval.

than I_s, the assembly converges to the low-point and remains quiescent. In contrast, currents higher than I_s bring the assembly to the high-point and force it to exhibit a high firing rate. In our framework external Poisson noise occasionally provides a transient synaptic current larger than the current of the switch point. The mechanism described above is the reason that the assembly switches from the low-point to high-point. Switching back from the high-point to the low-point is due to spike-frequency adaptation and will be discussed further below.

As discussed, a sufficiently large value of C_{fb} gives rise to two stable fixed points of the network activity, the low-point and the high-point. Since the assembly of connected weight-hub neurons exhibits high average synaptic weights (w_{h}) and high connection probability (p_{h}), the value of $C_{\mathrm{fb}} \propto w_h p_h$ for this subpopulation is high (see Materials and Methods, Eq. 2.17). But is such an assembly of weight-hub neurons necessary for producing the oscillations? Or can any highly connected group of neurons (not necessarily weight-hub neurons) generate the oscillation? Or even a group of neurons with very strong synaptic weights but sparse connectivity (similar to Mazzucato et al., 2015)? The relevant parameters for the configuration of fixed points is the value of C_{fb}, which can in principle be increased by an increase of either w_{h} or p_{h}, or both. However, we found some of these possibilities to be not consistent with the existing experimental data. In particular, fixing p_{h} and increasing w_{h} by a large factor yields a set of very strong synapses out of the range of reported experimental PSP values (Lefort et al., 2009). On the other hand, by fixing w_{h} we require a very high p_{h} (close to full connectivity, $p_{\mathrm{h}} = 1$) which does not look biologically plausible for cortical networks (for more details of relation between connection probability and other population parameters see Klinshov et al. (2014)). For example, in the case of the smallest assembly (containing 20 neurons), choosing sparse connectivity $p_{\mathrm{h}} = 0.2$ yields to very high synaptic weight value $w_{\mathrm{h}} = 3.55$mV, similarly choosing synaptic weight $w_{\mathrm{h}} = 0.71$mV (average synaptic weight in L5 excitatory population is 0.66mV) leads to full connectivity ($p_{\mathrm{h}} = 1$). Our solution was to increase both w_{h} and p_{h} by a moderate factor, so that both remain realistic and still lead to a sufficiently high value of C_{fb}.

We would like to highlight another characteristic of C_{fb}. Increasing its value increases the firing rate r_{h} in the high fixed point, and lowers the minimal value of the switching current I_s (Figure 2.7A, inset). Consequently, a high value of C_{fb} implies that only a small amount of transient external current is required to bring the population above the switch point. In our model, different assemblies have different numbers of neurons, therefore different values of C_{fb}, and different switching points. The different feedback coefficients of weight-hubs assemblies and non-hub neurons also explain the skewed distribution of firing rates (Figure 2.2B) in the model. Larger assemblies of weight-hub neurons switch more often to the high-point and produce higher firing rates than smaller assemblies. Hence, weight-hub neurons from different assemblies form the tail of firing rate distribution. Non-hub neurons do not switch to the high-point and are not able to produce high firing rate. Therefore, they form the peak of the firing rate distribution at low rates.

Let us now focus on the return of the assembly from the high-point to the low-point. At the high-point neurons exhibit a high firing rate but spike-frequency adaptation continuously decreases the probability of spike emission. Therefore, the neurons' gain function changes gradually (dashed curves in Figure 2.7B). The system eventually makes the transition to a new

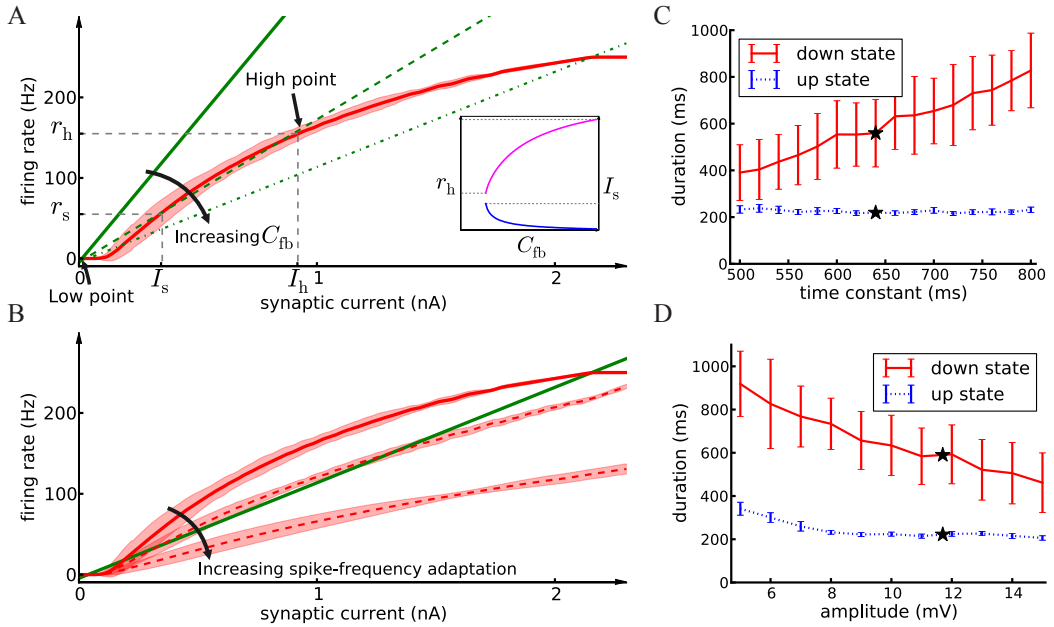

Figure 2.7: Mean-field analysis. **A**) The network feedback (C_{fb}, Eq. 2.17) affects the quasi-stationary dynamics of the system. The red curve is the noisy gain function g of the GIF neuron model (mean spike count in a group of 50 independent neurons over 10ms, divided by 50×10ms, shaded area marks ±3 SEM) measured during the initial 10ms after switching on a synaptic current of mean $\langle I_{\mathrm{syn}} \rangle$ (see Materials and Methods, Eq 2.14). The green lines (solid, dashed and dash-dotted) show the relation of firing rate and synaptic current caused by network feedback (see Materials and Methods, Eq. 2.16) for increasing C_{fb}. The slope of the green lines has an inverse relation with the effective coefficient C_{fb} of the population. Intersections of the red curve with one of the green lines indicate potential stationary states (fixed points) of a network of non-adapting neurons. Populations with a high C_{fb} (dashed and dash-dotted green lines) have three fixed points, stable low point, high point and unstable switch point. If the population described by a network feedback given by the dashed lines is driven by a mean current higher than I_{s}, it rapidly converges to the high point. On the other hand, a population with a low C_{fb} (solid green line) has only one intersection at the low point. Inset: Increasing C_{fb} causes an increase in the high firing rate r_{h} (magenta curve, left vertical scale) and a decrease of the switch current I_{s} (blue curve, right vertical scale). **B)** The noisy gain function of adaptive neurons is different during the first 10ms after stimulus onset (solid red curve) than later (dashed red curves) **C**) The duration of up- and down-states as a function of the time constant of the excitatory neuron firing threshold kernel $\gamma(s)$. Only the time constant of $\gamma_2(s)$ (the exponential with the longer time constant) was manipulated, while $\gamma_1(s)$ remained as reported in Table 2.1. The black stars indicate the experimentally extracted value of the time constant, which was used in the other figures. **D**) Same as C, except that here we manipulated the amplitude of $\gamma_1(s)$ (the exponential with the larger amplitude). The error bars show the standard deviation of up/down state durations over 10 simulation trials of 10s duration each.

configuration where the low-point is the only fixed point. When the system is at the low-point, both adaptation current and dynamic threshold decay, and eventually the dynamics of the subpopulation go back to the initial configuration in which both high- and low-point exist. In other words, the neurons recover from adaptation while they are in the low-point. Stochastic spike arrivals from other areas, described as Poisson neurons with constant firing rate here, provide the excitation necessary to make the assembly switch to the high-point. The resulting process of repetitive switching between the low-point and the high-point forms the oscillation in the system. The high point, corresponding to high firing rates of the weight-hub neurons in our model, can be interpreted as the up-state of a cortical network, and similarly the low-point corresponding to low firing rates of the down-state. Previous studies (Giugliano et al., 2004, 2008) addressed these dynamics for a simpler adaptive integrate-and-fire neuron model with similar analytical approaches.

Because spike-frequency adaptation in our model is responsible for progressively changing the gain function during the up-state, and eventually for its termination, we investigate the effects of the adaptation parameters on the duration of the up- and down states. Each time a neuron emits a spike, several adaptation processes are added to its firing threshold and spike-triggered current (denoted as "kernels" $\gamma(t)$ and $\eta(t)$ in Table 2.1). Each kernel has an exponential form of $be^{-t/\tau}$, where b and τ are amplitude and time constant of the kernel, respectively, and t is the time elapsed since the emission of the spike. By modifying the time constant τ of the firing-threshold kernel $\gamma_2(t)$ (which has a longer time constant than $\gamma_1(t)$) for the excitatory neurons, we are able to change the down-state duration strongly without affecting the up-state duration (Figure 2.7C). A longer time constant implies that neurons need more time to recover from adaptation, which leads to a longer duration of the down-state. On the other hand, manipulation of the kernel amplitude affects both up- and down-state durations, as shown by changing the amplitude of the exponential term of the kernel $\gamma_1(t)$ (Figure 2.7D). Longer values of the amplitude cause shorter up- and down-states. Note that because the switch from the down-state to the up-state in our model is caused by stochastic Poisson inputs, the down-state durations have a greater variability compared to the up-state durations (see error bars in Figure 2.7C, D). In general one could manipulate amplitudes and time constants of all exponential kernels in $\gamma(t)$ and $\eta(t)$ as well as other neuronal parameters. However, since all neural parameters of our model (including the adaptation parameters) are extracted from experiments (Mensi et al., 2012), we did not investigate manipulating them any further.

In order to examine whether the above network feedback mechanism is indeed causing the up-down state transitions, we simplified the model of L5 such that it contains a single assembly of densely connected weight-hubs (see Materials and Methods) embedded in a network of non-hubs with weak random connections. Figure 2.3C shows the dynamics of the network. Note that in this model the assembly acts as the driving force of the system and generates an oscillation by switching between its two stable fixed points. The non-hub neurons are enslaved by this oscillation and show only the passive behavior of followers. However, while embedding only one assembly in the excitatory population makes the system oscillate, the duration of up-states is short and has a narrow distribution (regular duration). In contrast, a combination of several assemblies, as in Figures 2.2, 2.3A, results in several oscillations with different frequencies,

each of which is generated by one assembly. Non-hub and inhibitory neurons receive these excitatory input signals and superimpose them. The result of the superposition are rather irregular up-states with a longer duration (Figure 2.2, 2.3A). The role of inhibitory neurons in the model is to regulate the firing rate of the assemblies in the up-state. This regulation is necessary because an excessively high firing rate in each assembly would cause rapid spike-frequency adaptation, and would therefore substantially reduce the duration of the up-states in that assembly. Consequently, the superimposed oscillations would also show short up-state durations.

We can also explain the light-evoked response of L5 and L2/3 (Figure 2.4) by the dynamics of the assemblies of weight-hub neurons. In order to understand the differences between the layers, let us suppose that most of the neurons that express the light-sensitive ion channel generate one or several spikes in response to the stimulus. Assuming a uniform spatial distribution of weight-hubs in the excitatory population, we estimate that $\sim$ 15% of both weight-hub and non-hub neurons are stimulated. Since synaptic weights among non-hubs are weak, non-hub neurons do not strongly excite neighboring non-hub neurons. However, since they send strong synapses to weight-hubs (according to our definition of weight-hubs), they contribute to the initial activation of weight-hub neurons. Recall that a densely connected assembly needs only little initial activation (to reach the switch point) to generate a high firing rate via self-excitation. Therefore, a densely connected assembly switches to the high point more easily so that each weight-hub neuron fires several spikes.

In contrast, since the connections from weight-hub neurons to non-hub neurons are weak, the stimulation does not generate a high overall firing rate in the network (non-hub neurons depolarize but do not show a high firing rate). After the weight-hub neurons have fired several spikes, spike-frequency adaptation changes the neuronal gain function. This switches the mean-field dynamics of the weight-hub assembly from a three-fixed-point to a one-fixed-point regime and brings the assembly to the low-point (Figure 2.7B), as discussed above. Consequently, both firing in weight-hubs and depolarization in non-hubs cease. In contrast, in the case of sparse connectivity between weight-hub neurons, due to a low value of the C_{fb}, this subpopulation is unlikely to transition to the high-point. Either such a fixed point does not exists because the system has only one fixed point (the low-point), or the value of the switch current (I_{s}) is very high and stimulated neurons cannot provide sufficient input current to reach it. Therefore, the absence of a densely connected weight-hub assembly leads to weak spreading of the induced activation in the population (Figure 2.4B). For the case of Figure 2.4C, since synaptic weight from non-hub neurons onto assembly neurons are weakened, assembly neurons do not receive enough synaptic current to cross the switch current. Consequently, they cannot produce notable number of spikes.

2.4 Discussion

In this paper, we suggest cortical microcircuits with a particular non-random network feature called assembly of densely connected weight-hub neurons, to explain two different experimen-

tal observations: Firstly, spontaneous slow oscillations (irregular up- and down- state) and, secondly, stimulus-evoked responses of cortical layers.

We argue that in our framework the existence of weight-hub neurons in a cortical network alone is not enough to cause significant changes in network dynamics. Since we want the values of network parameters (synaptic weights and connection probabilities) to remain in the experimentally observed range, we may not increase the synaptic weight of connections on weight-hub neurons by a huge factor. Therefore the value of network feedback cannot become high enough to produce oscillations by only modifying the weights. But if the connection probability between weight-hubs is also high (at least twice the connection probability between two arbitrary non-hub neurons), the emerging assembly of densely connected weight-hubs shapes the dynamics and the activity of the cortical layer. We have shown both qualitatively and quantitatively that a small but sufficient amount of initial activation brings the assembly of model neurons to a transient high-rate state that resembles cortical up-states.

A single assembly of weight-hub neurons together with a small amount of external noise (which here is provided by constant rate Poisson inputs) forms a slow oscillator. The reason is that this assembly switches between a high-rate state and a low-rate state repetitively. Fluctuations caused by external noise bring the assembly to the high-rate state, and spike-frequency adaptation brings it back to the near-zero, low-rate state. Several experimental studies (Sanchez-Vives and McCormick, 2000; Sakata and Harris, 2009; Chauvette et al., 2010; Beltramo et al., 2013) indicate that the cortical oscillations originate in infra-granular layers (mainly L5), and that supra-granular layers (L2/3) are subsidiary, i.e. the up-state is initiated in L5 and rises from the depth to L2/3. We suggest that the connectivity of weight-hub neurons in L5 is dense, while it is sparse in L2/3. Thus L2/3 follows oscillations generated in L5, but is not able to sustain oscillations on its own.

In slice cultures slow oscillations are rather regular (Sanchez-Vives and McCormick, 2000), whereas experiments done in the anesthetized animals (Stern et al., 1997; Lampl et al., 1999) show irregular up-down state transitions. In order to reproduce this irregularity, we embedded several densely connected weight-hub assemblies in the excitatory population. Non-hubs, the majority of excitatory cells, and inhibitory neurons receive synaptic input from these oscillations and superimpose them. Consequently a large fraction of model neurons show an irregular oscillation with a broad distribution of up-state durations.

The presence of one or several assemblies of weight-hub neurons may also explain layer-dependent differences of stimulus-evoked responses (Beltramo et al., 2013). While L2/3 exhibits weak depolarization in response to stimulation of a small fraction of it, in L5 the same stimulus induces a strong and long-lasting depolarization and a substantial number of spikes. Since the assembly of weight-hub neurons needs just a small amount of activation to switch to a high firing rate, and may propagate it within the network, we suggest that the connectivity of weight-hub neurons underlies the long-lasting response of L5. Conversely, we would hypothesize that weight-hub neurons in L2/3 are not strongly connected to each other.

While our multi-assembly architecture produces long tailed distribution of firing rates, there is at least one other way to produce such a skewed distribution. In a balanced network in the

asynchronous state Roxin et al. (2011) showed that a gaussian input distribution can lead to a lognormal firing rate distribution via an exponential nonlinearity of the current-frequency relation. In our network model, however, neurons are not in the balanced stationary regime but participate in synchronous transitions between up and down states. Similarly, in the study of Mazzucato et al. (2015) the long tailed distribution of firing rates results from metastable activity not from the balanced stationary state.

Definition of hub neuron. The term hub can have two meanings: Firstly, degree-hub, i.e. a neuron that receives more synaptic connections than an average neuron, and secondly, weight-hub, i.e. a neuron that receives stronger synapses than average. The second definition was used in the current work. The common definition of a hub (degree-hub) as a neuron that receives more synapses (Bullmore and Sporns, 2009; Feldt et al., 2011; Prettejohn et al., 2011) does not take into account the strength of synapses, called synaptic weights here. This topological definition of hubs is common in computer sciences, where the issue of degree and connections between nodes is more important than the weight structure. However, in neuronal microcircuit modeling, synaptic weights are as important as degree and connectivity. Surprisingly, the amount of previous modeling work done on degree manipulation and connectivity structure (Roxin, 2011; Hu et al., 2013; Pernice et al., 2013; Vasquez et al., 2013; Hu et al., 2014; Jahnke et al., 2014; Potjans and Diesmann, 2014; Rudolph-Lilith and Muller, 2014) by far exceeds work on non-homogeneous weight structure (Koulakov et al., 2009; Iyer et al., 2013; Tomm et al., 2014).

Here we adopted the less-common definition of a hub in terms of synaptic weights, to shed light on this less-well understood aspect of non-random neuronal network features. While manipulation of the degree distribution in the network and creating degree-hubs has the same effect as creating weight-hubs in producing a skewed firing rate distribution (Roxin, 2011), the two are not always interchangeable. Tomm et al. (2014) showed that for reproducing light-evoked responses in mouse barrel cortex slices, manipulation of both degree and weight distributions are needed under the simulated network conditions of this study. In our case, it would be possible to keep the connectivity random (without rewiring) and manipulate the weights more strongly to produce the oscillations. However, this would entail very strong synaptic weights outside of the experimentally observed range (Lefort et al., 2009), and thus would reduce the biological plausibility of the model. Our combined approach of introducing weight-hubs with dense connectivity overcomes this problem with minimal changes to both weight and degree distribution.

Several electrophysiological experiments indicate that the distribution of synaptic weights (EPSP amplitudes) has a lognormal shape (Lefort et al., 2009; Avermann et al., 2012; Ko et al., 2011), see also Chapeton et al. (2012). Therefore we used a lognormal distribution for modeling synaptic weights in neuronal populations. Using random (Erdős–Rényi) networks to define whether a synaptic connection is present or not, together with a lognormal distribution for the synaptic weight of the connection, entails that the sum of inward synaptic weights is similar for all neurons (Figure 2.1B). However, by modifying the topology of the excitatory network to have local inward correlation in synaptic weights (see Materials and Methods), we could produce a more broadly distributed sum of inward synaptic weights (Figure 2.1B). Therefore, a few exci-

tatory neurons receive larger total synaptic weights, while others receive smaller values. For the sake of concreteness, we have defined a classification boundary such that the 20% of neurons that receive the strongest inputs are called weight-hubs (see Figure 2.1B). The model is robust against varying this fraction, and shows similar dynamics for 15% and 25% of neurons (data not shown).

Throughout this article, only excitatory to excitatory connections were manipulated and all other connections (inhibitory to inhibitory, inhibitory to excitatory and excitatory to inhibitory) remained unchanged. However, evidence of hubs in inhibitory populations has been found in experiments (Bonifazi et al., 2009). Therefore, the effects of hubs in inhibitory networks remain to be investigated. Since in our model excitatory hubs suffice to explain the aforementioned aspects of cortical dynamics, we neglected inhibitory hubs here in favor of model simplicity. Another reason for not exploring the structure of inhibitory connections is the lack of experimental datasets for inhibitory connectivity in L5. In this work, we use the inhibitory connection properties of L2/3 as a substitute for L5 (see Materials and Methods). Therefore, any investigation on inhibitory connectivity of L5 would be based on this unconfirmed hypothesis.

Identifying weight-hub neurons from data. A network structure with densely connected weight-hubs is hypothetical. In this section we propose a method using machine learning tools which can help experimentalists to label neurons as weight-hub or non-hub using a set of recorded membrane potential. In order to perform such a classification, we need to consider distinct properties of weight-hub neurons. First, weight-hub neurons in our model receive a larger amount of excitation than non-hubs and therefore exhibit a higher firing rate. Therefore we might label neurons with relatively higher firing rate as weight-hubs. However, this property alone does not yield a robust way of identification, because besides the synaptic input, the firing rate of a neuron also depends on its electrophysiological parameters, such as its firing threshold. A non-hub neuron may therefore occasionally exhibit a higher firing rate than a weight-hub (Figure 2.2B). A second property of weight-hub neurons predicted in the context of our model is the regularity of transitions between up- and down-states. According to our model, regular up-state durations indicate that the neuron is a weight-hub.

Here we use a combined approach for identifying subpopulations of weight-hub and non-hub neurons. In the first step, we characterize each neuron by a vector of two elements: the overall firing rate and the CV of up-state durations of the neuron. We pass these vectors to a K-means clustering algorithm (see Section Materials and Methods), which clusters neurons into weight-hubs and non-hubs with 100% accuracy (Figure 2.8A). We identify the group with the lower coefficient of variation of up-state duration as the weight-hubs and other group as the non-hubs. In order to distinguish the assembly that each identified weight-hub neuron belongs to, we perform a second step and run the algorithm again on the weight-hub neurons found in the previous step. Here we define the feature vector of each neuron by the mean and the CV of up-state durations. The algorithm assigns the correct assembly to 89 out of 95 weight-hub neurons. Accordingly the accuracy of the second step is 93.7% (Figure 2.8B).

Although our approach works for identifying of weight-hub neurons in our simulations, finding these neurons in the cortex using intracellular recording will be more challenging. This is mainly

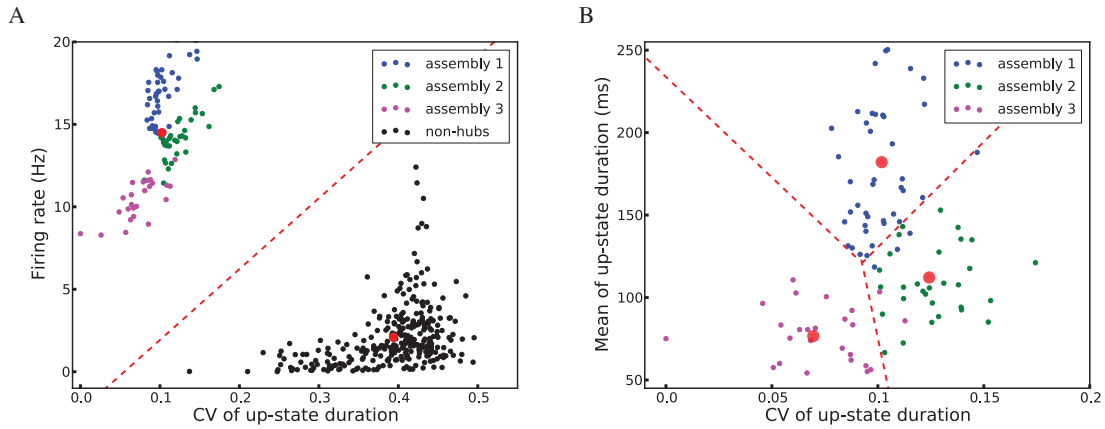

Figure 2.8: K-means clustering identifies weight-hub neuron assemblies. Each dot represents one neuron and its color denotes the corresponding subpopulation in the simulation shown in Figure 2.2. **A)** Clustering of all neurons into two clusters. The first stage of the classification algorithm successfully identifies weight-hubs and non-hubs, but does not distinguish between different assemblies of weight-hubs. The red circles show the center of the clusters and the dashed line displays the classification boundary. **B)** Clustering of weight-hub neurons (identified in A) into different assemblies. The K-means algorithm with three clusters identifies the assembly of each weight-hub neuron with 93.7% accuracy.

due to the fact that weight-hub neurons are likely to form only a small portion of all excitatory neurons. In our simulations of L5 of a single column in the barrel cortex $\sim 20\%$ of all excitatory neurons are weight-hubs. However, we can scale our model system up keeping the number of weight-hub neurons fixed, without a change to the overall dynamics. For example a similar model of L5 which contains both Layer 5A and Layer 5B (containing ~ 1000 excitatory neurons) needs the same number of weight-hubs to display up-down state oscillations. Therefore, in this example, the fraction of weight-hubs reduces to 10%. Analogously, in case of modeling an entire barrel column (containing ~ 5700 excitatory neurons), this number falls to about 1.7%. Therefore, we expect that weight-hub neurons are rarely recorded with present-day single-cell electrophysiological techniques.

Different models for reproducing up/down oscillations. Several models have been suggested to reproduce up-down state oscillations. The studies of Ghorbani et al. (2012) and Holcman and Tsodyks (2006) used mean-field analysis to show that short-term depression can give rise to the up/down state oscillation. Other works focused on numerical simulations on the neuronal level: Applying short-term facilitation on excitatory to inhibitory connections also produces oscillations (Melamed et al., 2008), as well as adding a non-linear term to the leaky integrate-and-fire model such that each neuron is bistable (Parga and Abbott, 2007). Giugliano et al. (2004) used a homogenous network of adaptive neurons to produce oscillations using a similar mechanism as in our model. However, in their model all the neurons switch between the high- and low-rate points. Hence they all have a high firing rate, and the distribution of firing rates is less skewed. On the other hand, if we used the average connection probability and synaptic weights obtained by the experiments (Lefort et al., 2009) for building a homogeneous

network with plausible size, the value of the network feedback would not be high enough to make the network oscillate. Therefore, we consider the proposed network with embedded weight-hub neuron assemblies to be the most plausible model with respect to these data.

Switching between up- and down-states. In slowly oscillating cortical microcircuits, the reason for the switch from the down-state to the up-state is a matter of debate (Chauvette et al., 2010). One possible reason could be the coincidence of spontaneous activity of several neurons (Timofeev et al., 2000; Bazhenov et al., 2002). Such a coincidence may provide enough input to several other neurons to make them fire. This phenomenon then repeats and propagates the activity to a notable number of neurons, and so the system may switch to the up-state. Another possibility is that a few neurons are active more than others on average, and show firing even in the down-state. One hypothesis about such neurons is that they receive a persistent sodium current which causes bursts of firing (Hill and Tononi, 2005; Bon-Jego and Yuste, 2007). Another hypothesis is that electrophysiological properties of these neurons make them fire more than others, e.g. they can have lower firing threshold (Compte et al., 2003). Therefore, these neurons play the role of pacemakers, or drivers of oscillations. Here we show that in order to make such an oscillator it is unnecessary to change the neuron model or introduce any persistent currents. In our model, we build the oscillation merely by increasing the connection probability between weight-hubs (to about 50%), while keeping the overall connection probability fixed at the value measured in experiments (Lefort et al., 2009).

The return of the cortex from the up-state to the down-state could have several reasons. In one approach, the accumulation or increase of inhibition shuts down the up-state: When the system goes to the up-state, the excitatory population receives excitation from itself and inhibition from an inhibitory population. The system remains in the up-state as long as the excitation dominates the inhibition. However, at some point the inhibition becomes dominant and brings the system back to the down-state (Melamed et al., 2008; Parga and Abbott, 2007). Instead of inhibition, synaptic short-term depression may weaken the excitatory to excitatory synapses during the up-state and cause a reduction of self-excitation received by the excitatory population, by which it can oscillate on its own (Holcman and Tsodyks, 2006). In Compte et al. (2003) and Giugliano et al. (2004) spike-frequency adaptation is responsible for bringing the system back to the down-state. In the up-state, Na^+ -activated K^+ channels reduce the firing rate of excitatory neurons gradually and the excitatory population looses the amount of self-excitation that is necessary for remaining in the up-state. Consequently it falls back to the down-state. Our model also uses adaptation for switching to the down-state. We have previously built a similar model which uses short-term depression instead of adaptation (Setareh et al., 2014). As shown here in a network of neurons that exhibit spike-frequency adaptation with parameters fitted from experiments, synaptic depression is not necessary, but we do not exclude that synaptic depression plays a role in cortical up-/down-states as well.

Competition based network models. An important point which distinguishes our work from several previous models (Shpiro et al., 2009; Krishnamurthy et al., 2012) is that there is no competition between the assemblies of weight-hub neurons in our model. In classic competition based models there are two or more populations of excitatory neurons, each trying to become active and suppress the other ones using either direct inhibition or indirectly by exciting an

inhibitory population of neurons. The dominant population keeps inhibiting others until it looses its activation by a negative feedback mechanism like short-term depression or spike-frequency adaptation, or until one of the suppressed populations becomes the dominant one by receiving a high amount of noise sufficient to overcome the inhibition. In contrast, in our model assemblies do not compete to win the activation. In contrast to inhibition-dominated networks, in our network, the active assembly helps other assemblies (and non-hubs) to become active by sending excitation more than indirect inhibition. As a consequence of our network parameters, several assemblies can be active simultaneously. Depending on the adaptation state of the assemblies at the time of receiving excitation, the number and order of transitions to the up-state are different. Such different patterns of activations cause different up-state duration in the non-hub and inhibitory neurons.

Models for producing multistable activity. While our model is not based on competition of assemblies, and several assemblies can be active at the same time, it is also different from clustered network models suggested for producing multistable activity states (Deco et al., 2011; Litwin-Kumar and Doiron, 2012; Mazzucato et al., 2015, 2016). In such models several clusters of neurons are embedded into the population of excitatory neurons. The connection probabilities inside clusters are increased (in Litwin-Kumar and Doiron (2012) both connection probabilities and synaptic weights are increased) compared to those between clusters. Therefore, each cluster acts as an attractor similar to the assemblies of weight-hub neurons in our model. Clusters receive noisy input and one or several of them become active at a time. The shared inhibitory population sends inhibition to all clusters and limits the number of active clusters. Once one of the quiescent clusters, which also receives noisy input, becomes active, due to shared inhibition, it deactivates one or several clusters which were previously active. This procedure repeats and consequently, each cluster switches between active and inactive states. In this architecture, coincidence of noisy inputs causes a cluster to switch to the active state and shared inhibition switches it back to the inactive state. Therefore, there is no need for a negative feedback mechanism like spike-frequency adaptation. Although the activity of this model looks similar to ours, the functionality is different. In these models, at least one cluster is active at each time during ongoing activity. In fact, a cluster deactivates because another one becomes active– the clusters pass on the activity amongst themselves. Therefore, after a first activation there is at least one active cluster which produces spikes and depolarizes other neurons including non-cluster excitatory neurons (the situation that all clusters become inactive at the same time rarely occurs). In contrast, in the down-state all neurons are silent and have a low membrane potential. Moreover, in the clustered network transitions into and out of the active state are anti-correlated: If one cluster activates, another one typically deactivates, i.e. the number of active clusters is constant most of the times, although we may rarely observe several active assemblies at the same time. In our model, transitions times to up- and down-states are correlated across the network. Moreover, each assembly is able to transition back to the inactive state (the low-point) on its own without need for inhibition or activation of other assemblies. The self-termination ability results from spike-frequency adaptation (see Materials and Methods). Therefore there are time intervals in which all assemblies are inactive and the whole network is silent. In summary, although the clustered architecture successfully reproduces the multistable states during ongoing

and evoked activity, it is not suitable to produce up-state/down-state oscillations.

To conclude we would like to highlight the predictive aspects of our study. First, central components of our model are the weight-hub neurons, i.e., those with strong synaptic inputs. Although, there is no direct experimental evidence for the existence of weight-hub neurons, we introduce this concept here as a prediction. Yet, our demonstrations that model networks using weight-hubs display biologically plausible dynamics, and explain cortical phenomena, may be considered as an indication of weight-hub existence. Second, on top of that, we predict that weight-hub neurons in L5 form an assembly of strongly connected cells, while the weight-hubs are sparsely connected in L2/3. Third, the up-down state transitions of neurons within a weight-hub assembly are more regular than that in the majority of other neurons. All of these predictions can be tested in future experiments.

Acknowledgments

We thank Christian Pozzorini, Skander Mensi and Tilo Schwalger for helpful discussions. This project was funded by the European Research Council (Grant Agreement no. 268 689; Hesam Setareh) and by the Swiss National Science Foundation (grant agreement no. 200020_147200; Moritz Deger).

Chapter 3

Excitable neuronal assemblies with adaptation as a building block of brain circuits for velocity-controlled signal propagation[1]

Abstract

The time scale of neuronal network dynamics is determined by synaptic interactions and neuronal signal integration, both of which occur on the time scale of milliseconds. Yet many behaviors like the generation of movements or vocalizations of sounds occur on the much slower time scale of seconds. Here we ask the question of how neuronal networks of the brain can support reliable behavior on this time scale. We argue that excitable neuronal assemblies with spike-frequency adaptation may serve as a building block that can flexibly adjust the speed of execution of neural circuit function. We show in simulations that a chain of neuronal assemblies can propagate signals reliably, similar to the well-known synfire chain, but with the crucial difference that the propagation speed is tunable to the behaviorally relevant range. Moreover we study a grid of excitable neuronal assemblies as a simplified model of the somatosensory barrel cortex of the mouse and demonstrate that various patterns of experimentally observed spatial activity propagation can be explained.

Author summary

Models of activity propagation in cortical networks have often been based on feedforward structures which have remained elusive in experiments. Here we propose a new model of activity

[1] Text copied from Setareh H, Deger M, and Gerstner W, manuscript is under review in PLOS Comput. Biol.

propagation, called excitation chain, which does not need such a feedforward structure. The model is composed of excitable neural assemblies with spike-frequency adaptation, connected bidirectionally in a row or a grid. This prototypical neural circuit can propagate activity forwards, backwards or in both directions. Furthermore, the propagation speed is tunable and may be as slow as necessary to model the generation of slow behaviors. The grid model is able to generate different activity propagation patterns, similar to spontaneous activity and stimulus-evoked responses in anesthetized mouse barrel cortex. We propose the excitation chain model as a basic component that can be employed in various ways to create spiking neural circuit models that generate signals on behavioral time scales. In contrast to abstract excitable networks, the model explicitly links to neuronal spikes.

3.1 Introduction

Reliable propagation of activity is necessary for processing and transmitting sensory signals in the brain. During the last two decades, two prominent types of computational models have been studied to address this issue. First, the synfire chain consists of groups of spiking neurons connected in a feedforward architecture (Abeles, 1982, 1991; Diesmann et al., 1999; Gewaltig, 2000) potentially embedded in recurrent networks (Kumar et al., 2008, 2010). Second, rate propagation models (van Rossum et al., 2002; Vogels and Abbott, 2005; Kumar et al., 2010) use a similar feedforward architecture, but instead of spikes they propagate fluctuations of the firing rate. Kistler and Gerstner (2002) investigated a synfire chain in feedforward structure and found that the refractory behavior of neurons after firing a spike is the crucial element of stable activity propagation. The derivative of the membrane potential shapes spike density and sharpens the activity pulse (Kistler and Gerstner, 2002; Goedeke and Diesmann, 2008). Statistical methods (Schrader et al., 2008; Torre et al., 2016) are proposed for detecting the firing pattern of synfire chains in spike train recordings. Reliable neuronal firing patterns compatible with synfire chains have been observed in area HVC of the song-bird (Hahnloser et al., 2002). The statistical significance of synfire chains in cortical neurons is questionable (Oram et al., 1999). Synfire chain models have been used for reproducing behavioral functions such as bird song generation (Hanuschkin et al., 2011a) and monkey scribbling (Hanuschkin et al., 2011b). Systems of interacting synfire chains were also used for building a large-scale model of cortex (Trengove et al., 2013, 2016).

While both synfire chain and rate propagation succeeded to model fast behaviors (behaviors on the order of milliseconds), they are expensive in terms of neuron numbers and therefore not suitable for reproducing behavioral phenomena that need a slower, and sometimes tunable, speed of activity propagation. Essentially synfire chains implement a clock, set by the propagation of neuronal spikes and transmission delays, running on the millisecond time scale (Gerstner et al., 1993; Izhikevich, 2006). In order to address this issue, we propose a new model, which we call *excitation chain*, for the activity propagation in a bidirectional chain of neuronal assemblies. Our model can be considered as a spiking version of excitable media (Wilson and Cowan, 1972, 1973; Jirsa and Haken, 1997; Coombes, 2006), with an explicit link to the neuronal time scale

of spikes.

In contrast to the previous synfire chain and rate propagation models, our model does not require an explicit feedforward architecture. Specific feedforward structures have not been observed in experiments in the neocortex so far. Here we propose an excitation chain model that is consistent with the following experimental connectivity data: First, inter- and intra-assemblies connection probability and synaptic weights are in the experimentally observed ranges (Lefort et al., 2009; Avermann et al., 2012); and second, clustered connectivity of neurons, necessary for neural assemblies (Perin et al., 2011). Hence, although the concept of the excitation chain as such is a rather generic and abstract model, its basic connectivity features are consistent with experimentally observed properties.

In the next section, we describe our model and its dynamics in detail. We also illustrate how activity propagation can be made faster or slower by changing synaptic weights. Then we analyze the behavior of the model and explain the role of its elements in forming the dynamics. Finally, we extend the excitation chain to a two-dimensional model, which we may call an excitation grid. We argue that this grid of assemblies can be considered as the skeleton of barrel cortex, which can generate different spatio-temporal modes of activity propagation observed experimentally in barrel cortex (Petersen et al., 2003a,b).

3.2 Results

3.2.1 The speed of activity propagation in a chain of excitable bistable assemblies

In order to propagate a signal of activation through several excitable assemblies, we first connect several groups of neurons in a chain (Figure 3.1A). Each group contains an excitatory assembly and a population of inhibitory neurons. Assemblies are defined as small populations of neurons with high connection probability. More precisely, inside each excitatory assembly synapses are strong and the connectivity is high (connection probability $p = 50\%$) whereas each inhibitory population has smaller synaptic weights and lower connectivity. Within each group, the excitatory assembly and inhibitory population are mutually connected. Moreover, the excitatory assembly is connected to the inhibitory population and excitatory assembly of neighboring groups. In contrast, the inhibitory populations do not have inter-group connections (see Materials and Methods for the details and parameters).

Basic mechanism and functionality If we stimulate the excitatory assembly of the first group of the chain with a transient stimulus of 25ms duration (see Materials and Methods), all of this groups' neurons fire several spikes. The activation of this first assembly is then propagated step by step through the chain of assemblies until the last group. Figure 3.1B shows the raster plot of all excitatory neurons as well as the population-averaged activity of excitatory and inhibitory populations of the chain. One can see that despite the reciprocal connections

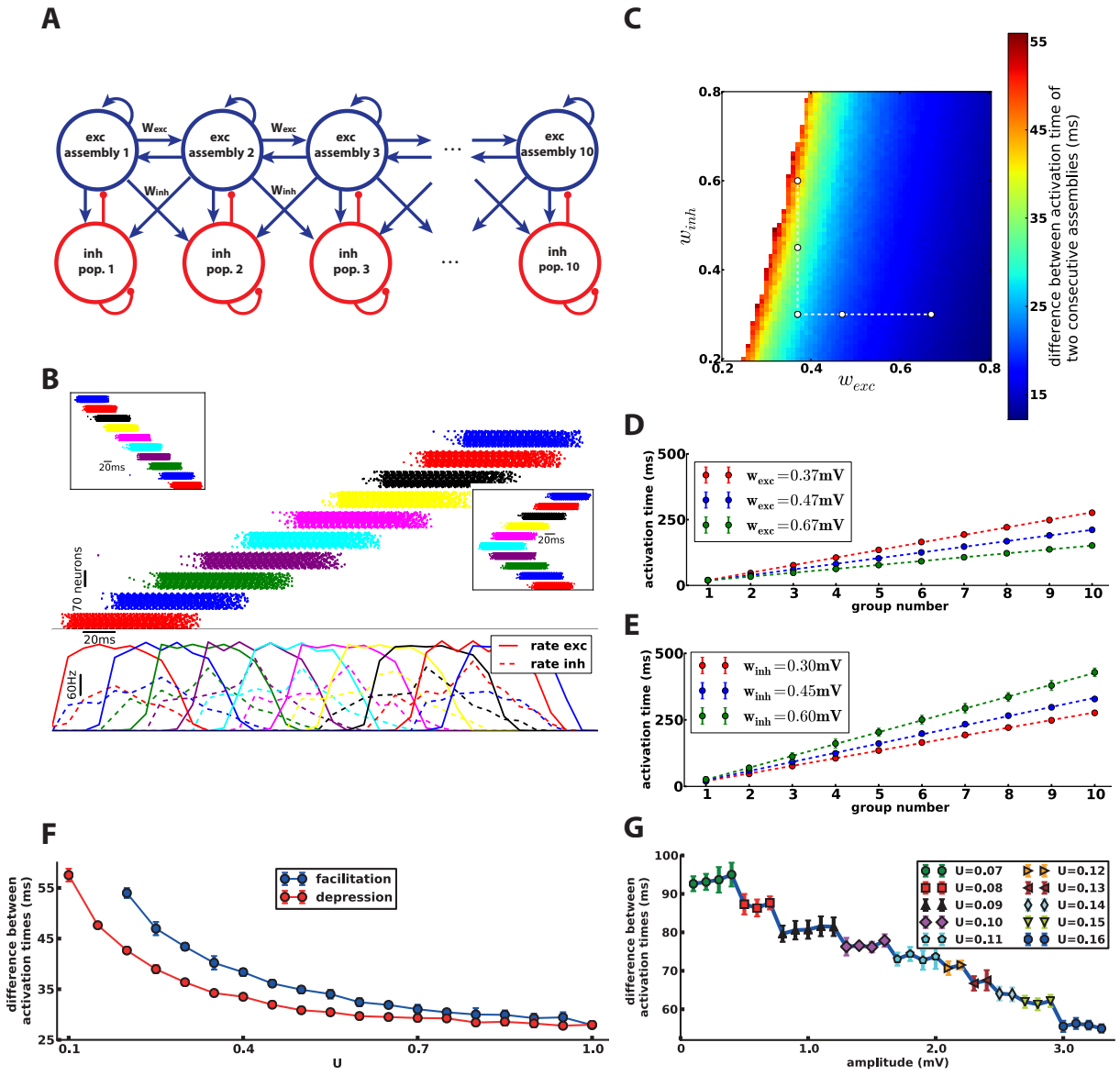

Figure 3.1: Excitation wave in a one-dimensional chain. **A**) Schematic of the excitation chain. Each excitatory assembly is connected to the excitatory assemblies and inhibitory populations of its neighboring groups in the chain, while the inhibitory population is only connected to the excitatory assembly of its own group. **B**) spike raster of excitatory assemblies (top) and average rate of each assembly (bottom, estimated in bins of 10ms). Based on the place of the stimulation, the chain can propagate the spiking activity forwards, backwards (top-left inset) or in both directions (bottom-right inset). **C**) The difference of the activation times of two consecutive assemblies can be adjusted by changing synaptic weights. The delay is increased by increasing the weights from excitatory assemblies to their neighboring inhibitory assemblies (w_{inh}) or by decreasing the weights between excitatory assemblies (w_{exc}). The white area denotes the parameter region in which the chain cannot propagate

Figure 3.1: ***(Continued)*** the activation (The intersection of the two dashed lines in **C** denotes the parameters used in **B**). **D**)The total delay of the chain (and inversely the propagation speed) depends on w_{exc} (compare white dots on horizontal dashed line in **C**). **E**) The total delay also depends on w_{inh} (compare white dots on vertical dashed line in **C**). **F)** Regulation of propagation speed using short-term plasticity parameter. Increasing the parameter U decreases the difference of activation times of two consecutive assemblies for both depression and facilitation. In the case of facilitating synapses, the activity cannot propagate for low values of U. The other parameters of the model (including w_{exc} and w_{inh}) are the same as in **B**. **G)** Decreasing the amplitude of $\gamma_1(t)$ together with a readjustment of the parameter U of short-term plasticity influences the difference of activation times (horizontal axis). For each value of amplitude, we found the value of parameter U (shown in the legend) which yields the larger delay. Every point in **C**, **D**, **E**, **F** and **G** is the mean over 10 different trials. Errorbars indicate standard deviations. The right-most circle repeats the left-most blue point in **F**.

between excitatory assemblies, the activity is propagated in a feedforward manner. We repeated the simulation several times with different transient stimuli (data not shown). Whenever the transient input stimulus is able to activate the first excitatory assembly, the activity is then propagated through the chain to the last group reliably. For a vast range of parameters (Figure 3.1C), we have observed neither a termination of the activity wave nor an instability in the whole network (such as convergence to synchronous firing of all excitatory neurons).

If we stimulate the excitatory assembly of the last group, we see that the activity propagates backwards (Figure 3.1.inset). The excitation wave can also spread in both direction simultaneously. Stimulating an excitatory assembly in the middle of the chain produces two traveling waves, one towards the beginning of the chain and another one towards its end (Figure 3.1.inset). The property of activity propagation in different directions has been observed in multi-electrode extracellular recordings of the neocortex. For example, based on the place of local application of glutamate, neural firing is initiated in a forward, backward or bidirectional manner (Sanchez-Vives and McCormick, 2000).

Speed depends on synaptic weights The speed of activity propagation in our excitation chain is much lower than in previously suggested chain structures like the synfire chain (Diesmann et al., 1999). In synfire chains the time needed for the activation to jump to next group is on the order of the synaptic transmission delay ($1 - 5$ms), while in our model this time is roughly 13-55ms, although we have used a short synaptic transmission delay of 1ms. This slow propagation allows us to model phenomena on the time scale of several hundreds of milliseconds or even seconds.

The speed of propagation in the excitation chain is controlled by the inter-assembly synaptic weights. Let us first define how to measure the delay (and consequently the speed) of activity propagation. We define the activation time of each excitatory assembly by the average time of the first spike of each neuron in the assembly. The difference of the activation time of two neighboring assemblies can be considered as the time needed for transmitting the activity signal from one group to the next group. The inverse of the activation time difference of the first and the last assembly can be used as a measure for propagation speed.

Let us denote the synaptic weights between neighboring excitatory assemblies with w_{exc} and

the synaptic weight from excitatory assemblies to the neighboring inhibitory populations with w_{inh}. Figures 3.1C, D and E show that increasing w_{exc} increases the speed, while increasing w_{inh} reduces it. The activity wave remains stable and propagates reliably over a broad range of parameter values.

Removing the inhibitory populations Excitatory assemblies are the essential elements of the excitation chain, while the role of inhibitory populations in the chain lies mostly in reducing the propagation speed. Therefore, we may simplify our model by removing all inhibitory populations. A chain of excitatory assemblies only (Figure 3.2A) is able to propagate the activity in different directions (Figure 3.2B) similar to chain containing also inhibitory neurons. The propagation speed is regulated by modifying w_{exc} (Figure 3.2C). However, because of the lack of inhibition, the speed cannot be lower than a critical value below which transmission becomes unreliable. In our simulations, we found a maximum delay of 34ms instead of 56ms with inhibition.

3.2.2 Analysis of excitation chain dynamics

Excitation chains rely on bistable assembly dynamics In order to understand the dynamics of the chain and to identify the components that determine the propagation speed, we first focus on one assembly of excitatory neurons. The dynamics of each assembly can be described by self-consistent equations relating the firing rate of the assembly to the average synaptic input of the neurons (see Materials and Methods). In case the assembly has a high network feedback coefficient C_{fb} (Eq. 3.9), the dynamics of the system has three fixed points (Figure 3.3A): the *low point* which is a stable fixed point with zero firing rate, the *switch point* which is the unstable middle fixed point and a high-rate fixed point which is called the *high point*. If the assembly is driven by synaptic input greater than the switch point's current (I_{s}), it approaches the high point and produces a high firing rate. Since the intra-assembly synaptic weights (w_{exc}) and connection probability (p) are high, the network feedback coefficient ($C_{\text{fb}} \propto pw_{\text{exc}}$) is also high. Therefore, the dynamics of the assembly can be explained by this three-fixed-point configuration, which we call the *excitable mode* of the assembly. However, because of spike-frequency adaptation of our excitatory neuron model, the frequency of spike emission progressively decreases during the high-rate state. Consequently, the neurons' gain function changes gradually (Figure 3.3B) and the system goes to a new configuration which has only one fixed point, the low point. (Note that, for the same reason, the assembly does not fully converge to the high point as it is shown in Figure 3.3A. While the assembly is approaching the high point, changes of the gain function move the position of the fixed point.) Therefore the assembly eventually becomes quiet and stops firing. We refer to this configuration as the *dormant mode* of the assembly. In this mode, receiving synaptic input does not activate the assembly. It takes a while for the assembly to recover from the dormant mode and return to the three-fixed-point configuration, which is the excitable mode.

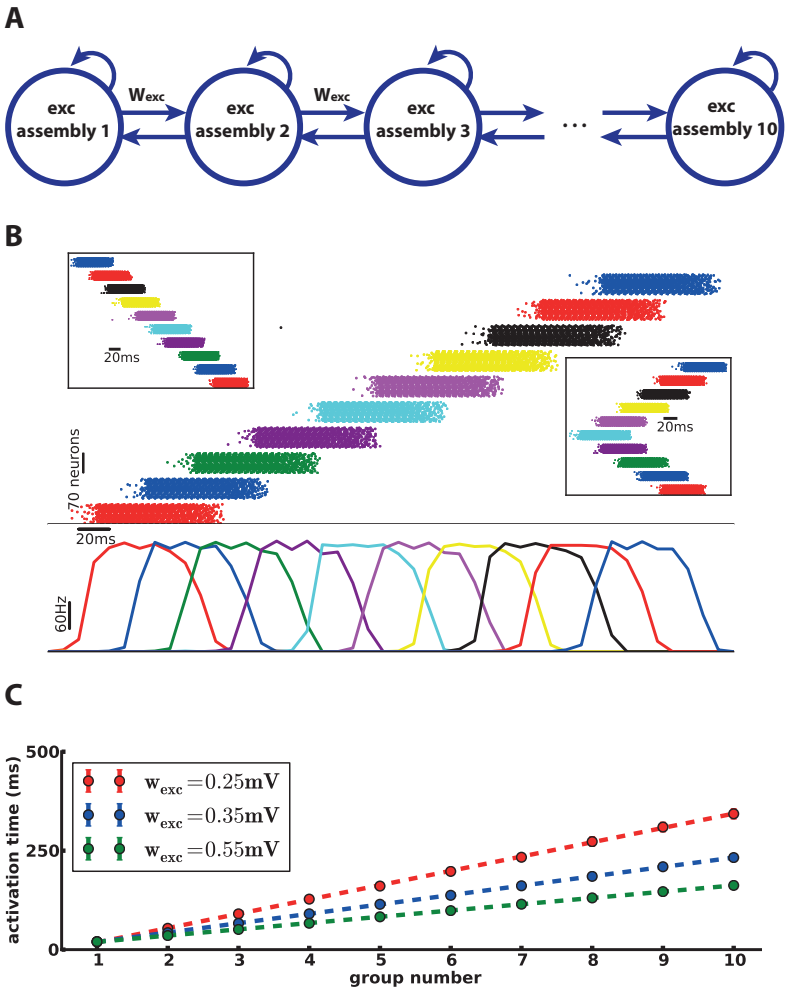

Figure 3.2: Inhibitory populations are not necessary. The chain containing only excitatory assemblies (**A**) propagates the spiking activities in both directions (**B**) similar to the case with inhibitory assemblies (Figure **3.1**B). The propagation speed can be tuned (**C**) by modifying the synaptic weights between excitatory assemblies (w_{exc}), albeit in a smaller range, than in Figure 3.1.

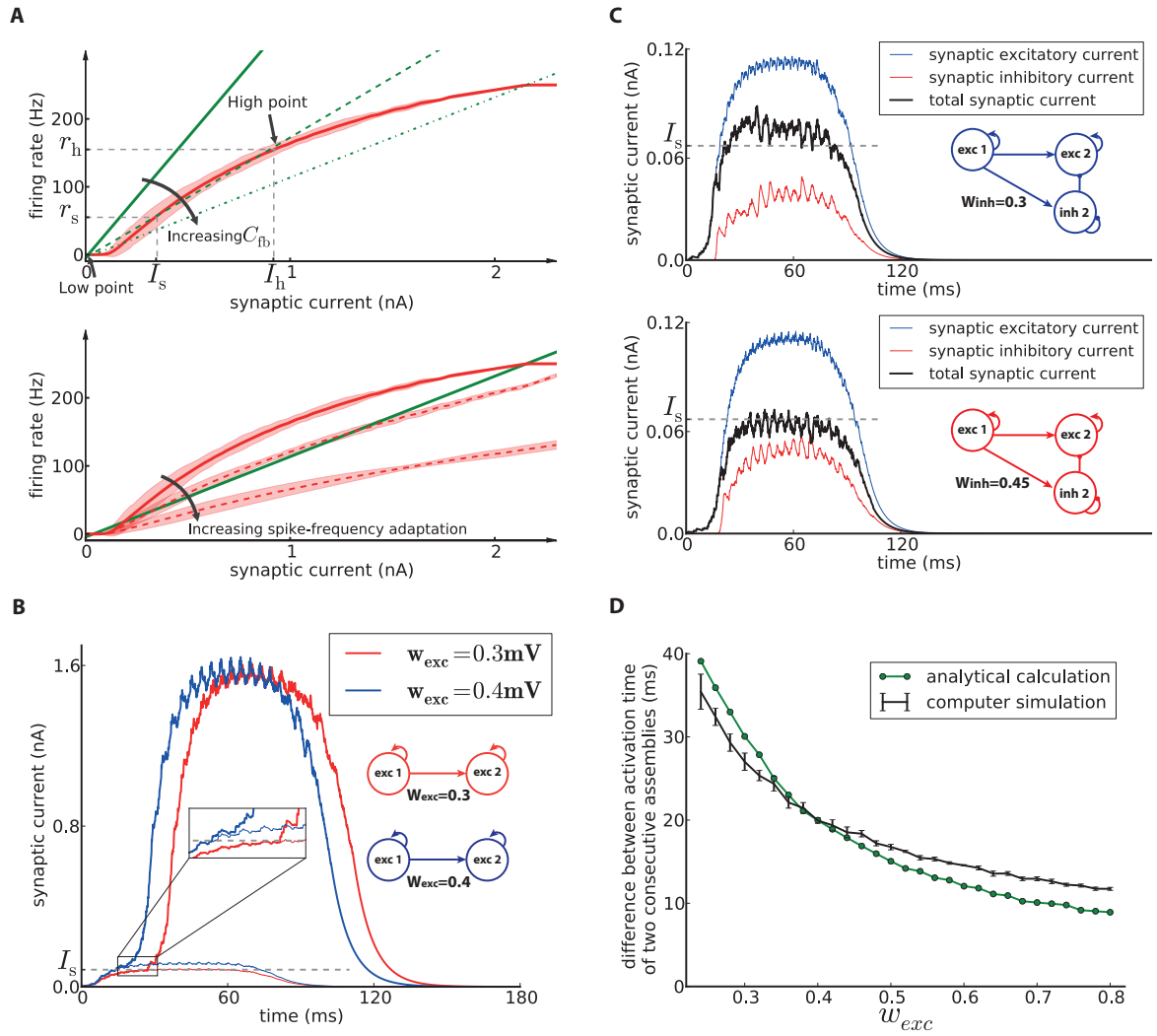

Figure 3.3: **A**-Top) The network feedback (C_{fb}, Eq. 3.9) affects the dynamics of the system. The red curve is the noisy gain function of the GIF neuron model (mean spike count in a group of 50 independent neurons over 10ms, divided by 50×10ms, shaded area marks ± 3 SEM) measured during the initial 10ms after switching on a synaptic current of mean $\langle I_{\mathrm{syn}} \rangle$. The green lines (solid, dashed and dash-dotted) show the relation of firing rate and synaptic current caused by network feedback (see Materials and Methods, Eq. 3.8) for increasing C_{fb}. The slope of the green lines has an inverse relation with the effective coefficient C_{fb} of the population. Intersections of the red curve with one of the green lines indicate potential stationary states (fixed points) of a network of non-adapting neurons. **A**-Bottom) The noisy gain function of adapting neurons during the first 10ms after stimulus onset (solid red curve) is different from that later (dashed red curves). **B)** Synaptic current received by the second assembly (averaged over the assembly's neurons) in two chains with different inter-assembly synaptic weights. The thin lines show the averaged synaptic current each neuron receives from the previous assembly, while the thick lines show the total synaptic current received from both the assembly itself and the previous assembly. When the thick line separates from the thin line, the assembly starts to fire spikes on its own. This is the moment when the assembly crosses the switch point and approaches the high activity fix point. This occurs

Figure 3.3: ***(Continued)*** earlier if inter-assembly synaptic weights are increased (blue). Consequently the propagation speed along the excitation chain increases. **C**) Total synaptic current received by the second assembly (averaged over the assembly's neurons). The second assembly receives excitation (blue) from the first assembly and inhibition (red traces show the absolute value of inhibitory currents) from the second inhibitory population. When the total input (black) crosses the threshold, the assembly switches to the high-point and becomes activated. Increasing synaptic weights from the first assembly to the second inhibitory population increases the inhibition and decreases the total input received by the second assembly. Hence it delays the activation time. **D**) Analytical approach (green line, see Materials and Methods) approximates the difference between the activation time of two consecutive assemblies with an error of less than 4ms. The black line shows the value of the difference obtained by averaging over 10 simulations. Error bars indicate standard deviation.

Synaptic weights determine the propagation speed For the second step of the analysis, we take into account the interaction of neighboring assemblies in the chain. Consider the case of a chain of excitatory assemblies only. When assembly 1 goes to the high point and each of its neurons fire several spikes within a short time, it sends strong synaptic input to assembly 2. However, since the synaptic weight between assemblies are relatively low, early volleys of spikes of assembly 1 do not yet suffice for assembly 2 to cross the switch point. Therefore it takes some time for assembly 2 to accumulate enough input from assembly 1. This is the reason why the propagation of activity is slow in the excitation chain and the difference of activation time is much higher than the synaptic delay. If we increase the inter-assembly weight, then a smaller number of spikes of assembly 1 are needed to produce the switch current in assembly 2, which means it will be activated sooner (Figure 3.3C). This explains the increase of the propagation speed along the chain when we strengthen the inter-assembly synapses (Figure 3.2C).

Inhibitory neurons delay the activation of each group Let us now discuss the effect of adding the inhibitory populations to the chain. Each inhibitory population sends an inhibitory input to the excitatory assembly in the same group and thus reduces the effect of the synaptic input provided by the neighboring excitatory assemblies. Therefore, the inhibition delays the time at which the switch current is reached. If we increase the inter-group synaptic weight onto inhibitory neurons w_{inh}, the inhibitory neurons fire more and produce more inhibition. This, again, increases the amount of synaptic input needed from the neighboring excitatory assembly and therefore delays the activation time. Figure 3.3C illustrates the effect of w_{inh} on the synaptic inputs.

Adaptation gives rises to directed activity propagation Suppose that assembly 1 has become active and sends synaptic current to assembly 2. When excitatory assembly 2 receives enough synaptic current to cross the switch point, it becomes active at a high firing rate. It then sends synaptic current to its neighbors, excitatory assembly 1 and 3. However, by that time, excitatory assembly 1 is about to fall into the dormant mode and cannot generate many spikes. Therefore, only excitatory assembly 3 switches to the high point. This procedure repeats until the end of the chain. Therefore activity propagates in one direction only although connections between assemblies are bidirectional. An analogous situation happens for the backwards propagation. In case of stimulating an assembly in the middle of a previously quiet chain, since

both of its neighbor assemblies are in the excitable mode, they both switch to the high point. Consequently, the activity propagates in both directions from then on.

Spike-frequency adaptation also has a second, equally important role. It is responsible for progressively changing the gain function (Figure 3.3B) during the active phase of an assembly (the duration that assembly stays in the high-point), and eventually for its termination. By modification of the adaptation parameters of excitatory neurons, we are able to adjust the duration of the activate phase of each assembly (Setareh et al., 2017).

The effect of other synaptic weights on the dynamics After having analyzed the effect of inter-group synaptic weights (w_{exc} and w_{inh}) on the propagation speed of the chain, we now focus on the the weights of inhibitory to excitatory neurons inside the same group. Since intra-group inhibition contributes to the total inhibition of the assembly, it can have effects similar to w_{inh} on the propagation speed. In order to avoid redundant parameter search, we kept the intra-group inhibition constant and explored w_{inh}. Likewise, the intra-group excitatory to excitatory connections (connections inside each assembly) are also important. As we mentioned earlier, assemblies should have a high network feedback coefficient ($C_{\text{fb}} \propto pw$). Otherwise, they would not be able to switch to the high point and produce high firing rates in case of receiving relatively low synaptic input.

Both connection probability and synaptic weight of the intra-group connections affect the network feedback coefficient and therefore shape the core of the excitation chain. Other intragroup connections (excitatory to inhibitory and inhibitory to inhibitory connections) are less important. However, one should avoid choosing values that inject huge inhibition into the assembly. Too much inhibition may shut down the assembly by finishing its activation rapidly so that not enough synaptic input arrives at the next assembly. Therefore, it may lead to a loss of signal propagation.

Obtaining the propagation speed using an analytical approach The self-consistent approach relating the firing rate to the average synaptic input which we mentioned earlier is useful for a qualitative explanation of the dynamics of the excitation chain. However, it is not suitable for a quantitative calculation of the propagation speed, because we cannot calculate the exact gain function for this neuron model (see Materials and Methods) if the effects of spike-frequency adaptation become strong. Therefore, we developed another analytical approach (see Materials and Methods) in order to obtain the difference between activation times of two consecutive assemblies in the chain of only excitatory assemblies (Figure 3.2). Figure 3.3D compares the results of simulation and the analytical approach for different values of w_{exc}. Our theory estimates the activation time difference with an error of less than 4ms.

Embedding short-term plasticity in the model We can also add short-term facilitation and depression (Tsodyks and Markram, 1997; Tsodyks et al., 1998) (see Materials and Methods) to the model. In these cases, we are able to adjust the activity speed by manipulating the parameters of the facilitation and depression, while we keep w_{exc} and w_{inh} fixed. In the first

variation, we added facilitation to the excitatory synapses between assemblies. We observed that increasing the value of the usage parameter U decreases the difference between activation times of two consecutive assemblies (Figure 3.1F). In the presence of facilitation, the amplitude of post-synaptic currents (PSC) are initially lower compared to case of not having facilitation. When a presynaptic neuron fires several spikes within a short interval, the amplitude of each PSC in the post-synaptic neuron increases. After a suitable number of spikes, the PSC amplitude reaches the amplitude of the case without facilitation. Therefore, it takes time for an assembly to provide sufficient amount of synaptic input to activate the next assembly. Modification of the recovery time constant τ_{rec}, however, does not affect the propagation speed (data not shown).

In the second variation, we neglected facilitation and added depression in inter-group excitatory to inhibitory connections. We also increased the intragroup inhibitory to excitatory synaptic weight by $\sim$ 7 times (1.07mV instead of 0.16mV). The propagation delay decreased as we increased the value of U (Figure 3.1F). The reason is that a large amount of inhibition from the inhibitory subpopulation does not allow the excitatory assembly to become active. If we shutdown the inhibitory subpopulation after a while, the inhibition ceases and leads to the activation of assembly. Depressing synapses from one assembly to the neighboring inhibitory subpopulation play this role. Depressing synapses reduce the amount of PSC onto inhibitory subpopulation after a while. Therefore, the activity of an inhibitory subpopulation and its projecting inhibition drop off. Similar to the previous case, the time constant (τ_{facil}) does not affect the propagation speed (data not shown).

Note that we still need spike-frequency adaptation in the above cases because it is the adaptation that terminates the activation of the assemblies. Without adaptation, an assembly switches to active and remains active for the rest of the simulation. It is important to notice that our model is not based on a competition between assemblies (see Discussion) and every assembly switches to the low point on its own.

In addition to connectivity, the duration of the active phase of assemblies plays important role in the propagation speed. The duration should be long enough, such that each assembly can provide the synaptic input needed to activate the next assembly in the chain. If an assembly becomes inactive before having provided enough synaptic input, the next assembly cannot switch to the high point and the propagation stops at this point. Therefore, if we want to achieve a slower propagation speed, we need to increase the duration of the active phase.

The duration of the active phase can be adjusted by modification of adaptation parameters of excitatory neurons (Setareh et al., 2017). Each time a neuron fires a spike, several adaptation process on several time scales are triggered and generates both spike-triggered currents and increase in firing threshold (Pozzorini et al., 2013). To describe these adaptation effects we use several exponential decaying kernels, $\eta_k(t)$ $(k = 1, 2)$ for spike-triggered currents and $\gamma_k(t)$ $(k = 1, 2)$ for dynamic threshold. Here we decreased the amplitude of kernel $\gamma_1(t)$ (the kernel with the smaller time constant). Then we used short-term facilitation for changing the propagation speed (similar to Figure 3.1F). For each value of the kernel amplitude, we found the value of the usage parameter U which causes slowest propagation. Figure 3.1G summarizes the values of parameters and difference between activation times of assemblies. We achieved a maximum

delay of 95ms between one assembly and the next using this approach. Hence, we conclude that a linear chain of 11 assemblies are sufficient to cover a typical behavioral time scale of above 1 second.

3.2.3 A grid of assemblies as a skeleton for barrel cortex

While the previous section focused on a one-dimensional structure, in this section we consider an excitation wave in a two-dimensional grid structure inspired by the layout of barrel cortex. Barrel cortex processes sensory information from the whiskers and is a part of the rodent somatosensory system. It consists of vertical modules called barrel columns, each of which relates to one principle whisker (Petersen, 2007). Here we make a multicolumn model of barrel cortex which contains 25 columns, organized in the shape of 5 arcs while each arc contains 5 rows). The actual mouse barrel cortex includes 33 columns in an unordered shape. It contains an arc of 4 rows, 4 arcs of 5 rows and 3 arcs of 3 rows (Petersen, 2007). For simplicity, we only consider one cortical layer of the barrel cortex. In our model, every column consists of excitatory and inhibitory neurons. Excitatory neurons are divided into two groups, a minority of assembly neurons and a majority of non-assembly neurons (see Table 3.2). Figure 3.4 shows the schematic of the model. While assembly neurons have high internal synaptic weights and connection probability, the connections between assembly and non-assembly neurons as well as connections inside non-assembly neurons are sparse and weak. Inside a column, all three groups have connections to each other, but inter-column connections are different from intra-column connections. (see Table 3.2). Columns are identical in terms of number of neurons, neural parameters and connections between neurons. Inhibitory neurons in our model form only intra-column connections and are not connected to the neurons of other columns, consistent with the common assumption that inhibitory neurons send short axons and contact only local targets (Fino et al., 2013). In contrast, excitatory neurons of each column of our model connect to the excitatory neurons of the four nearest-neighbor columns. However, due to the relatively long distance between two neighboring columns, the connection probability between columns is low ($p = 10\%$), consistent with experimental observations (Boucsein et al., 2011).

Just as in the excitation chain of the previous section, the dynamics of each assembly can be explained by the three-fixed-point configuration. However, the subpopulations of non-assembly neurons have low network feedback coefficients (Eq. 3.9) so that their dynamics exhibit only the low-activity fixed point. Hence the assemblies govern the dynamics of the whole grid model. Neglecting non-assembly and inhibitory neurons for a moment, we can consider this barrel cortex model merely as a grid of assembly neurons. We may think of this grid as the skeleton of our model for barrel cortex. Just as in the chain model, the synaptic weight between assemblies determines the propagation speed. Here, we adjusted the value of the inter-column synaptic weight ($w_{\text{exc}} = 0.32\text{mV}$) such that the the speed of activity propagation in the model is similar to the experimental data (Petersen et al., 2003a,b; Ferezou et al., 2007). We did not need to use short-term facilitation or depression to achieve the desired speed. The remaining parameters of the model are reported in section Materials and Methods.

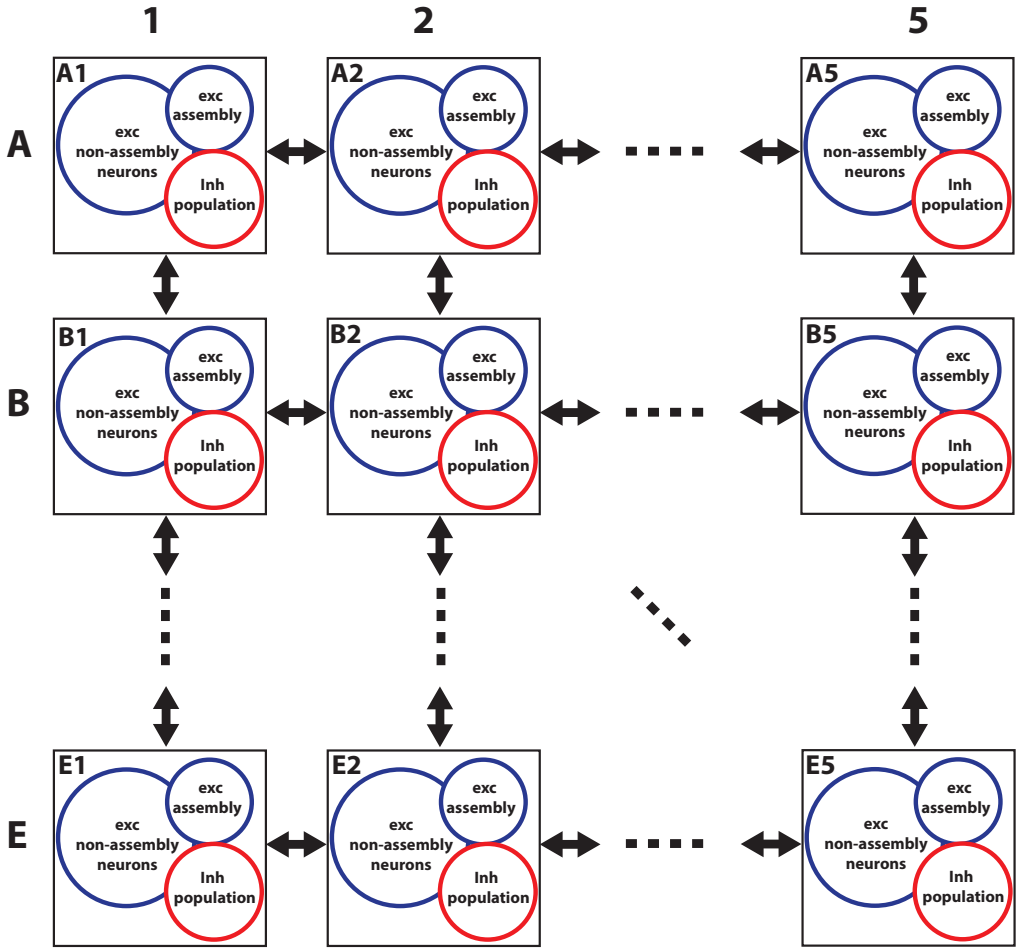

Figure 3.4: Schematic of a multi-column model of barrel cortex. Each column contains three groups: excitatory assembly and non-assembly groups, and an inhibitory group. Inside each column all groups are connected to each other, while between neighboring columns only excitatory neurons are connected. Non-neighboring columns have no connection in this model. One vertical line is called an 'arc', e.g. A2, B2, ..., E2.

Qualitative comparison with experiments The grid model is able to reproduce several aspects of the dynamics of anesthetized barrel cortex in the stimulus-evoked and spontaneous regime. In the stimulus-evoked experiments (Petersen et al., 2003a; Civillico and Contreras, 2006; Ferezou et al., 2006; Lustig et al., 2013), a sensory signal was triggered by a brief deflection of a whisker. Voltage-sensitive dye imaging showed that the neural activity starts in the barrel column corresponding to the stimulated whisker and propagates to the neighbor columns. After spreading over the whole field of view of barrel cortex, the activation vanished.

Figure 3.5A shows the simulated evolution of neuronal firing rate in the grid model after stimulating the neurons of the central column. The dynamics of the model are similar to the experimental recording. For better visibility, the voltage traces of the model were temporally filtered with a Gaussian function ($\sigma = 30$ms). We show only 64 neurons of each column: each panel in Figure 3.5A shows 25 squares (= columns) and each square contains 64 pixels (= neurons). These neurons are randomly selected from all neurons of the column (excitatory assembly and non-assembly neurons and inhibitory neurons). While the assembly neurons receive a high amount of synaptic input (due to their strong synaptic weights) and show a high firing rate, non-assembly and inhibitory neurons receive weaker weights and show lower firing rates ($0 - 20Hz$). Since assembly neurons form only a minority of all neurons in a column (see Materials and Methods), the average firing rate is close to firing rate of non-assembly and inhibitory neurons.

For the case of spontaneous activity, the experiment (Petersen et al., 2003b; Ferezou et al., 2007) shows that neural activity starts on one side of the barrel cortex and only in a few columns. Then it moves from column to column in a circular fashion. Our model is able to reproduce the circulation of activity, on the same time scale. If we stimulate a model column on the upper-left side, the activity starts circulating in the down- and the leftward direction (Figure 3.5C). The activity orbits around the central column several times and then terminates.

Experimental data also report another interesting observation. Petersen et al. (2003a) found that in some experiments, after the stimulation, the activity spreads faster along the row (horizontal spread in our model) than the arc (vertical spread in our model). The authors suggested that this could be due to the axonal length of excitatory cells, i.e. axons of excitatory neurons extend longer along a row as along an arc. In order to interpret this phenomenon we assume that the connection probability between columns connected in the row direction ($p = 15\%$) is greater than the connection probability along the arc direction ($p = 10\%$). Simulations of this modified model exhibit a higher propagation speed along rows comparing to arcs (Figure 3.5B).

Qualitative analysis of activity wave To understand the origin of the model's dynamics we consider again the regular grid of assemblies. Similar to the assemblies of the excitation chain, each grid assembly is either in the dormant or the excitable mode depending on the adaptation level of its neurons. The dormant mode corresponds to high values of neuronal adaptation variables (spike-triggered current and firing threshold). This mode appears after the neurons of the assembly have emitted a burst of spikes or if high initial values have been assigned to these variables. After recovering from the dormant mode, neurons of the assembly have weak

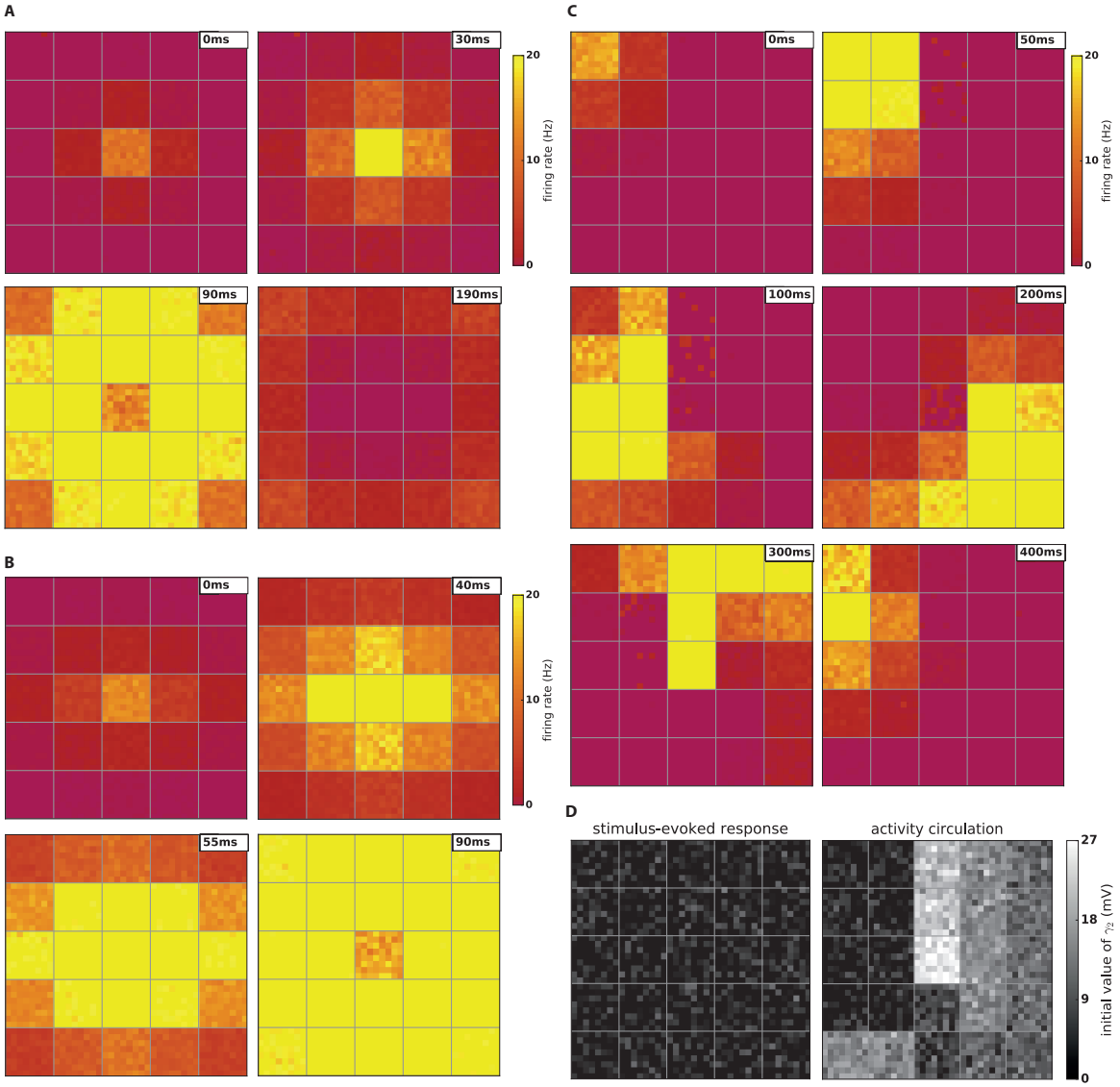

Figure 3.5: **A**) Dynamics of the multi-column model after stimulation of the central column. The activity spreads over the barrel cortex. Each square in the figure shows 64 neurons randomly chosen from all three neuronal groups of a column. **B**) Similar to (**A**) with different connection probabilities between vertical (10%) and horizontal neighbors (15%). The difference in connectivity causes different propagation speed along the row compared to the speed along the arc. Note that in (**A**) both connectivities were 10% and the propagation speeds were identical. **C**) Circulation of activity in the multi-column model. After stimulation of a corner column, the activity propagates between columns and circulates across the model for several rounds. Eventually activity vanishes. This type of dynamic has been observed in spontaneous activity in mouse barrel cortex in vivo (Petersen et al., 2003b). **D**) Initial values of the second adaptation kernel (γ_2), which describes spike-triggered movement of the firing threshold (see Eq. 3.3). For the stimulus-evoked response (shown in **A**) all initial values are drawn from a normal distribution with zero mean and standard deviation of 3mV. Any negative values are

Figure 3.5: ***(Continued)*** clamped to zero. For activity circulation (shown in **C**) we tuned the initial values to make a path for propagating the activity. For each column, we first choose a mean value for the normal distribution, while standard deviation of all distributions are the same (3mV). Again we clamped the negative values to zero. A high value of the mean adaptation variable for a column makes it dormant and does not allow it to activate until it recovers from the dormant mode. A low value, however, makes it excitable and ready to propagate the activity.

spike-triggered current and relatively low firing threshold. Hence the assembly has returned to the excitable mode and can now generate a burst of spikes in case of sufficient excitation. After activation, it switches again to the dormant mode.

In our model, we manipulate the initial value of firing threshold kernel with longer time constant ($\gamma_2(t)$) of neurons in the assembly in order to set the initial mode of each assembly. High initial values cause the dormant mode, while low initial values make it excitable. Note that the kernel with shorter time constant ($\gamma_1(t)$) is not suitable for this kind of manipulation. Since the value of the kernel converges to zero quickly, the assembly does not remain in the dormant mode for a sufficiently long time.

For simulating the stimulus-evoked response we initialize all assemblies in the excitable mode. The initial value of $\gamma_2(t)$ for neurons are selected from a random distribution with zero-mean and $\sigma = 3$mV. All negative values are clipped to zero (Figure 3.5D (left)). After stimulation of the central assembly, it converges to the high point and produces a burst of spikes. As a result, neighboring assemblies receive some synaptic input. Although the value of this input current is low due to low inter-column connectivity, it suffices for the neighboring assemblies to pass the switch point. This causes rapid increase of the firing rate during convergence to the high point. This scenario repeats, and so the activation spreads over all assemblies. The assemblies go to the dormant mode after a burst of activity , consistent with the experimental data.

The simulation of activity circulation is more complicated and needs careful tuning of the initial values of the adaptation variables of the neurons. Figuratively speaking we carve a path for the activation by choosing suitable initial values for the firing thresholds (Figure 3.5D (right)). Again we use a random distribution with $\sigma = 3$mV for neurons inside each column. The distribution's mean is different in each column. The means are selected such that there is path of excitable assemblies from top-left of grid to the column below the center. The activity propagates only in the path of excitable assemblies, and dormant assemblies do not switch to the high point in case of receiving the synaptic current. Once the activity has passed through the initially excitable assemblies, they become dormant. At the same time, the assemblies that were dormant initially recover and become excitable. Therefore, the activity continues its path along those assemblies which were dormant initially. This phenomenon repeats and causes activity circulating on the grid. After several rounds the circulation terminates because of a shortcut problem (see below). Non-assembly and inhibitory neurons do not contribute to shape the circular activation pattern. They merely receive the activation from the assembly of their own column and show depolarization and a few spikes.

One may think that pre-shaping an activation pattern by initialization is artificial. However,

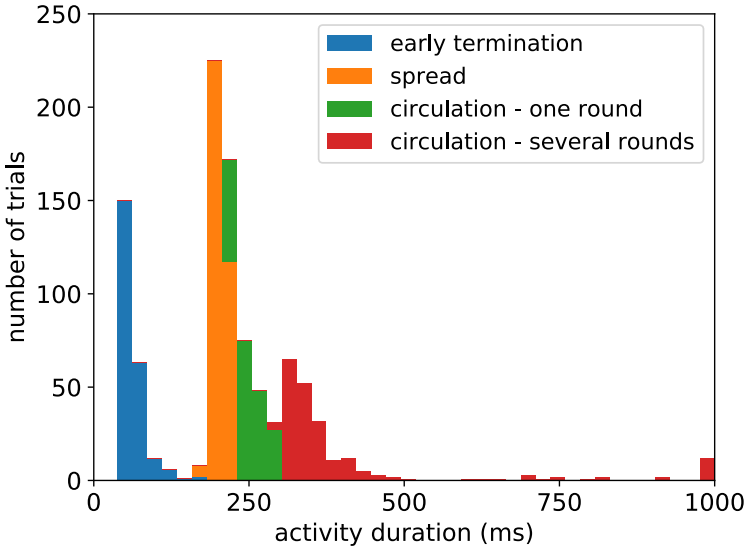

Figure 3.6: Histogram of activity survival durations for 1000 trials of grid simulations with different initial values of the second adaptation kernel (γ_2). For each trial we took the initial values shown in Figure 3.5D (right) and shuffled the columns. In $\sim$ 23% of trials the activity ceases before reaching all columns. In $\sim$ 35% of trials we observed that the activity spreads instead of circulating. In the remaining trials, we observed circulation with different patterns and durations depending on the path made by initial values. The durations longer than 1000ms are clamped to 1000ms for better visibility.

any distribution of initial values which make several neighboring assemblies excitable and leave others in the dormant mode has potentially such a "shaping" property. Different patterns of initial values lead to different patterns of activity propagation observed in the cortex. In other words, we suggest that the great trial to trial variability of activity previously observed via voltage-sensitive dye imaging in the cortex (Arieli et al., 1996; Kenet et al., 2003) might be due to different initial values of neurons in each trial. Here we tuned our pattern to make a path in order to specifically reproduce the particular dynamics observed in the experiments,. In order to investigate the role of initial values, we simulate 1000 trials. For the initial values of each trial, we randomly chose a shuffled version of initial values shown in Figure 3.5D (right). We only shuffled the mean of initial values of each column. Then, we used a random distribution with $\sigma = 3$mV and the desired mean for neurons inside each column. Figure 3.6 indicates the types of activity propagation and the durations that activity survives in the grid. In $\sim$ 23% of trials the activity does not spread over all columns. In $\sim$ 35% of trials the activity spreads over all columns without repetition. In the rest of trials, cortical columns form a path of activation and the activity circulates for one or several rounds.

Termination of activity Even with a highly tuned path, the activity terminates after several rounds. In order to understand the reason for this, we compare the activity path in early rounds and late rounds (Figure 3.7). In the early rounds, activity orbits around the central assembly and

passes through all marginal assemblies to eventually reach the starting point at the corner again. Since, in our simulations, the central assembly has been assigned a very high initial value for the neuronal firing thresholds, it does not synchronize with its neighbors and does not initially follow them. However, after a while the central assembly becomes excitable and eventually activates when its, say, right-sided neighbor becomes active. Thereby it creates a shortcut for the activity which reaches the left-sided assemblies before the recovery from the dormant mode is complete. Since these assemblies are not recovered yet, they cannot become active. Therefore, the activity terminates and does not circulate any further. If we remove the central assembly or prevent it from being excitable (e.g. by decreasing its network feedback or increasing the value of inhibition it receives from the inhibitory neurons inside its column by strengthening its intra-column inhibitory to excitatory synaptic weights), the activity can circulate for a very long time (green dots in Figure 3.8). This is also the reason why we used absorbing boundaries for the grid. In case of reflecting boundaries (i.e., the activation wave reflects when it reaches the boundary) assemblies in the dormant mode do not have enough time for recovery and cause termination of the wave. Applying periodic boundary (i.e., when the activation wave passes a boundary, it jumps to the other side of grid) is not realistic, because once activity passes the boundary of a cortical area in the cortex, it generates (weak) propagation into a neighboring area rather than returning to the same area. Hence, we consider absorbing boundary as a good compromise and a step toward a very large scale model of neocortex. Due to large number of neurons, simulating a large scale model needs high performance computations and is beyond this research.

As we described above, in our model the circulation of activity terminates spontaneously. This is consistent with spontaneous barrel cortex dynamics observed in vivo (Petersen et al., 2003b). More specifically, every time the activity vanishes in the model, there is need for stimulation of a corner assembly which is in the excitable mode. If such stimulation is provided, the activity can circulate again for several rounds. Such a stimulus could potentially be provided by other cortical areas adjacent to the barrel cortex or reverberations of activity in thalamo-cortical loops.

3.3 Discussion

We have shown that a network of spiking neurons consisting of 11 assemblies can generate reliable temporally structured activity, that extends around one second, which has been described previously for an excitable medium with discrete structures (Murray, 2001). While two well-known models of activity propagation, the synfire chain and rate propagation, require a feedforward network structure, our excitation chain works with a bidirectional activity pattern, similar to excitable media (Wilson and Cowan, 1972, 1973; Jirsa and Haken, 1997; Murray, 2001). This is advantageous because there is no direct experimental confirmation for the existence of systematic feedforward connectivity pattern in the brain (Abeles, 1982, 1991; Diesmann et al., 1999; van Rossum et al., 2002). Moreover, the biophysical prerequisites of the excitation chain model, namely neuronal clustering, spike-frequency adaptation, recurrent connectivity

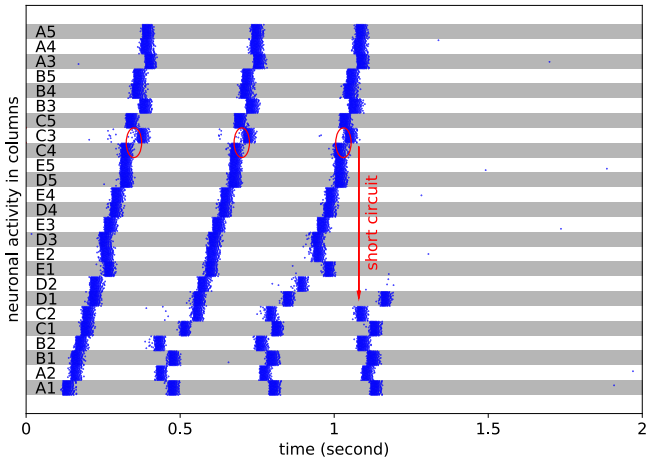

Figure 3.7: The activity circulation in the grid terminates after several rounds because of a short circuit in central assemblies (C4→C3→C2). In early rounds the difference of activation time between C4 and C3 are shorter compared to the late rounds (red ellipses). In other words, C3 becomes active sooner than it is expected. Therefore, C3 is able to activate C2 (red arrow), while C2 is supposed to be activated by B2. This short circuit generates activity before assemblies recover from the dormant mode. Hence, other assemblies are not able to become active and the circulation ceases. The initial values are the same as shown in Figure 3.5D (right). Column A1 is stimulated at $t = 100$ms in order to start the circulation.

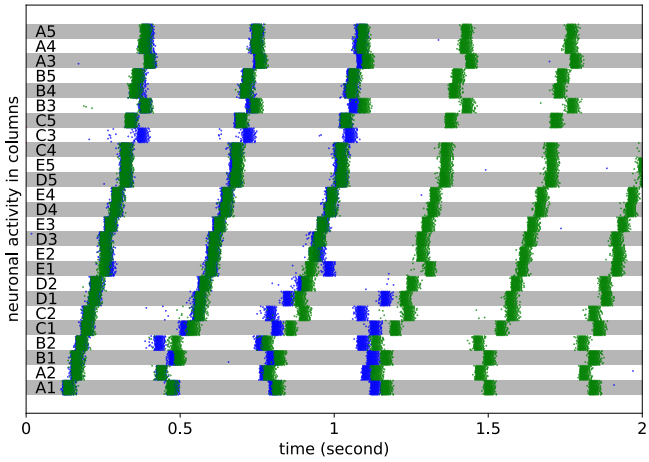

Figure 3.8: Long duration of circulation by removing column C3. We repeat the simulation of Figure 3.7 with same condition except that we removed column C3. Green dots show the dynamics of the new configuration while we keep blue dots from the Figure 3.7 for better comparison. In the new configuration, the circulation runs for much longer. In the figure, we have only shown the first two seconds, but we have not seen termination for 10 seconds.

and short-range inhibitory connections, are in principle consistent with experimental findings (Sanchez-Vives and McCormick, 2000; Perin et al., 2011; Mensi et al., 2012; Fino et al., 2013).

The excitation chain carries the signal by a wave of synchronous activity. Seen from this perspective, it is more similar to the synfire chain than to the fluctuating rate propagation which relies on asynchronous activity and rate coding (Kumar et al., 2010). However, the excitation chain is fundamentally different from the synfire chain and rate propagation in its ability to adjust the propagation speed without modifying the synaptic delay or synaptic time constant. While the propagation speed is nearly constant in a synfire chain (Wennekers and Palm, 1996), and is very close to the synaptic time scale in fluctuating rate propagation (van Rossum et al., 2002) and two-dimensional systems of neurons (Kistler et al., 1998), we can slow down and adjust the speed in the excitation chain by changing the strength of inter-assembly synapses. Hence, we suggest that the excitation chain can be used for population coding across slow time scales (Buonomano and Maass, 2009; Runyan et al., 2017). It is also possible that changes in synaptic weights are caused by neuro-modulators or various forms of activity-dependent synaptic plasticity. Suppose that a part of a neuronal structure which produces a complex cognitive behavior is an excitation chain, such that each assembly is responsible for performing one primitive of the behavior. Repeating the behavior, the assemblies become active one after each other in a systematic and reliable manner. In this case, a Hebbian learning rule will strengthen the synapses between excitatory assemblies and thus will work towards an increase of the execution speed of the behavior as we observed in Figures 3.1 and 3.2. This may explain why practicing sequential or rhythmic movements, such as in playing a musical instrument, can increase the speed at which the movement can be performed.

The bistability of neuronal assemblies is a key component of the excitation chain model's functionality. While the mechanism of assembly activation (jumping to the high point) is based on network feedback and is independent from the neuron model, the return of the assembly to the low point (in the dormant mode) needs an element of fatigue. In our model, we use spike-frequency adaptation for this purpose. However, replacing adaption by short-term depression (Tsodyks and Markram, 1997) of intra-assembly synapses yields similar results. In a previous abstract (Setareh et al., 2015), we removed spike-frequency adaptation and built a chain using leaky integrate-and-fire neurons while the synapses within each assembly expressed short-term depression. With strong connections inside assemblies, and relatively weak connections between them, the chain could propagate the activation forward, backward and in both directions. Similar to what is presented here, the propagation speed was tunable by changing the inter-assembly maximum synaptic weights.

In the grid model, assemblies are responsible for transmitting the activity between barrel columns. Removing the inhibitory and non-assembly neurons from the model, the grid of assemblies is able to propagate and circulate the activity on its own (data not shown). Therefore we consider the grid of assemblies the skeleton of the model, while the other neurons just follow the activity wave. This, however, is not meant to imply that inhibitory and non-assembly neurons do not play an important role in the cortex. Whereas in our model, we only consider the anesthetized state, information processing in the awake cortex very likely involves more than just the assembly neurons and requires the contribution of the other neurons.

In the literature, there exist several competition-based models for reproducing cortical trial-to-trial variability (Litwin-Kumar and Doiron, 2012; Doiron and Litwin-Kumar, 2014; Mazzucato et al., 2015, 2016) and for modeling working memory using continuous attractors (Compte et al., 2000; Wang et al., 2013). In these models, individual neurons or neural assemblies (also called neural clusters) try to become active and to suppress others by direct inhibitory connections or global inhibition. However, in the two models considered here (the chain and grid of assemblies) the situation is completely different. Instead of competition, the assemblies cooperate with each other to propagate activity signals through the tissue. Hence, in this type of model there is no need for global inhibition.

Similar to bump attractor models proposed for implementing working memory (Compte et al., 2000; Wang et al., 2013) and attractor maps used for encoding spatial location in hippocampus (Samsonovich and McNaughton, 1997; Tsodyks, 1999; McNaughton et al., 2006), our model relies on strong recurrent excitatory connections. However, while these encoding-models are designed to stabilize neuronal activity in time in order to provide a memory of a continuous variable, our model's aim is to propagate the activity with a specified speed and path to relay sensory information or to perform slow behavioral tasks.

Activity propagation was studied previously using the Wilson-Cowan model of neuronal population dynamics (Wilson and Cowan, 1972, 1973) and the dynamics of neural fields (Jirsa and Haken, 1997; Bressloff, 1999; Murray, 2001; Coombes, 2005, 2006). However, it is often hard to link network parameters used in these abstract models to neuronal and synaptic parameters. In our approach, we start directly from neural parameters extracted from experiments (Mensi et al., 2012; Pozzorini et al., 2015) and explore the influence of synaptic weight or short-term plasticity (Tsodyks and Markram, 1997). Despite the richness of the biological parameter space, the essential mathematical features of excitable media (Wilson and Cowan, 1972, 1973; Jirsa and Haken, 1997; Coombes, 2006) are still apparent in the models examined here.

The multicolumn model presented in this work is able to produce dynamics similar to the spontaneous regime of cortical activity (Petersen et al., 2003b). However, it is different from resting-state networks (Honey et al., 2007; Ghosh et al., 2008; Deco et al., 2009, 2011; Gilson et al., 2016) designed for explaining the synchrony of different brain regions. In these models, each brain region is typically considered as a nonlinear oscillator. The coupling strength between oscillators (Honey et al., 2007) as well as synaptic transmission delay and noise (Ghosh et al., 2008; Deco et al., 2009) are tuned such that different brain regions show synchrony similar to observed data. While such models are very successful in representing resting-state activity, their focus on macroscopic network structure may limit the range of dynamics produced by the models. In contrast, in our model we focus on a particular element of neuronal circuit-level connectivity, namely local assemblies of neurons, which may be contained in a small part of each cortical column. Such assemblies may make only a small contribution to the average (or resting-state) activity. Nonetheless propagation of activity across barrel columns or brain regions may depend on such assemblies, and chains or other functional structures built of them. In systems with excitable elements such as ours, the type of dynamics strongly depends on initial conditions of the neurons and nonlinearly on the inputs (Helias et al., 2010). Therefore embedded excitable assemblies provide nonlinear mesoscopic processing characteristics to the

circuits that may easily be overlooked in resting-state or other macroscopic models relying on averaged measures of connectivity between areas.

3.4 Materials and Methods

Neuron model and population parameters Neuronal parameters used in the simulations are reported in Table 3.1. Table 3.2 summarizes the network parameters.

As our neuron model we use a current-based generalized integrate-and-fire (GIF) model which implements spike-frequency adaptation using a spike-triggered current and a moving firing-threshold mechanisms (Mensi et al., 2012). The dynamics of the neuron's sub-threshold membrane potential ($V(t)$) is described by:

$$C\frac{dV(t)}{dt} = -g_L(V(t) - E_L) - \sum_{\hat{t}_j<t} \eta(t - \hat{t}_j) + I(t) \tag{3.1}$$

where parameters C, g_L and E_L are the passive parameters of the neuron. $I(t)$ is the synaptic input and $\eta(t)$ is the shape of the spike-triggered current caused by spikes of the neuron itself at times $\hat{t}_j$. After each spike emission, the membrane potential is reset to V_{reset}, integration of Eq. 3.1 restarts and the neuron goes through an absolute refractory period of duration τ_{ref}.

Spikes are produced stochastically (similar to an inhomogeneous Poisson process) with the firing intensity:

$$\lambda(t) = \lambda_0 \exp(\frac{V(t) - V_{\text{T}}(t)}{\Delta V}) \tag{3.2}$$

where λ_0 is the stochastic intensity at the firing threshold V_{T}, and ΔV is a constant which defines the level of stochasticity. The threshold V_{T} follows the dynamic:

$$V_{\text{T}}(t) = V_{\text{T}}^* + \sum_{\hat{t}_j<t} \gamma(t - \hat{t}_j) \tag{3.3}$$

where V_{T}^* is constant and $\gamma(t)$ describes the time course of the threshold after a spike emission. In Eq. (3.1), the synaptic input $I_i(t)$ received by neuron i is determined by the spikes of synaptically connected neurons:

$$I_i(t) = \sum_j w_{ij} \sum_f \alpha(t - t_j^f) = \sum_j w_{ij} \int_0^\infty \alpha(s) S_j(t - s) ds \tag{3.4}$$

where w_{ij} is the weight of the synapse connecting neuron j to neuron i, and $\alpha(t) = e^{-(t-\Delta)/\tau_{\text{syn}}}$ for $t \geq \Delta$ is the post-synaptic current (PSC) shape. The synaptic transmission delay (Δ) in all simulation is 1ms. $S_j(t) = \sum_f \delta(t - t_j^k)$ is the spike train of neuron j, δ denotes the Dirac δ-function and t_j^k is the k^{th} spike of neuron j. The synaptic weight w_{ij} indicates the PSC amplitude. Given the neuronal parameters, one can relate the PSC to the post-synaptic potential (PSP). We report values both of PSC and PSP amplitudes used in our simulations.

We ran simulations using the Brian simulator (Goodman and Brette, 2008) for simulating the chain and NEST (Gewaltig and Diesmann, 2007) for simulating the grid.

Table 3.1: Neuron model parameters used in simulations.

Parameter	Excitatory	Inhibitory
C (pF)	63.0	54.2
g_L (nS)	8.1	5.5
E_L (mV)	-58.6	-59.8
$\eta(t)$	$\eta_1(t) + \eta_2(t)$	$\eta_1(t) + \eta_2(t)$
$\eta_1(t)$ (pA) for $(t \geq 0)$	$36.3e^{-t/39.2\text{ms}}$	$47.4e^{-t/19.1\text{ms}}$
$\eta_2(t)$ (pA) for $(t \geq 0)$	$0.7e^{-t/700.0\text{ms}}$	$-0.8e^{-t/282.1\text{ms}}$
$\gamma(t)$	$\gamma_1(t) + \gamma_2(t)$	$\gamma_1(t) + \gamma_2(t)$
$\gamma_1(t)$ (mV) for $(t \geq 0)$	$3.26e^{-t/45.0\text{ms}}$ (*)	$-7.3e^{-t/28.3\text{ms}}$
$\gamma_2(t)$ (mV) for $(t \geq 0)$	$2.52e^{-t/204.3\text{ms}}$	$3.7e^{-t/347.7\text{ms}}$
λ_0 (Hz)	0.1	0.1
ΔV (mV)	1.76	1.24
V_T^* (mV)	-56	-44.5
τ_{ref} (ms)	4.0	4.0
V_{reset} (mV)	-31.9	-38.7

(*) This is value is $13.05e^{-t/45.0\text{ms}}$ for the simulation of multicolumn model (Figure 3.5).

Transient stimulus In order to initiate the activity in the chain, we stimulate one assembly of the chain (for example the first assembly, the last assembly or an assembly in the middle of the chain.). For stimulating an assembly, we connect each of its neurons to 25 Poisson neurons which fire with the rate of 5Hz each for 25ms. The synaptic weight between the Poisson neurons and the assembly neurons is 0.18nA.

Rate-current relations Here we present some theory necessary to explain the dynamics of excitable assemblies. The dynamics of a neuronal population can be described by two equations relating the firing rate averaged over all neurons and the mean of the synaptic input received by them. The first relation is called the neuron's gain function. Injecting a weakly fluctuating current I_{syn} into a neuron produces an average firing rate of

$$r = g(\langle I_{\text{syn}} \rangle, \sigma_{\text{I}}) \tag{3.5}$$

where $\langle I_{\text{syn}} \rangle$ and σ_{I} are the average and the standard deviation of the synaptic current over time, respectively, and g is the gain function. Although there are ways to compute the firing rate of adaptive integrate-and-fire neuron models in closed-form (Fourcaud-Trocmé et al., 2003; Hertäg et al., 2014) or by using a self-consistent numerical approach (La Camera et al., 2004; Richardson, 2007, 2009), there is no straightforward analytical solution for computing the gain function of the GIF model that we use here. We obtain the gain function (3.5) by numerical simulation (Setareh et al., 2017). For the simulations to determine the gain function numerically

Table 3.2: Parameters of networks used in simulations (exc: excitatory, inh: inhibitory, pop: population, amp: amplitude, CP: connection probability, PSP: postsynaptic potential, PSC: postsynaptic current)

Simulation of excitation chain (Figure 3.1 and 3.2)

Size of exc. assembly	70
Size of inh. pop.*	70

	Connections	PSP amp. (mV)	PSC amp. (pA)	CP	τ_{syn} (ms)
Inter-column connections	exc. to exc.	Variable	Variable	10%	7.7
	exc. to inh.*	Variable	Variable	30%	9.9
Intra-column connections	exc. to exc.	1.0	22.1	50%	7.7
	exc. to inh.*	0.25	3.7	10%	9.9
	inh. to exc.*	0.16	3.5	22%	7.7
	inh. to inh.*	0.56	10.2	30%	6.7

* Not applicable for the chain of only excitatory assemblies (Figure 3.2)

Simulation of multicolumn barrel cortex model (Figure 3.5)

Size of exc. assembly	70
Size of exc. non-assembly	380
Size of inh. pop.	70

	Connections	PSP amp. (mV)	PSC amp. (pA)	CP	τ_{syn} (ms)
Inter-column connections	exc. to exc.*	0.32	7.1	10%	7.7
Intra-column connections	assembly to assembly	1.0	22.1	50%	7.7
	assembly to non-assembly	0.15	3.3	15%	7.7
	non-assembly to non-assembly	0.15	3.3	15%	7.7
	non-assembly to assembly	0.15	3.3	15%	7.7
	inh. to exc.*	0.16	3.5	22%	7.7
	exc. to inh.*	0.25	3.7	10%	9.9
	inh. to inh.	0.56	10.2	30%	6.7

* exc. indicates both assembly and non-assembly groups.

the injected current is given by

$$I(t) = \langle I_{\text{syn}} \rangle + \frac{\sigma_{\text{I}}}{\sqrt{q_2}} \int_0^\infty \alpha(s)\xi(t-s)ds \tag{3.6}$$

where $\xi(t)$ is white noise with mean $\langle \xi(t) \rangle = 0$ and covariance $\langle \xi(t)\, \xi(t') \rangle = \delta(t-t')$, $\alpha(t)$ is the shape of the PSC defined above and $q_2 = \int_0^\infty \alpha^2(t)dt$. Depending on the duration of injection, the neuron goes into different adaptation states. By injecting the current (3.6) for a short episode of 10ms, we can estimate the firing rate in the non-adapted state. In case of a longer stimulation period, we can divide the time into intervals of 10ms and extract the rate-current relation in the different, progressively more adapted states. This method has been used to obtain the gain functions displayed in Figure 3.3A and B.

The network activity gives rise to the second relation between the average firing rate and the average synaptic current. The synaptic input of an arbitrary neuron i is described by:

$$I_{i,\text{syn}=} \sum_j w_{ij} \left(\int_0^\infty \alpha(s) S_j(t-s)ds \right) \tag{3.7}$$

where w_{ij} is the weight of the synapse connecting neuron j to neuron i and $S_j(t)$ is the spike train of neuron j. The sum runs over all other neurons j in the assembly. Averaging both sides over time and input neurons gives the average input current: $\langle I_{\text{syn}} \rangle = Npqwr$, where N is the number of neurons inside the population, p is the connection probability between neurons, w is the synaptic weight and q is the total charge of one PSC pulse: $q = \int_0^\infty \alpha(t)dt$. Rearranging this equation yields:

$$r = \frac{\langle I_{\text{syn}} \rangle}{Npqw} \tag{3.8}$$

We refer to the denominator of eq. 3.8 as the network feedback (C_{fb}) of the population (Setareh et al., 2017):

$$C_{\text{fb}} = Npqw \tag{3.9}$$

We use these two relations for analysis of the behavior of excitatory assemblies in the "Results" section.

Analytical approach for obtaining the propagation speed of the excitation chain
Our aim is to estimate the difference between activation times of two consecutive assemblies (which is a measure of propagation speed) using an analytical approach. We assume that the values of the parameters are given and the time course $r(t)$ of the population rate signal of an arbitrary assembly in the chain is known. Furthermore, we assume that the populations are silent before activation ($r(t) = 0$ for $t < t_{\text{a}}$).

Suppose that we have two excitatory assemblies, assembly1 and assembly2. We refer to their activation time as $\bar{t}_1$ and $\bar{t}_2$ respectively. The aim of the calculation is to find the difference in activation times $x = \bar{t}_2 - \bar{t}_1$. Recall that the activation time has been defined above as the expected time at which each assembly neuron has spiked once. Assuming independent Poisson

firing of the assembly with rate $r(t)$, we can find $\bar{t}_1$ as the moment when the expected spike count reaches 1, $n(0;\ \bar{t}_1)/N = 1$, where $n(a;\ b)$ is the number of spikes in time interval $[a,\ b)$ and N is the number of neuron in the assembly. Inserting the shape of assembly population rate we obtain

$$\int_0^{\bar{t}_1} r(t)dt \ = \ 1 \tag{3.10}$$

which we can solve for $\bar{t}_1$. Note, however, that the Poisson assumption made here does not ensure that no neuron fires more than one spike before $\bar{t}_1$. Therefore Eq. 3.10 yields an approximate value of $\bar{t}_1$.

Finding the value of $\bar{t}_2$ is more complicated. After activation of assembly1, its neurons send synaptic input to assembly2. The average input received by each assembly2 neuron can be computed:

$$I_{\text{syn\_fwd}}(t) = Np_{\text{exc}}w_{\text{exc}}(\alpha(t) * r(t-\Delta)) \tag{3.11}$$

where p_{exc} and w_{exc} are inter-assemblies connection probability and synaptic weight respectively, $*$ denotes the convolution operator and Δ is synaptic transmission delay. However, this is not the only synaptic input received by neurons in assembly2. Even before $\bar{t}_2$, several neurons of assembly2 may already fire spikes (due to random fluctuations) and send some feedback current to other neurons. This averaged current can be computed similarly:

$$I_{\text{syn\_self}}(t) = (N-1)p_{\text{self}}w_{\text{self}}(\alpha(t) * r(t-\Delta-x)) \tag{3.12}$$

where p_{self} and w_{self} are intra-assemblies connection probability and synaptic weight respectively, and x is the difference of activation times. Note that the shape of $r(t)$ is assumed to be the same for all assemblies of the chain. However, we must be careful about the timing of each current. Suppose that at the time $t = 0$ assembly1 starts to fire, therefore assembly2 receives a first input at the time $t = \Delta$. After a while, assembly2 starts to fire. The difference between these two starting times is denoted by x. Therefore the feedback current is received by assembly2 neurons at the time $t = \Delta + x$.

The total synaptic input received by neurons of assembly2 is the summation of $I_{\text{syn\_fwd}}$ and $I_{\text{syn\_self}}$. Consequently, we can write the the total input received by assembly2 neurons as

$$I_{\text{syn}}(t) = I_{\text{syn\_fwd}}(t) + I_{\text{syn\_self}}(t) \tag{3.13}$$

Now we can calculate the subthreshold membrane potential of neurons in assembly2 by solving Eq. 3.1:

$$V(t) = E_{\text{L}} + \frac{1}{C}(e^{-t/\tau_{\text{m}}} * I_{\text{syn}}(t)) \tag{3.14}$$

Note that since we want to calculate the time of first spikes of neurons, we can neglect the spike-triggered current and the moving firing threshold. The firing intensity is then given as a function of $V(t)$ by Eq. (3.2), except that $V_{\text{T}}(t) = V_{\text{T}}^*$ because we assumed that neurons are not adapted and all $\gamma(t)$ equal zero.

Then using the distribution of first spikes $P(t)$, we are able to calculate the average time of first spikes of assembly2:

$$P(t) = \lambda(t)\exp(-\int_0^t \lambda(t')dt') \tag{3.15}$$

$$\bar{t}_2 = \int_0^\infty tP(t)dt \tag{3.16}$$

Finally, using Eq. 3.10 and Eq. 3.16, we can calculate the time difference between activation times:

$$x = \bar{t}_2 - \bar{t}_1 \tag{3.17}$$

Note, however, that $\bar{t}_2$ in Eq. (3.17) depends on the value of x through Eq. (3.12). Therefore, we have formed a self-consistent equation for x. We feed this value in Eq. 3.12 and get it back in Eq. 3.17. If the output value of x equals its input value, we found the proper value. Using a simple search, we are able to find this value numerically.

We apply this approach for our chain and calculate the value of x for different values of w_{exc}; these results are presented in Figure 3.3D. Note that we need to obtain the shape of the assembly population rate $r(t)$ by neural simulation beforehand. However, the same shape $r(t)$ can be used for all values of w_{exc}, because for $p_{\text{exc}}w_{\text{exc}} \ll p_{\text{self}}w_{\text{self}}$ the time course of the initial rise is dominated by the self-feedback (see Figure 3.3B).

Short-term plasticity We use short-term plasticity (Tsodyks and Markram, 1997; Tsodyks et al., 1998) in one series of our simulations (Figure 3.1F). This synaptic model supposes that each synapse has a certain amount of resource denoted by x, with dynamics

$$\frac{dx}{dt} = \frac{1-x}{\tau_{\text{rec}}} - ux\delta(t-t_f) \tag{3.18}$$

$$\frac{du}{dt} = \frac{U-u}{\tau_{\text{facil}}} + U(1-u)\delta(t-t_f) \tag{3.19}$$

where U (jump of release fraction), τ_{rec} (recovery time constant) and τ_{facil} (facilitation time constant) are three parameters of the model. u (release fraction) and x are the two variables of the system. Whenever a neuron fires a spike (t_f denotes the firing time), it produces a PSC with amplitude of uxw (w is the synaptic weight). Then, the amount of resource is decreased by ux and the release fraction is increased by $U(1-u)$. In our simulations, we either used facilitation or depression. We chose the values $\tau_{\text{rec}} = 0.001$ms and $\tau_{\text{facil}} = 500$ms for the facilitation case and $\tau_{\text{rec}} = 800$ms and $\tau_{\text{facil}} = 0.001$ms for the depression case. The value of U is different in each simulation. Note that for the depression case, we have to fix the amplitude of the first PSC regardless of value of U. We did that by adjusting the value of the synaptic weight.

Acknowledgments

We thank Carl Petersen and Tilo Schwalger for helpful discussions. This project was supported by the European Research Council (Grant Agreement no. 268 689; Hesam Setareh) and by the Swiss National Science Foundation (grant agreement no. 200020_147200; Moritz Deger).

Chapter 4

In vitro cortical network firing is homeostatically regulated: A model for sleep regulation[1]

Abstract

Prolonged wakefulness leads to a homeostatic response manifested in increased amplitude and number of electroencephalogram (EEG) slow waves during recovery sleep. Cortical networks show a slow oscillation when the excitatory inputs are reduced (during slow wave sleep, anesthesia), or absent (in vitro preparations). It was recently shown that a homeostatic response to electrical stimulation can be induced in cortical cultures. Here we used cortical cultures grown on microelectrode arrays and stimulated them with a cocktail of waking neuromodulators. We found that recovery from stimulation resulted in a dose-dependent homeostatic response. Specifically, the inter-burst intervals decreased, the burst duration increased, the network showed higher cross-correlation and strong phasic synchronized burst activity. Spectral power below <1 Hz significantly increased and the increase was related to steeper slopes of bursts. Computer simulation suggested that a small number of clustered neurons could potently drive the behavior of the network both at baseline and during recovery. Thus, this in vitro model appears valuable for dissecting network mechanisms of sleep homeostasis.

4.1 Introduction

Sleep regulation is one of the most intriguing topics in the field of neuroscience. Sleep is a complex brain state and is believed to be necessary for normal functioning during waking. Two main stages constitute sleep: rapid eye movement sleep (REM or paradoxical sleep), and non-rapid

[1]Text copied from Saberi-Moghadam S, Simi A*, Setareh H*, Mikhail M and Tafti M, manuscript is under review in Int. J. Neural Sys. (* contributed equally to this work).

eye movement sleep (NREM or slow wave sleep, SWS). NREM sleep is characterized by high amplitude and low frequency quasi-synchronous cortical network activity (Borbély et al., 1981). The NREM slow wave network oscillations are divided in the electroencephalogram (EEG) slow oscillation (<1 Hz) (Steriade et al., 1993b; Achermann and AABorbely, 1997) and slow wave or delta activity (EEG power density between 0.5-4 Hz, SWA) (Borbély et al., 1981; Steriade et al., 1993a). Sleep is homeostatically regulated. Prolonged periods of spontaneous wakefulness or sleep deprivation lead to an increased sleep need that is manifested in a proportional increase in EEG SWA and an increased incidence of high amplitude slow oscillations during recovery sleep (Borbély et al., 1984; Esser et al., 2007; Vyazovskiy et al., 2011a). Homeostatic regulation of sleep is not limited to an increase in EEG SWA in mammalian species but extends to an increased sleep duration and reduced response to external stimuli in nearly all species so far studied (Cirelli and Giulio, 2008; Vyazovskiy and D, 2013; Tononi and Chiara, 2014). Nevertheless, the underlying cellular, network, and molecular mechanisms of sleep homeostasis are poorly understood.

Intracellular recordings of cortical neurons during SWS or anesthesia revealed a robust slow oscillation characterized by a period of active firing (UP state) followed by a long-lasting period of neuronal silence (DOWN state) (Steriade et al., 1993b; Timofeev et al., 2001). This pattern of network activity can be reliably recorded during SWS in intact animals (by local field potential "LFP" and multiunit activity recordings) and in humans (by the EEG) (Achermann and AABorbely, 1997; Sirota and Buzsáki, 2005; Ji and A, 2007; Riedner et al., 2007; Vyazovskiy et al., 2007; Bersagliere and Achermann, 2010; Vyazovskiy et al., 2011a). Interestingly, this slow oscillation occurs spontaneously in thalamic inactivated cortical regions or isolated cortical slabs (Lemieux et al., 2014), cortical slices (Sanchez-Vives and McCormick, 2000), or even in mature cortical cultures (Wagenaar et al., 2006; Corner et al., 2008; Hinard et al., 2012; Jewett et al., 2015; Colombi et al., 2016). By using multielectrode arrays (MEA) and mouse primary cortical cultures, we showed that not only these dish-wide slow oscillations can be recorded for long periods of time but that cultures can be stimulated by a waking chemical cocktail (hereinafter called "CCK", including monoaminergic, glutamatergic, cholinergic, and orexinergic neurotransmitters or agonists) to induce tonic firing that returns to the default synchronous burst firing 24h later (Hinard et al., 2012). Notably, stimulated cultures show remarkably similar transcriptional and metabolic changes as cortical tissues of animals subjected to 6h of sleep deprivation (Hinard et al., 2012). One important finding in this study, which was confirmed and extended by Kaufman et al. 2014, is that even continuous stimulation of such cultures cannot prevent the invariable return of slow oscillations, strongly indicating that homeostatic processes are activated to compensate for imposed tonic firing. Here we performed continuous recording of mouse cortical cultures before stimulation by two different concentrations of our CCK and 24 hours later during recovery. Detailed analysis of burst firing in these preparations revealed a dose-depended homeostatic response of the network activity, which showed remarkable similarities to homeostatic regulation of cortical activity during physiological sleep in vivo.

4.2 Materials and Methods

Cell cultures

Cortical cultures were prepared from C57BL/6J mouse brains at embryonic days 18–20. The brain tissue was separated and dissected in a phosphate buffer solution containing HEPES, 33 mM glucose, and 40 mM sucrose. The isolated cortices were digested with a solution containing 50 U of papain for 30 min at 37°C. Digestion was stopped by the addition of trypsin inhibitor for 10 min. Cells were then mechanically dissociated and plated in neurobasal medium supplemented with 2% B-27, 0.5 mM glutamax, and penicillin/streptomycin. Before seeding (200,000 neurons / MEA), the microelectrode array biosensors (MEAs; Multichannel Systems, Germany) were coated with 0.1% polyethyleneimine and 5 µg/ml of laminin to promote cell adhesion. Cultures were maintained in a humidified CO2 incubator (5% CO2, 37°C) and half of the medium was changed once a week with the complete neurobasal medium. All cultures were recorded between 12 and 14DIV when stable burst-pause activity was observed (Hinard et al., 2012) and were either sham (H2O) stimulated or stimulated with a cocktail of neuromodulators: 1 µM NMDA, AMPA, kainate, ibotenic acid, serotonin, histamine, dopamine and noradrenaline; 10 µM carbachol; and 0.01 µM orexin (Hinard et al., 2012). This coctail (1CCK) was two-fold diluted to prepare the 0.5CCK. All experimental procedures were conducted in accordance with regulatory standards and approved by the Vaud Veterinary Office, Switzerland.

Micro Electrode Array (MEA) recording

Electrophysiological signals were acquired using the complete MEA60-BC system (Multi Channel Systems, Germany). The set-up consists of a MEA 1060-Inv-BC amplifier integrating 60 channels and filter amplifiers with a bandwidth of 0.1 Hz–10 KHz and a gain of 1100. The set-up was connected to a computer equipped with a PCI data acquisition board and raw data were acquired and analyzed using MCRack software (Multichannel Systems, Germany). Primary neuronal cultures were seeded on standard MEA biosensors containing 59 planar TiN/SiN micro- electrodes (30 µm diameter, 200 µm interelectrode distances) plus one internal reference electrode (Figure 4.1A). Spontaneous firing activity (Figure 4.1B) was recorded after 2 weeks in vitro when a stable network activity was established (which appears approximately after 10 days in murine cortical cultures (Hinard et al., 2012)). All recordings (300 seconds long) from MEAs were performed in a humidified CO2 incubator 10-15 minutes after the transfer of the MEAs into the recording stage. The raw signals were recorded at 25 kHz sampling frequency, high pass filtered at 200 Hz and low pass filtered at 2 kHz, and amplified spikes were isolated at 1ms resolution. Several cultures were recorded at baseline and every 3 to 6h after stimulation till dish-wide burst activity resumed at around 24h (Figure 4.2). Each recording lasted for 5 minutes. A total of 29 cultures were analyzed; 12 cultures were stimulated at high concentration (1CCK), 8 at low concentration (0.5CCK, half of the 1CCK concentration) and 9 were sham (H2O) stimulated.

Spikes and synchronized bursts detection

Neuronal spikes were sorted from the biological noise using the threshold tool of MCRack software when the amplitude (peak-to-peak) of the extracellular potential exceeded a noise-based threshold set at 7 times the standard deviation of the noise for each MEA channel (Chiappalone et al., 2006). The spike time stamps were stored in the MCRack software. The recorded spike train is time-varying spontaneous multi-unit activity in the vicinity of each MEA electrode. The network activity is composed by both spikes and synchronized bursts (Figure 4.1B). To calculate the network firing rate, we computed a spike density function (SDF) for each MEA electrode during the five minute long recordings. Briefly, spike trains were convolved by a Gaussian function with a total area of 1 and a width (SD) of 100ms. The population firing rate or mean of SDF (mSDF) was then calculated by averaging the firing rate across all channels at each time point (Figure 4.1E).

Primary cortical cultures are characterized by repetitive burst activity. Synchronized network activity across all channels were detected by using a method described in Mukai et al. 2003 and Ito et al. 2010. Briefly, the total number of spikes contained in a 100ms time window were counted over all electrodes. By convolving the window on the spike train, a firing rate histogram was obtained over time. Finally, all the events exceeding a 40 spikes/window threshold were defined as a synchronized burst (Figure 4.1F). In order to avoid any biased results due to inter-variability across cultures, all detection procedures for single spikes and synchronized bursts were tested in accordance to specific acceptance criteria as described in (Novellino et al., 2011).

Characteristics of synchronized burst activity

To characterize multiple features in the time domain, the detected burst-pause activity was analyzed during baseline and its variation during the recovery period (24 hours after stimulation). Different parameters were analyzed such as the number of spikes per channel, number of bursts, burst duration (BD), Inter-Burst-Interval (IBI), and the number of spikes per burst (Figure 4.1F, J).

To detect burst's slopes, we first normalized each burst activity distribution by dividing to the maximum of the burst amplitude. For each detected burst, the slope was defined as the first derivative of the normalized burst activity. The ascending and descending phases are denoted as initial and final slope, respectively.

It is believed that spiking activity is correlated across neurons in a population of neural networks. Cross-correlation is a method to detect the degree of interdependency (synchrony) between firing of paired neurons or electrodes (Chiappalone et al., 2007; Rocha et al., 2007; Poli et al., 2015). For all pairs of MEA channels, the cross-correlation was computed as follows. First, all spikes were placed into bins of 1ms. Then, within a time window ($T = 1000$ms), $C_{ij}(\tau) = \Sigma_{\tau=0}^{T} x_i[s]x_j[s+\tau]$ was calculated, where s is the starting time of the window and $x_i[s]$ is the number of spikes filtered by a Gaussian Kernel with a width (SD) of 100ms in time interval $[s, s+1]$ ms in channel i. This value ($C_{ij}(\tau)$) was divided to $\sqrt{C_{ii}(0)C_{jj}(0)}$, and the maximum

value was selected: $C_{ij}(\tau)$ over $\tau = 1, 2, 3, \ldots, T$ for all time windows. This calculation for each culture was repeated and averaged across all cultures. Note that the auto-correlations were excluded. For statistical analysis, histograms of all averaged cross-correlation coefficients were constructed and the difference between baseline and recovery was tested by Kolmogorov-Smirnov test.

Spectral analysis

The spectral components are lost during the extraction of temporal features of the signal. To better understand the network oscillation, a Fast Fourier Transform (FFT) was performed on burst-paused mSDF population firing rate with a 100ms bin width at 1kHz sampling rate (Mok et al., 2012). Before FFT, the DC component was removed by subtracting the mean from the data. The obtained power spectrum across all cultures showed a typical dominant frequency with the highest peak within the slow oscillation band frequency ($\leq$1 Hz).

Neural Trajectory

To consider the network properties at the population level, there are two concerns. First, salient features of the channel responses may be masked by averaging across channels. Second, it is difficult to characterize multiple spatiotemporal features of a high-dimensional oscillating network. To address these concerns, we assessed representative 2-d linear projections of the 60 channel responses. For example, principal component analysis (PCA) can be applied to the channel responses to assess the top two principal components. While this projection captures the greatest amount of variance, it is not guaranteed to capture the oscillatory nature of the data. Instead, we used the DataHigh software (Cowley et al., 2013) to view many 2-d projections of the data. DataHigh first smooths the spike counts of each channel across time with a 50 ms Gaussian kernel. Next, DataHigh applies PCA to the smoothed channel responses (60-dimentional spike count vectors) and takes the top K dimensions that explain 90% of variance (where K is typically greater than 2). This helps to remove dimensions with small amount of variance. DataHigh then allows the user to view many 2-d projections of the K principal components by plotting the data as a 'neural trajectory', where two consecutive time points are connected by a line. Thus, the neural trajectory represents the temporal evolution of the channel responses, which may oscillate from one region of firing rate space to another. These regions correspond to states, where an 'UP' state corresponds to elevated firing rates, whereas 'DOWN' state corresponds to low firing rates.

Simulation

For the neuron model, we used a current-based generalized integrate-and-fire (GIF) model (Mensi et al., 2012), which implements spike-frequency adaptation. It is shown that the GIF model is able to capture both subthreshold dynamics of membrane potentials and spikes recorded

from neurons in the cortex with high accuracy during current injection (Mensi et al., 2012). The model describes the dynamics of the membrane potential $V(t)$ by the differential equation:

$$C\frac{dV(t)}{dt} = -g_{\mathrm{L}}(V(t) - E_{\mathrm{L}}) - \sum_{\hat{t}_j<t} \eta(t - \hat{t}_j) + I(t) \tag{4.1}$$

where $I(t)$ is the input current. C, g_L and E_L are parameters of the neuron model and $\{\hat{t_j}\}$ are the spike times. In case of spike emission, a current with the shape $\eta(t)$ is triggered. The neuron goes through a refractory period with the duration of τ_{ref} and the membrane potential is reset to V_{reset}. Spikes are produced stochastically with the firing intensity

$$\lambda(t) = \lambda_0 \exp\left(\frac{V(t) - V_{\mathrm{T}}(t)}{\Delta V}\right) \tag{4.2}$$

where λ_0 and ΔV are the parameters of the firing intensity. $V_T(t)$ is firing threshold:

$$V_{\mathrm{T}}(t) = V_T^* + \sum_{\hat{t}_j<t} \gamma(t - \hat{t}_j) \tag{4.3}$$

where V_T^* is a constant. After each spike emission, a shape $\gamma(t)$ is added to the firing threshold. Table 4.1 summarizes the parameters and shapes of $\eta(t)$ and $\gamma(t)$ used for excitatory and inhibitory neurons in the simulations.

Parameter	Excitatory	Inhibitory
C (pF)	83.1	46.1
g_L (nS)	3.7	6.6
E_L (mV)	-67.0	-71.2
τ_{ref} (ms)	4.0	4.0
V_{reset} (mV)	-36.7	-48.4
$\eta(t)$	$\eta_1(t) + \eta_2(t)$	$\eta_1(t) + \eta_2(t)$
$\eta_1(t)$ (pA)	$56.7e^{-t/57.8\mathrm{ms}}$	$31.8e^{-t/11.5\mathrm{ms}}$
$\eta_2(t)$ (pA)	$-6.9e^{-t/218.2\mathrm{ms}}$	$1.6e^{-t/500.1\mathrm{ms}}$
$\gamma(t)$	$\gamma_1(t) + \gamma_2(t)$	$\gamma_1(t) + \gamma_2(t)$
$\gamma_1(t)$ (mV)	$11.7e^{-t/53.8\mathrm{ms}}$	$5.6e^{-t/11.5\mathrm{ms}}$
$\gamma_2(t)$ (mV)	$1.8e^{-t/640.0\mathrm{ms}}$	$0.6e^{-t/473.7\mathrm{ms}}$
λ_0 (kHz)	10	10
ΔV (mV)	1.4	0.6
V_T^* (mV)	-39.6	-41.2

Table 4.1: Parameter of GIF neuron model used in simulations of cell cultures.

Simulation	Connection	CP	τ_{syn} (ms)	w_{ij} (pA)
First culture, baseline mode (Figure 4.1)	cluster→cluster	50%	16.3	18.6
	cluster→non-cluster	15%	16.3	4.4
	non-cluster→cluster	10%	16.3	4.4
	non-cluster→non-cluster	15%	16.3	4.4
	excitatory→inhibitory	37%	6.9	14.8
	inhibitory→excitatory	25%	1.3	39.6
	inhibitory→inhibitory	35%	6.9	10.1
First culture, recovery mode (Figure 4.1)	cluster1→cluster1	50%	16.3	18.6
	cluster2→cluster2	50%	16.3	18.6
	cluster1→cluster2	10%	16.3	2.6
	cluster2→cluster1	10%	16.3	4.4
	cluster1→non-cluster	15%	16.3	4.4
	cluster2→non-cluster	15%	16.3	4.4
	non-cluster→cluster1	5%	16.3	4.4
	non-cluster→cluster2	15%	16.3	4.4
	non-cluster→non-cluster	15%	16.3	4.4
	excitatory→inhibitory	37%	6.9	14.8
	inhibitory→excitatory	25%	1.3	39.6
	inhibitory→inhibitory	35%	6.9	10.1
Second culture, baseline mode (Figure 4.7)	cluster1→cluster1	55%	16.3	18.6
	cluster2→cluster2	55%	16.3	18.6
	cluster1→cluster2	5%	16.3	3.5
	cluster2→cluster1	5%	16.3	3.5
	cluster1→non-cluster	18%	16.3	3.1
	cluster2→non-cluster	18%	16.3	2.6
	non-cluster→cluster1	18%	16.3	4.4
	non-cluster→cluster2	18%	16.3	4
	non-cluster→non-cluster	18%	16.3	4.4
	excitatory→inhibitory	18%	6.9	14.8
	inhibitory→excitatory	25%	1.3	39.6
	inhibitory→inhibitory	35%	6.9	10.1
Second culture, recovery mode (Figure 4.7)	cluster→cluster	45%	16.3	18.6
	cluster→non-cluster	12%	16.3	2.4
	non-cluster→cluster	12%	16.3	3
	non-cluster→non-cluster	18%	16.3	4.4
	excitatory→inhibitory	18%	6.9	14.8
	inhibitory→excitatory	25%	1.3	39.6
	inhibitory→inhibitory	35%	6.9	10.1

Table 4.2: Network parameters used for each simulation. Excitatory neurons include cluster and non-clustered neurons. Connections between inhibitory neurons and cluster neurons are same as connections between inhibitory neurons and non-clustered neurons. cluster: clustered neurons, non-cluster: non-cluster neurons, CP: connection probability

Simulation	Connection	r (Hz)	τ_{syn} (ms)	w_{ij} (pA)
First culture, baseline mode (Figure 4.1)	Poisson→cluster	95	16.3	16
	Poisson→non-cluster	95	16.3	9
	Poisson→inhibitory	100	6.9	30
First culture, recovery mode (Figure 4.1)	Poisson→cluster1	95	16.3	16
	Poisson→cluster2	100	16.3	12
	Poisson→non-cluster	95	16.3	9
	Poisson→inhibitory	100	6.9	30
Second culture, baseline mode (Figure 4.7)	Poisson→cluster1	48	16.3	28
	Poisson→cluster2	95	16.3	19
	Poisson→non-cluster	95	16.3	4
	Poisson→inhibitory	100	6.9	30
Second culture, baseline mode (Figure 4.7)	Poisson→cluster	66	16.3	23
	Poisson→non-cluster	95	16.3	4
	Poisson→inhibitory	100	6.9	30

Table 4.3: Parameters of external Poisson noise. Each neuron receives independent Poisson input with constant rate r and a synaptic weight w. cluster: clustered neurons, non-cluster: non-cluster neurons

Neurons receive synaptic current as the input ($I(t)$). The input received by neuron i is generated by the spikes of synaptically connected neurons:

$$I_i(t) = \sum_j w_{ij} \sum_f \alpha(t - t_j^f) = \sum_j w_{ij} \int_0^\infty \alpha(s) S_j(t-s) ds \tag{4.4}$$

where w_{ij} is the synaptic weight of connection from neuron i to j. t_j^f is the f^{th} spike of neuron j. Postsynaptic current shape is described by: $\alpha(t) = we^{-(t-\Delta)/\tau_{\text{syn}}}$ for $t \geq \Delta$, where τ_{syn} is synaptic time constant. The transmission delay (Δ) for all synapses is 2ms. $S_j = \sum_f \delta(t - t_j^f)$ is the spike train of neuron j where δ denotes the Dirac δ-function. The synaptic weights, connection probabilities and time constants between different subgroups of neurons are different. Table 4.2 shows the parameters used for building the network.

We assume that each neuron receives noise, beside the synaptic input from other neurons. This noise is modeled with a stochastic Poisson input. Table 4.3 displays the properties of the Poisson input each neuron receives. All simulations were performed by Brian simulator (Goodman and Brette, 2008).

Statistical analysis

All analyzed parameters were first tested for normality by the Kolmogorov-Smirnov test. The extracted network-burst parameters were first expressed relative to the sham condition followed by Student's paired t-test. The power spectra were compared among conditions by 2-way ANOVA

followed by Tukey test. The distributions of cross-correlation coefficients were compared by Kolmogorov-Smirnov test. Statistical significance level was set at $p < 0.05$.

4.3 Results

Developing cortical networks in vitro show initially a random firing that gradually is transformed into a synchronized bursting pattern within a two weeks period (14 days in vitro "DIV") and remains stable thereafter (Maeda et al., 1995; Kamioka et al., 1996). Synchronized bursting in vitro tightly correlates with the membrane depolarization (UP state) of single neurons by intracellular recordings (Kaufman et al., 2014) and show similarities to the firing activity of cortical neurons during SWS sleep in vivo (Timofeev et al., 2001). Also, similar to the in vivo activity, the burst-pause firing in vitro occurs at low frequency (typically between 0.1 to 0.5 Hz) (Hinard et al., 2012). Examples of 5-minute recordings of a culture at 14DIV before and 24h after stimulation with our waking neuromodulator cocktail (Hinard et al., 2012; Mikhail et al., 2017) are shown in Figure 4.1. Note that, the waking cocktail was added to each culture but the medium was not changed (no washing) during the recordings. Bursting activity was characterized as described in Materials and Methods and the burst parameters analyzed here are indicated in Figure 4.1F, J. CCK but not sham stimulation rapidly suppressed burst firing (Figure 4.2). We hypothesized that similar to early phase of sleep, signs of recovery must be seen at the re-emergence of burst activity (24h after stimulation).

4.3.1 Spectral analysis, burst duration and interburst interval

Slow waves during NREM sleep arise from a synchronized occurrence of UP and DOWN states among large cortical neuronal populations (Timofeev et al., 2001). More specifically, the negative segment of the slow waves coincides with network silence (Contreras and Steriade, 1995). This activity can be approximated by the envelope of bursts (spike density function) as shown in Figure 4.1E,I. Time series of smoothed firing activities were subjected to a fast Fourier transform (FFT) analysis.

Cultures recorded 24h after stimulation showed a dose-dependent increase in spectral power below 1 Hz (Figure 4.3A). In addition, a right shift in the dominant frequency was observed (Figure 4.3A). The increase in power density can result from an increase in the incidence of bursts and/or an increase in their amplitude.

We therefore calculated both the duration and the inter-burst interval as outlined in Figure 4.1J. None of the burst parameters at baseline differed significantly between sham, 1 and 0.5 CCK (one-way ANOVA, $p > 0.1$). We therefore normalized these parameters by dividing to the mean of the sham condition (both at baseline and recovery) followed by paired t-test to detect the effect of stimulation Figure 4.3A-D). It was proposed that a higher homeostatic need for recovery results in less neuronal activity (Rodriguez et al., 2016). This can be achieved by a decrease in the incidence of UP states and/or longer neuronal silent periods (DOWN states).

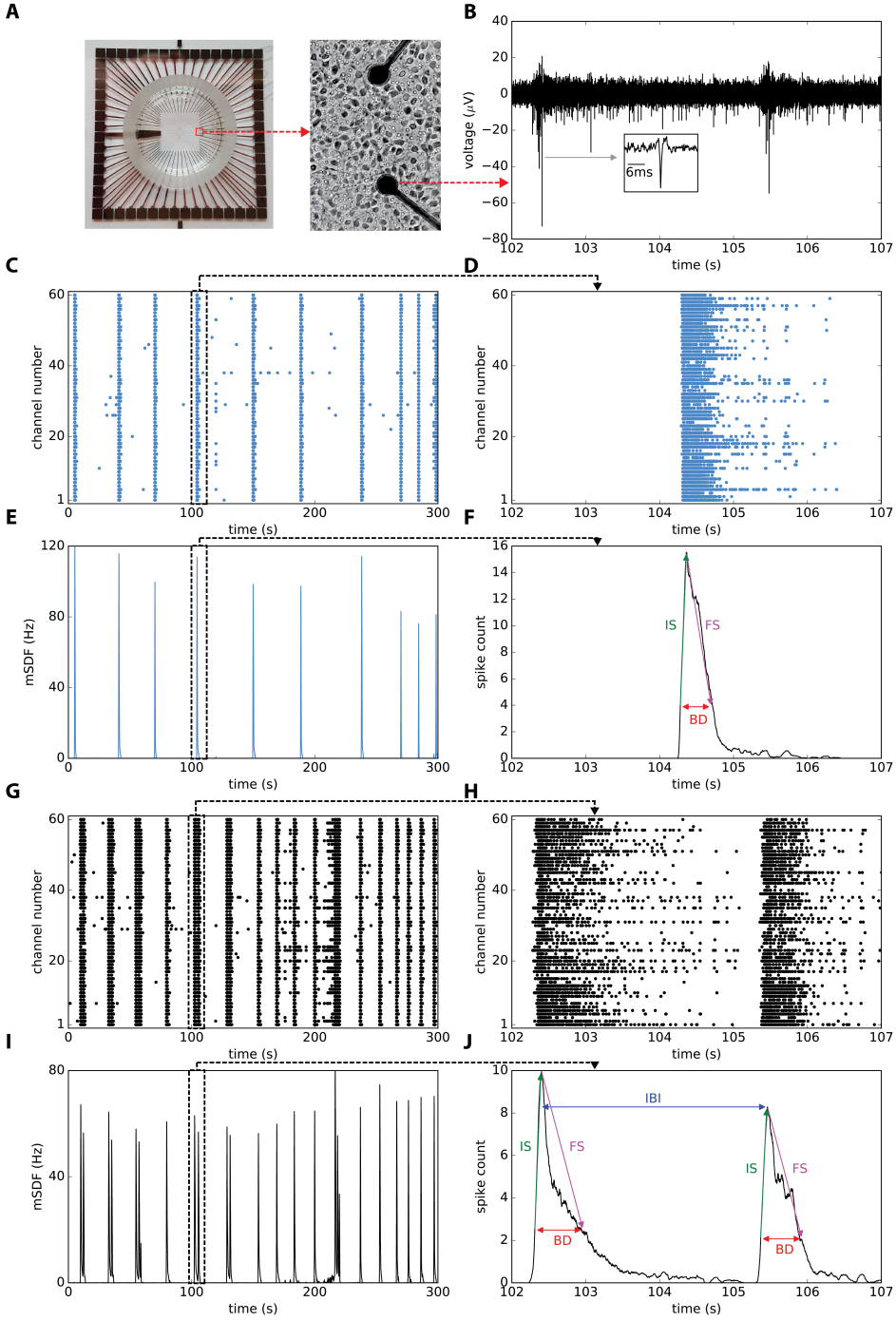

Figure 4.1: Synchronized burst firing and burst characteristics in representative MEA recordings of a 14DIV mouse cortical culture at baseline and during recovery. **A**) Picture of an MEA with 60 electrodes and zoomed figure of two electrodes with neuronal culture. **B**) Five seconds of raw MEA recording. The inset shows a typical spike at higher resolution. Five minutes raster plots and mean spike density function (mSDF) recorded in one culture at baseline (**C**, **E**) and during recovery (**G**, **I**). Zoomed figures of raster plots (**D**, **H**) and mean spike density (**F**, **J**) provide higher resolutions. Automatic detection of bursts with their parameters are shown in **F** and **J**. IS: initial slope, FS: final slope, BD: burst duration, and IBD: inter-burst duration.

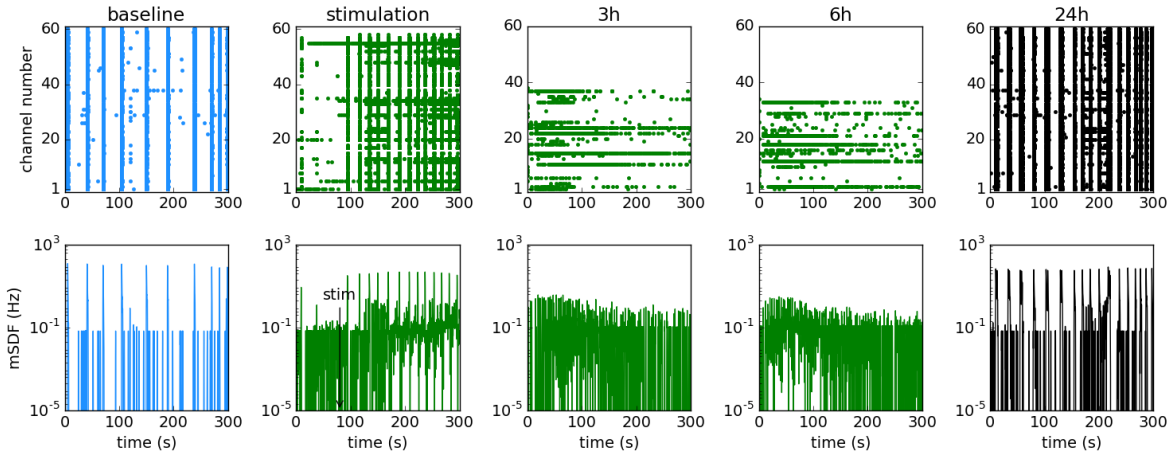

Figure 4.2: Time course of the network firing behavior. A representative MEA recording at baseline and following stimulation with a cocktail of neuromodulators. Tope panels show the raster plots and lower panels the mean spike density functions. Stimulation results in the disappearance of bursting activity which is replaced by tonic firing. The bursting activity recovers after 24h. Lower panels are presented in log scale to visualize the low amplitude high frequency tonic activities after stimulation.

In vivo intracellular recordings of cortical neurons during recovery sleep after sleep deprivation are lacking, but our results clearly show that the burst duration during recovery is significantly increased after both 1 ($p < 0.04$) and 0.5 ($p < 0.02$) CCK stimulation and inter-burst interval is significantly decreased after 1CCK stimulation ($p < 0.02$) (Figure 4.3B,C). These findings suggest that higher homeostatic pressure in vitro results in an increased incidence of bursts (UP state) and a decreased inter-burst interval (DOWN state).

4.3.2 Burst slopes

In vivo EEG recordings in humans and LFP recordings in rats, as well as computational simulations, indicated that the right shift in the major slow frequency power density is related to steeper slopes of slow waves (Riedner et al., 2007; Vyazovskiy et al., 2007). Changes in the slope of slow waves are caused by the synchronization of neuronal activity in the network, so that faster synchronization events lead to steeper slopes (Vyazovskiy et al., 2009). In our recordings the shape of the bursts depends on the firing activity recorded across electrodes (spike density) and therefore the height of the burst envelops is limited by the density of spikes recorded and the number of active electrodes. We therefore calculated the slopes of the rising and decaying segments of the burst envelops (Figure 4.1J) and compared them between baseline and recovery (24h after stimulation) recordings. Both initial and final slopes significantly increased during recovery and these changes were larger after 1CCK (initial slope, $p < 0.05$, final slope, $p < 0.01$) than after 0.5CCK stimulation (initial slope, $p < 0.05$, final slope, $p < 0.05$), while no changes were observed after sham stimulation (initial slope, $p = 1$, final slope, $p > 0.40$) (Figure 4.3D,E). Note that the final slope, which we found highly significantly steeper, is equivalent to the first

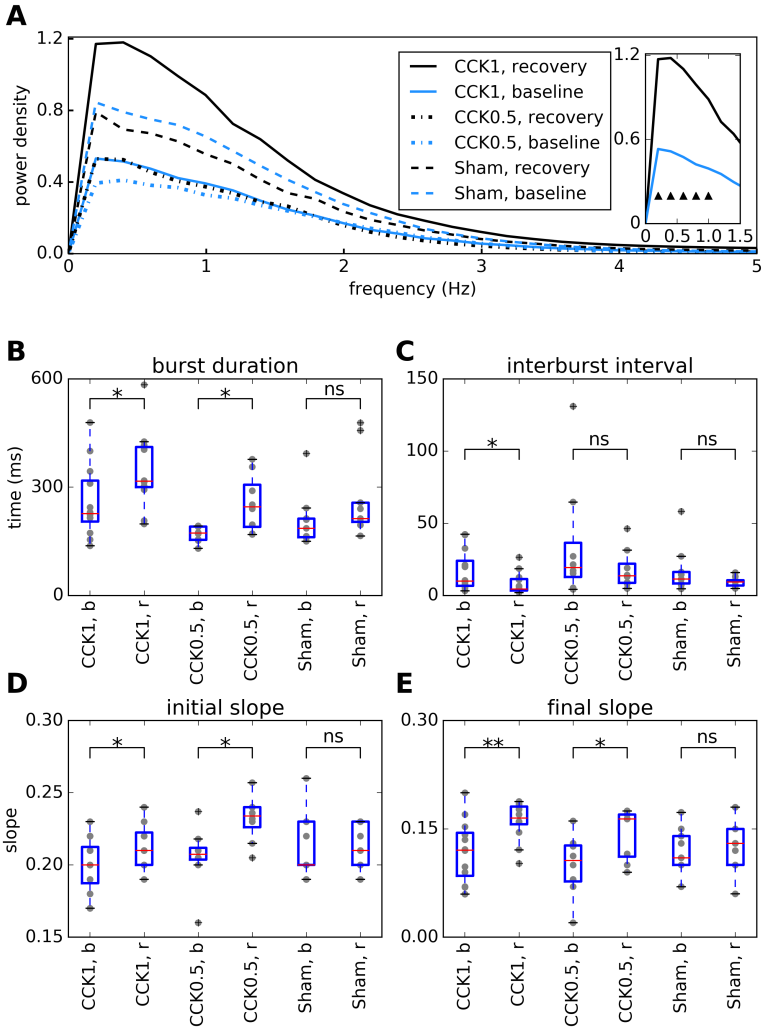

Figure 4.3: Spectral and burst properties of in vitro cortical networks at baseline and during recovery after neuromodulatory or sham stimulation. **A**) Spectral power density of bursting activity of cultures during baseline (blue lines) and recovery (black lines) for 1CCK ($n = 12$), 0.5CCK ($n = 8$), and sham stimulation ($n = 9$). The power spectrum shows an increase with a shift toward higher prominent peak (~ 0.45Hz) during recovery compared to baseline (~ 0.31Hz). The inset indicates the significant increase (triangles) and shift in power for 1CCK ($p < 0.05$; post hoc Tukey test after 2-way ANOVA with repeated measures). (**B**) Burst Duration (BD) is significantly longer and (**C**) the inter-burst interval (IBI) is shorter during recovery for 1CCK and 0.5 CCK while there is no change in sham stimulated cultures. (**D**) Initial and (**E**) final slopes are significantly increased after 1CCK and 0.5 CCK stimulation while no change is observed after sham stimulation. Each dot represents a single culture. B: baseline, r: recovery, ns: non-significant, * $p < 0.05$, ** $p < 0.01$; paired t-test on relative values (to the sham condition).

segment of negative waves as recorded by the LFP and the EEG.

4.3.3 Cross correlation

The homeostatic response after prolonged wakefulness in vivo, is manifested during recovery sleep in an increase in neuronal synchronization across large cortical regions. In our preparations, the level of synchronization in spatiotemporal neural network can be reliably measured by cross-correlation between electrode pairs. As shown in Figure 4.4, cultures recorded 24h after stimulation at 1CCK show a higher cross-correlation than baseline, indicating that recovery from stimulation leads to a stronger and larger synchronization across the network. However, the increase in synchronization does not occur across the entire recording dish but is restricted to clusters of electrodes (Figure 4.3B).

4.3.4 Firing rate, burst duration histogram and neural trajectory

Increase in sleep need not only increases synchronization but also increases excitability during the UP state and in susceptible human subjects may lead to seizures (Steriade, 2006; Lawn et al., 2014). Overall, spike rates did not significantly change between the three conditions or between baseline and recovery. Nevertheless, frequency distribution of spike counts indicated more channels with higher spike rates during recovery after 1 and 0.5CCK stimulation (Figure 4.5A,B, right shift in spike rate distribution), while no difference was found after sham stimulation (Figure 4.5C).

The temporal structure of the network activity was also analyzed by two additional methods. First, there is a positive correlation between BD and the number of spikes across all channels, so that longer bursts recruit more channels with higher spike numbers both at baseline and during recovery (Figure 4.5D). Nevertheless, during recovery there is a stronger correlation (between regression lines, $p < 0.005$, z-score, Figure 4.5D) with a clear increase in longer bursts ($p < 0.05$, cross-tabulation) with higher spike numbers ($p = 0.07$), resulting in the appearance of a second peak in the distribution of BD and spike numbers (Figure 4.5D).

Second, to analyze the temporal evolution of the firing rate (network behavior) we used neural trajectory analysis. A neural trajectory describes the time evolution of network population activity that can be traced over time in the space (Cowley et al., 2013). By using a 2-d projection of firing rate space, we mapped the network activity, with different phase and amplitude, that starts at a local temporal space (dense central neural activity) and propagates globally over the network. Figure 4.5E,F show neural trajectories of two representative cultures at baseline and during recovery after 1CCK stimulation. Increased number of black circle traces in both cultures during recovery indicates a strong phasic synchronized activity compared to baseline (blue circle traces). Differences in neural trajectories suggest that not all neurons but selected groups of neurons (local clusters) contribute to the network population activity.

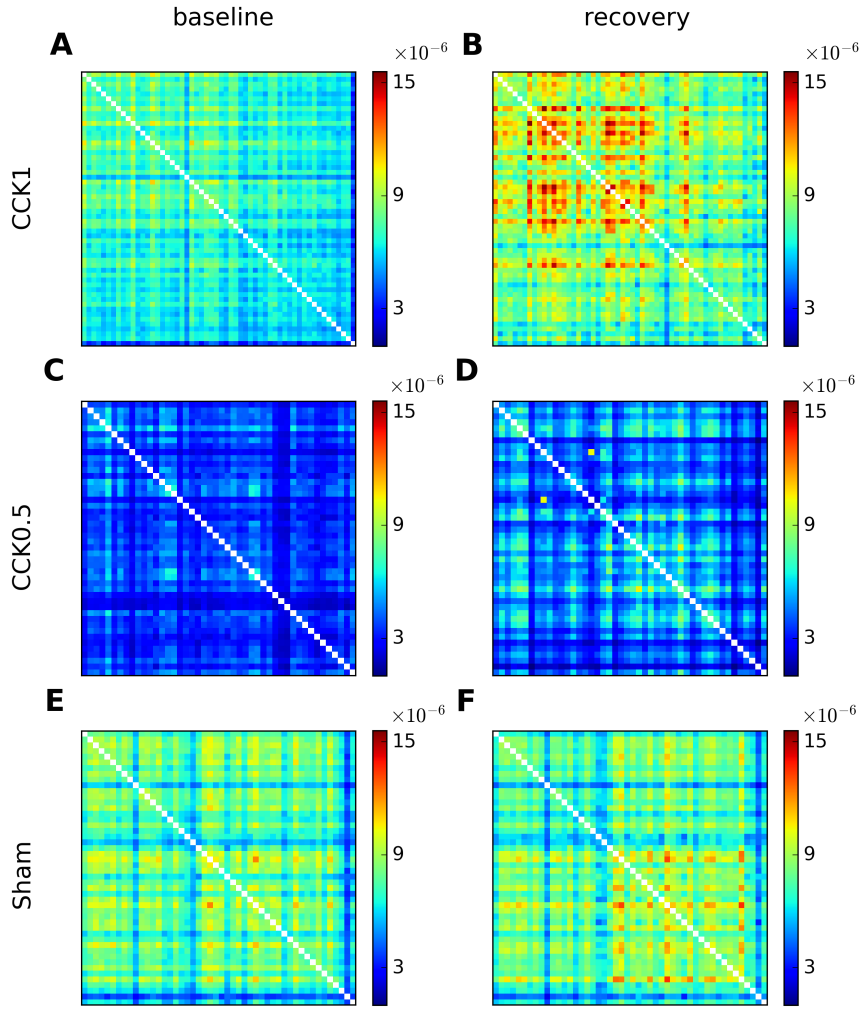

Figure 4.4: Cross-correlations between paired MEA channels averaged across all cultures. **A-F**) The cross-correlation of spike trains between paired MEA channels at baseline (**A**, **C**, **E**) and during recovery (**B**, **D**, **F**) after 1CCK (**B**), 0.5CCK (**D**), and sham (**F**) stimulation. The population channel activity reveals higher temporal cross-correlation between discharge times of spikes during recovery for 1CCK (**B**) where the level of synchrony is increased. There is no change between baseline and recovery after 0.5CCK (**D**) and sham stimulation (**F**). 1CCK ($p < 0.05$, Kolmogorov-Smirnov test).

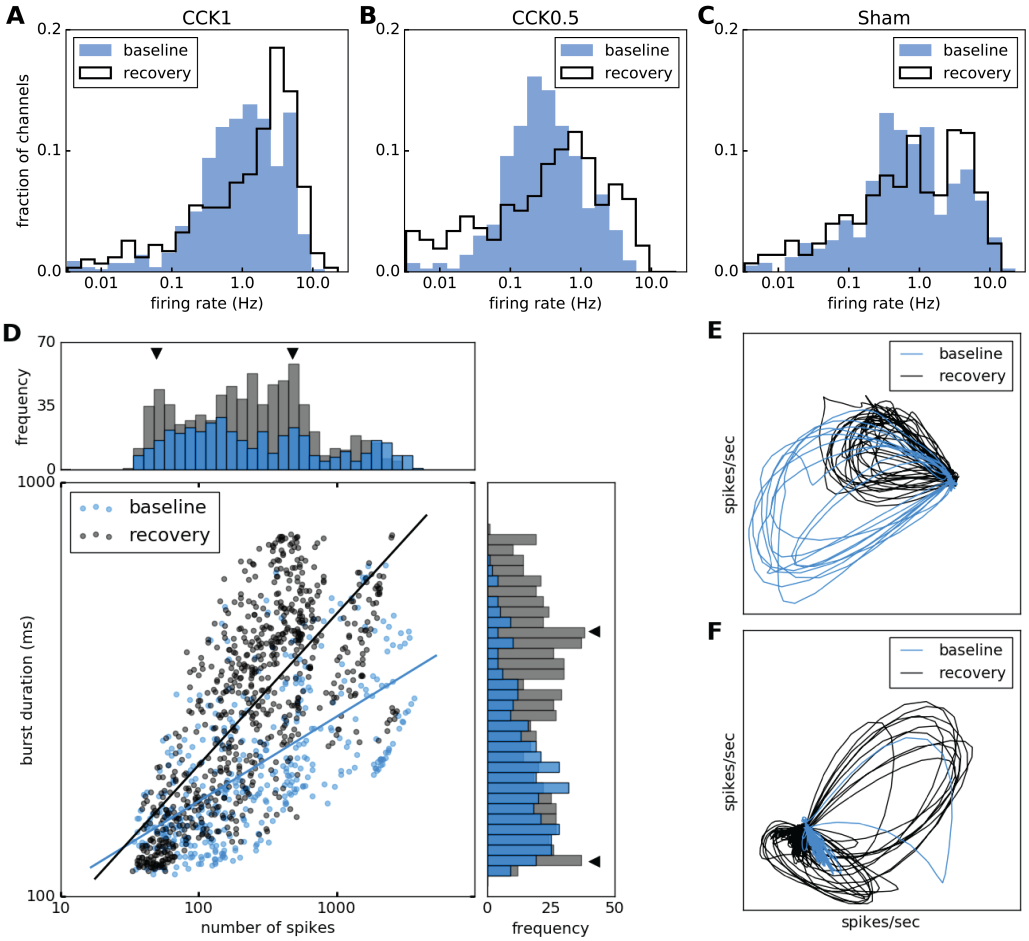

Figure 4.5: Changes in firing rate during bursts. **A-C**) Firing rate distributions at baseline (blue) and during recovery (black) after stimulation with the neuromodulatory cocktail at 1 and 0.5 CCK or after sham stimulation. More MEA channels present higher spike rate during recovery after 1 and 0.5CCK stimulations (right shift in the distribution). (**D**) Correlation between the burst duration and the number of spikes (log scales) at baseline (blue) and during recovery (black) and the corresponding frequency histograms. Triangles indicate changes in frequency histograms during recovery. (**E-F**) Neural trajectories for two representative cultures captured by a 2-d projection of firing rate space. (**E**) The neural trajectory of spontaneous activity in one culture for baseline (blue) and recovery (black). The X and Y axes correspond to projection vectors that are linear combinations of firing rates. Two characteristics are detected: phase and amplitude. The strong phase between up and down states are reflected more in recovery (circle traces) with lower amplitude. (**F**) Increasing number of circle traces with higher amplitude in this culture during recovery (black) compared to lower one in baseline (blue). For both cultures the neural trajectories start from one point locally and propagate in firing rate space with various phases.

4.3.5 Simulation of neural network behavior and topology

Sleep is local and use-dependent (Krueger et al., 2008). Cortical networks or even individual cortical columns that are highly stimulated during wakefulness show higher probability to enter sleep with larger increase in SWA (Kattler et al., 1994; Rector et al., 2005, 2009). Also, small cortical networks can show signs of sleep in otherwise awake and sleep deprived animals (Vyazovskiy et al., 2011b). Therefore, the recruitment of larger cortical areas by small neural clusters might result to the whole network sleeping behavior while individual neurons might not. To test if the network behavior can be predicated by local (cluster) activity shaping the overall network behavior we built several neural networks with different topologies and obtained their behavior at baseline and during recovery using computer simulation. Recovery processes include changes in synaptic weight and network topology (connectivity). Obviously, cortical cultures lack the intact cortical connectivity and each culture is unique in terms of established network. We propose that the structure and topology of neural networks in vitro plays an important role in generating the network oscillation and establishing its properties (e.g., duration of bursts or the regularity of oscillations). A network feature which is often used for modeling neural networks is the neural cluster (also called neural assembly). A neural cluster is a subgroup of neurons with dense connectivity or strong synaptic weight. Previous studies showed that embedding neural clusters in a larger network significantly changes the dynamics and behavior of the whole network (Litwin-Kumar and Doiron, 2012; Mazzucato et al., 2015). Here we embedded one or two clusters of excitatory neurons to produce oscillations.

We built a network with 900 inhibitory neurons and 3000 excitatory neurons (see Materials and Methods). To reproduce the dynamics of the recorded culture in Figure 4.1, we embedded a cluster of 95 neurons in the excitatory population. Figure 4.6D shows the schematic of the network at baseline. Both synaptic weight and connection probability are higher inside clustered neurons compared to the connections between non-clustered neurons and between non-clustered and clustered neurons (see Materials and Methods). To display the results as multielectrode array recordings, we defined 60 channels. For each channel, we randomly picked 4 neurons from the network and aggregated their spikes. Figure 4.6A-C shows the raster plot of channels and simulated mean firing rate (filtered with a Gaussian function, $\sigma = 100$ms) at baseline. Simulated multiunit firing of a 9 second recording in Figure 4.6A is shown at higher resolution in Figure 4.6. We assume that increasing the firing rate of neurons after stimulation with the waking cocktail triggers long-term synaptic plasticity and modifies the synaptic weight between neurons. Therefore, this might lead to a new connectivity structure in the neuronal network. In this simulated culture, we suggest that the new structure has two clusters with 95 and 90 neurons (Figure 4.6H). In other words, the stimulation adds another cluster in excitatory neurons population. Therefore, the culture exhibits a different oscillatory behavior (Figure 4.6E,G). As observed in the experimental data, changes in burst duration (Figure 4.6I) and inter-burst intervals (Figure 4.6J) are very similar between the experimental and simulated data. Using a similar number of simulated inhibitory and excitatory neurons we also reproduced the behavior of another culture with a different connectivity structure (Figure 4.7). During the baseline phase, we defined two clusters with 65 and 40 neurons. This structure showed a similar dynamics to the baseline recording (Figure 4.7). To simulate the dynamics of

the culture during recovery, we assumed that stimulation results in merging of the two clusters with a new and bigger cluster with 100 neurons (5 clustered neurons lost their connections to other neurons). This new structure reliably showed a network oscillation similar to the experimental data (Figure 4.7). In summary, we showed that the network topology (number of neural clusters and size of each cluster) determines the properties of oscillations and behavior of neurons. We assumed that the different oscillatory behavior of each cluster is due to different topologies. Also, stimulation may change the topology of the network, which leads to different burst durations and inter-burst intervals at baseline and during recovery.

4.4 Discussion

In this work we studied the network activity of cultured cortical neurons at baseline and during recovery after stimulation by a cocktail of waking neuromodulators. Our aim was to investigate if the behavior of the network during recovery (when slow oscillations reappear) shows homeostatic changes as seen during sleep in living animals. We found that during recovery the inter-burst interval is decreased while the burst duration is increased. Moreover, the power density in slow frequencies is increased together with the slope of UP and DOWN states. Our results clearly indicate that during recovery the neural network correlated activity shows a higher temporal and spatial synchrony, reminiscent of the patterns observed during recovery sleep after sleep deprivation in vivo. The overall changes during recovery are dose-dependent with stronger stimulations (1CCK) leading to larger differences, similar to longer wakefulness durations leading to larger sleep changes in vivo. We also show that neural trajectory method could trace temporal evolution of neuronal firing during recovery as a result of a higher synchrony with stronger phasic neural oscillation (UP and DOWN). Our simulations strongly suggest that the overall network behavior can be predicted by changes in activity of clusters within the network. One important finding resulting from in vitro preparations or isolated cortical islands is that neural networks default activity state is synchronized slow oscillations (sleep-like state) (Corner et al., 2008; Hinard et al., 2012; Kaufman et al., 2014; Lemieux et al., 2014; Jewett et al., 2015). More importantly, continuous stimulation or inhibition cannot prevent the return to this default mode (Kaufman et al., 2014; Slomowitz et al., 2015). Note that in our experiments, the cultures were stimulated with a cocktail of neuromodulators without wash out. Although different neuromodulators might have different half-lives, signaling mechanisms, and time courses of feed-back induction (Mikhail et al., 2017), our cultures are most probably nearly continuously stimulated. In an elegant experiment, cortical cultures were continuously stimulated with carbachol or noradrenaline leading to the disappearance of synchronous bursting that recovered within 24 hours (Kaufman et al., 2014). Therefore, the default slow oscillation is regulated by homeostatic processes that play as strong attractors bringing the network activity back to its set-point. The underlying cellular and molecular mechanisms remain unknown. Obviously receptor desensitization might not be involved since for instance continuous cholinergic stimulation renders the cortical networks insensitive to noradrenergic stimulation (Kaufman et al., 2014), although changes in overall receptor trafficking cannot be excluded. Recent observations also suggest that changes in firing rate are not compatible with transcriptional modifications

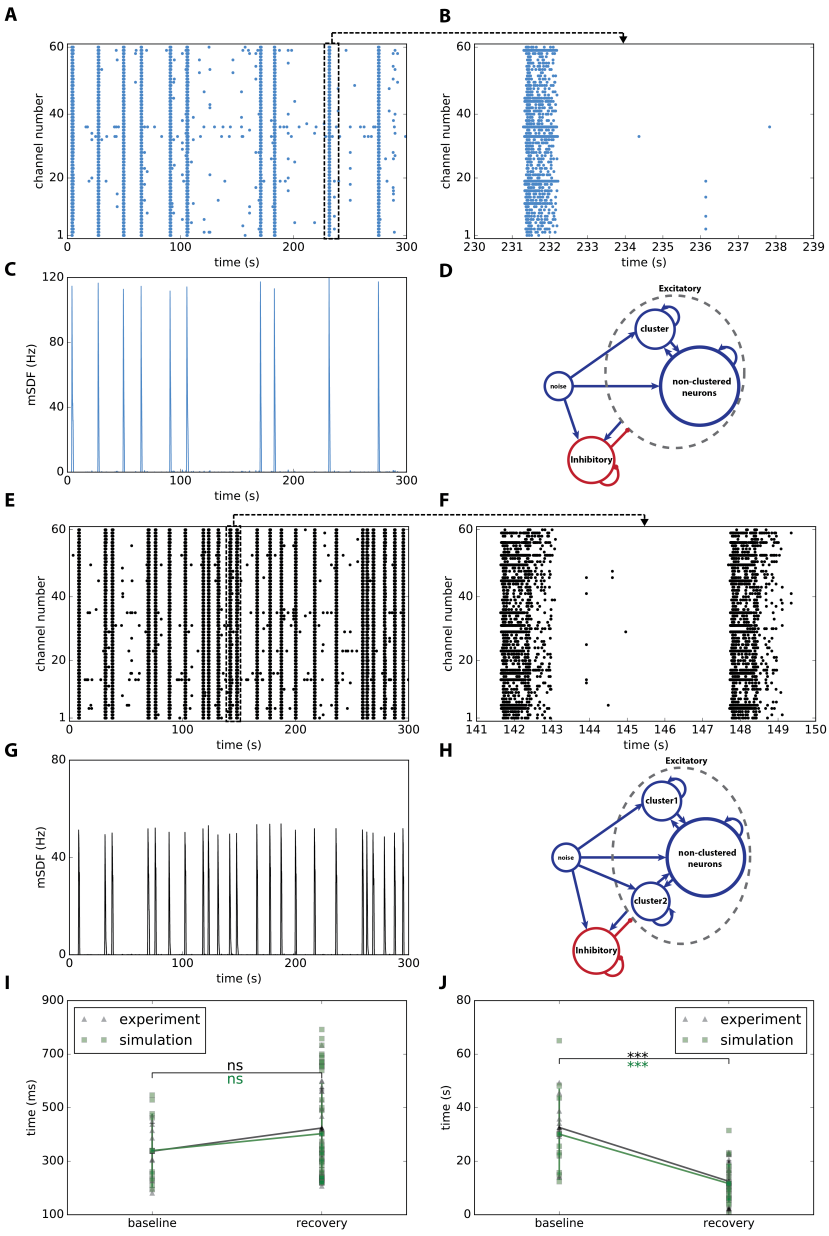

Figure 4.6: Computer simulation of the network firing behavior of the culture shown in Figure 4.1. Network topology changes after the stimulation: while we used only one cluster at baseline (**D**), we assumed that another cluster appeared in recovery (**H**). Simulated raster plots (baseline **A**, recovery **E**) and mean spike densities (baseline **C**, recovery **G**) are similar to experimental data (Figure 4.1). A 9 second higher resolution of simulated multiunit activity (baseline **B**, recovery **F**) shows typical bursts. Comparisons of burst durations (**I**) and inter-burst intervals (**J**) between experimental and simulation data indicate a very similar pattern (inter-burst intervals are significantly longer in both conditions during recovery; *** $p < 0.001$, ns: non-significant).

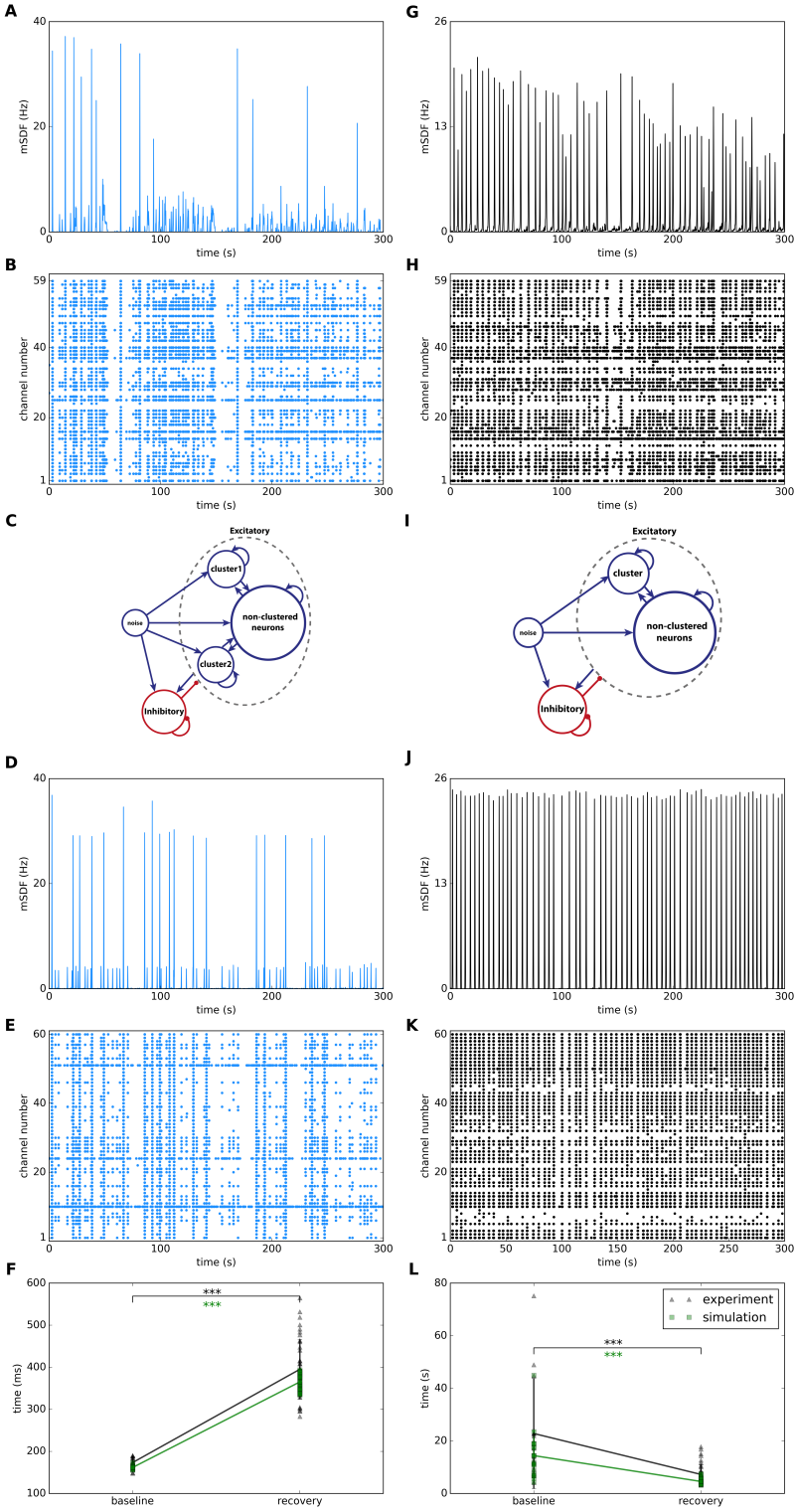

Figure 4.7: Computer Simulation of the network firing behavior of the second culture. Experimentally recorded

Figure 4.7: ***(Continued)*** mean spike density function and raster plot of the culture in culture in the baseline mode (**A**, **B**) is different with the recovery mode (**G**, **H**). In order to reproduce similar dynamics with the computer simulation we assumed that the network has two clusters in the baseline mode (**C**), while they merge into one cluster after the injection (**I**). Simulated mean spike density functions (baseline **D**, recovery **J**) and raster plots (baseline **E**, recovery **K**) are similar to the recorded data. Comparisons of burst durations (**F**) and interburst intervals (**L**) between experimental and simulation data indicate a very similar pattern (burst durations and interburst intervals are significantly longer in both conditions during recovery; *** $p < 0.001$, t-test).

(Hengen et al., 2016). Other mechanisms such as intracellular calcium or membrane homeostasis might be involved (Maret et al., 2007; Hinard et al., 2012; Ding et al., 2016). Interestingly, by using different methods and electrical or TNF alpha stimulation of cortical cultures, a similar pattern of homeostatic regulation was also observed (Jewett et al., 2015). The cellular mechanisms of recovery during sleep are poorly investigated. Nevertheless, detailed analysis of slow oscillations during human sleep at baseline and during recovery indicated very similar changes as reported here (Bersagliere and Achermann, 2010). As opposed to the recent report by Rodriguez et al., 2016 multiunit activity in freely behaving mice, where an increase in OFF state was reported (longer inactivity periods), both in vivo and our results indicate that recovery leads to more frequent UP and DOWN states (Bersagliere and Achermann, 2010) with longer UP and shorter DOWN state. Also, experimental and computational data indicated that higher sleep need leads to steeper slope of the slow oscillation (Riedner et al., 2007; Vyazovskiy et al., 2007) as reported here. In previous studies, the homeostatic recovery of firing rate was investigated mainly by inhibition, such as visual deprivation in vivo (Hengen et al., 2016) or $GABA_B$-mediated silencing in vitro (Slomowitz et al., 2015), with in vivo findings favoring a cell-autonomous while in vitro results favoring a network homeostatic process. Nevertheless, even in the visual deprivation paradigm, the homeostatic regulation of firing rate set-point was found dramatically affected by ongoing network activity (wakefulness promoting and sleep inhibiting recovery) (Hengen et al., 2016). Obviously, neuronal activity depression requires activity (wakefulness) while over-activation requires sleep.

Whether the homeostatic mechanisms are cell autonomous or properties of networks remain controversial (Slomowitz et al., 2015; Hengen et al., 2016). In vitro observations strongly favor the network hypothesis (Slomowitz et al., 2015). Also, the recent development of high density MEAs based on CMOS technology (with 4096 microelectroldes) revealed a high number of random firing activity while the overall network behavior was driven by synchronized bursts (Lonardoni et al., 2015). Excitatory cortical neurons are known to form privileged synaptic connections to form clusters (Perin et al., 2011). We show that similar to intact cortex, the number of clusters, number of neurons in each cluster, synaptic weights, and connection probability inside and outside the clusters, as well as the amount of noise that each neuron receives affect the shape of the oscillations. Using our simulation model, we expected weak connections between neurons during the early days of cell cultures to be able to establish neural clusters and network oscillations. As the cell culture proceeds to maturation, connections are formed between neurons and stronger connections maintained by synaptic plasticity. These neurons form the clusters through long-term synaptic plasticity rules (Zenke et al., 2015) and the network

produces oscillations during the baseline phase. Stimulation with our waking cocktail forces neurons to discharge at higher rates for a long period of time (nearly 24h). Based on the firing pattern, synaptic plasticity modifies the structural connectivity between neurons leading to the formation of new clusters or the collapse of existing ones. The number of neurons in the cluster may also change. The new structure leads to a new oscillation (recovery mode) with different properties compared to the baseline oscillation (before stimulation). It might happen that the new architecture is unable to produce oscillations.

A major discrepancy between sleep homeostasis as indexed by the EEG SWA and neuronal firing homeostasis is the large difference in their time course. While SWA shows a fast kinetics, typically within tens of minutes in rodents and a few hours in humans, network homeostasis, both in vitro and in vivo takes up to two days (Slomowitz et al., 2015; Hengen et al., 2016).

Although the slow oscillation (<1 Hz) is at the basis of slow waves recorded by the EEG, other oscillations such as delta waves and spindles are critically modulated and/or generated by the cortico-thalamic network. How such oscillations are regulated remains unknown. Nevertheless, the spontaneous generation of such oscillations in more complex thalamo-cortical co-cultures (or interconnected through microfluidics devices) may be obtained and being subjected to detailed analysis as reported here.

Acknowledgment

The work was supported by the Swiss National Science Foundation (146615 to Mehdi Tafti), the University of Lausanne, and the Novartis Foundation (to Mehdi Tafti). Hesam Setareh is supported by the European Research Council (grant 268689). We thank V. Hinard for her original contribution to this work. We also thank V. Vyazovskiy and A. Becchetti for their comments.

Chapter 5

Conclusion and future work

5.1 Conclusion

In this thesis, we developed a specific model of neural assemblies and networks containing these assemblies in order to explain a large amount of experimental data extracted from cortical networks and cell cultures similar to related works on Hopfield models (Hopfield, 1984, 1987) and attractor memory models (Amit and Brunel, 1997). We have shown that a neural assembly can have a bistable dynamics. The assembly is either quiet or generates high firing rates. Adding background noise or a transient stimulus forces the assembly to switch to the high-rate state. Spike-frequency adaptation enables the assembly to switch back from the high-rate state to the quiet state. Therefore, the neural assembly together with synaptic input and spike-frequency adaptation is able to switch between two different dynamical regimes. These dynamics provide a unifying model feature which is the basis of all network models presented in this thesis.

We combined neural assemblies in different forms and each instance produced a biologically plausible network dynamic. In chapter 2 we embedded several assemblies in bigger networks for generating up-state/down-state oscillations observed in anesthetized cortex. These networks were also able to exhibit different stimulus-evoked responses observed in cortical layers. In chapter 4 we repeated the same approach for reproducing oscillations of cell culture networks. We illustrated that manipulating the number and size of assemblies affect the properties of oscillations. Hence, we were able to generate different oscillations observed in cultures using different formations of assemblies. In chapter 3 we formed a chain of bidirectionally connected assemblies in order to propagate neural activity with tunable speed. Then, we extended the chain to a 2-dimensional grid and used it for simulating different activity patterns observed in mice barrel cortex.

In the models presented in this thesis we used neuron and network parameters extracted from experiments (Lefort et al., 2009; Avermann et al., 2012; Mensi et al., 2012; Pozzorini et al., 2015). Using these biologically observed parameters, spike-frequency adaptation and neural assemblies, we reproduced experimentally observed behaviors, e.g., slow oscillations of cortical neurons (Steriade et al., 1993a; Petersen et al., 2003b), stimulus-evoked responses (Beltramo

et al., 2013), activity circulation in barrel cortex (Petersen et al., 2003a,b) and slow oscillations observed in cell cultures (experimental data are shown in chapter 4).

In summary, we stated that small groups of neurons (assemblies) are able to drive a big network and shape their dynamics. Therefore, in order to build a network model for reproducing a desired dynamic, it is better, in our view, to focus on assemblies first and find a good formation of them. Then, we can add non-assembly neurons. This approach reduces simulation time and makes the modeling process easier and faster.

5.2 Future work

The models introduced in this thesis can be extended in several aspects. In this section we present some ideas that could be investigated in future.

In this work, we did not explore the role of inhibitory neurons. Their role was limited to regulating assemblies and reducing firing rates. In chapter 3 inhibitory populations reduced the propagation speed. While we used one type of inhibitory neurons, experiments (Rudy et al., 2011; Gentet et al., 2012) unravel different inhibitory neuron types with different properties and probably different roles in the cortex. One may use several inhibitory populations in the model and define different functionality for each of them. For example, in chapter 3, while one inhibitory neuron type reduces the propagation speed, another inhibitory neuron type can decrease the firing rate of assemblies by providing a significant amount of inhibition.

We mentioned in chapter 3 that using a learning rule we can strengthen the synaptic weights between assemblies and increase the propagation speed. Therefore, if we use the chain as sequence generator for a behavioral task, repetition of the task will lead to stronger synapses and therefore increase the speed of performing the task. However, we did not implement this idea and left it for future work.

We may scale up the multicolumn model of barrel cortex introduced in chapter 3 in order to simulate the dynamics of whole cortex. If we do this, we speculate that we will be able to maintain several activity waves in the model and generate more complicated dynamical patterns. However, such a big model contains huge numbers of neurons and populations. Hence, the simulation becomes very slow. One solution is using parallel programming technics and running the simulation on several machines for simulation instead of one. Another solution is using population models which approximate the activity of a homogenous neuron population with a set of equations (Deco et al., 2008; Naud and Gerstner, 2012a; Deger et al., 2014; Schwalger et al., 2017). In this case, we replace each population by a population model and reduce each column (that we used in chapter 3) to three population models: assembly, non-assembly and inhibitory neurons. Such a population model should be able to simulate whole cortex and preserve time efficiency.

Appendix A

Reproducing monkey scribbling using the chain of assemblies

Here we propose an architecture for reproducing the drawing movement of a monkey (Polyakov et al., 2009). The excitation chain, introduced in chapter 3, plays a key role in forming the rhythm of generated movements as well as the speed of drawing.

Several studies (Hogan, 1984; Hogan and Sternad, 2012; Giszter, 2015) showed that complex motions are composed of motor primitives, which can be considered as building blocks for constructing motions. In other words what we observe as a complex movement may arise from a sequence of simple patterns. Polyakov et al. (2009) studied two monkeys and let their right hands operate a two-joint low-friction manipulandum. In order to motivate monkeys to generate scribbling movements, a random target in a tiled grid of many possible targets was chosen. The monkeys only saw a cursor indicating the position of the hand while the target was invisible. Since the monkeys had no knowledge of target location, they produced trajectories that covered the entire workspace and moved the hand until reaching the target. If they could reach the target within 5 seconds, they were rewarded. Otherwise another target was chosen randomly. This procedure repeated several times. The analysis showed that the scribbling trajectories made by the monkeys were combinations of parabolic movement primitives. Consequently, in the architecture of our movement generator model we have blocks that produce parabolic trajectories in case of receiving activation signals. We refer to these blocks as *translator units*, as they translate the input activation signal to movement parabolas.

Figure A.1A shows the schematic of our model. The two main neuronal elements are the rhythm generator and the translator units. The excitation chain works as the rhythm generator and activates the translator units one after each other. The translator units are designed to send out four signals, one for each direction that the monkey's hand can move (right, left, up and down). Once a translator unit becomes activated, the model produces a parabolic motion (a particular movement primitive) with special properties (concavity, horizontal/vertical symmetry, as discussed below). These properties depend on the internal implementation of the translator unit. A biomechanical block then receives the direction signals from the translator

units and employs muscles in order to move the monkey's hand into the respective direction. However, we do not implement neither the biomechanical block nor the muscles into in our architecture and consider the output of the model to be the four direction signals provided by the translator units. These four signals suffice to sketch the trajectories. Supposing that the firing rate (estimated with 2ms bin size) of each directional output of the translator units denotes the velocity of movement in that direction at any moment in time, we can visualize the scribbling made by the model (Figure A.1B).

According to the experimental study (Polyakov et al., 2009) the speed of drawing increases as the monkeys continue to practice. Our model provides a possible interpretation of this finding. During the scribbling, the assemblies of the excitation chain become active sequentially, i.e. the spiking activity of each assembly drives the next one to also spike . Synaptic learning rules such as Hebbian spike-timing dependent plasticity imply that this kind of activity will potentiate the synapses between these assemblies. Now, as we have shown in chapter 3, increasing the inter-assembly weights increases the speed of activity propagation in the chain. Therefore, the chain assemblies activate the translator units more quickly than before, and thus increases the speed of drawing (Figure A.1B).

Figure A.1C shows the internal structure of a neuronal translator unit which generates a parabolic movement from top-left to top-right on the screen (Network parameters are reported in Table A.1.). This parabola has horizontal symmetry and is concave. The translator unit receives an activation signal from an assembly of the excitation chain. Since, in this case, the hand always moves to right, the left direction signal remains inactive. Conversely, the right direction signal should be active during the presence of input activation signal. In order to implement this, a neuronal population receives the activation signal and fires. Its firing rate denotes the right signal strength. The down signal should be sent out immediately after starting the activation and should last during almost the first half of activation. The down signal is implemented by a similar neuronal population as the right signal. The difference here is that the synapses between the assembly and the down population express short-term depression (Tsodyks and Markram, 1997). Therefore, the amount of excitation that the down population receives from the assembly gradually decreases and the firing rate of the down population and consequently the strength of the down signal decays. On the contrary, the up signal should remain quiet during the first half and rise after that. The firing rate of a fourth population, which is called up population, is used to code the strength of the up signal. By using weak synapses from the assembly to the up population, it takes some time until enough input accumulates until the up population starts to fire. In this manner, with carefully tuned parameters, the translator unit can produce the parabola. Figures A.1D and E illustrate the firing rate of each population and the parabola made by the unit during the presence of activation signal. By rearranging the internal structure of the unit, it can be used to produce different parabolas. For instance, if we interchange the up and down populations respectively by the right and left populations, the unit produces a vertical symmetry parabola with concavity to the right. Neuron model and parameters as well as parameters of the chain are the same as parameters we used in chapter 3 (Reported in Table 3.1 and 3.2).

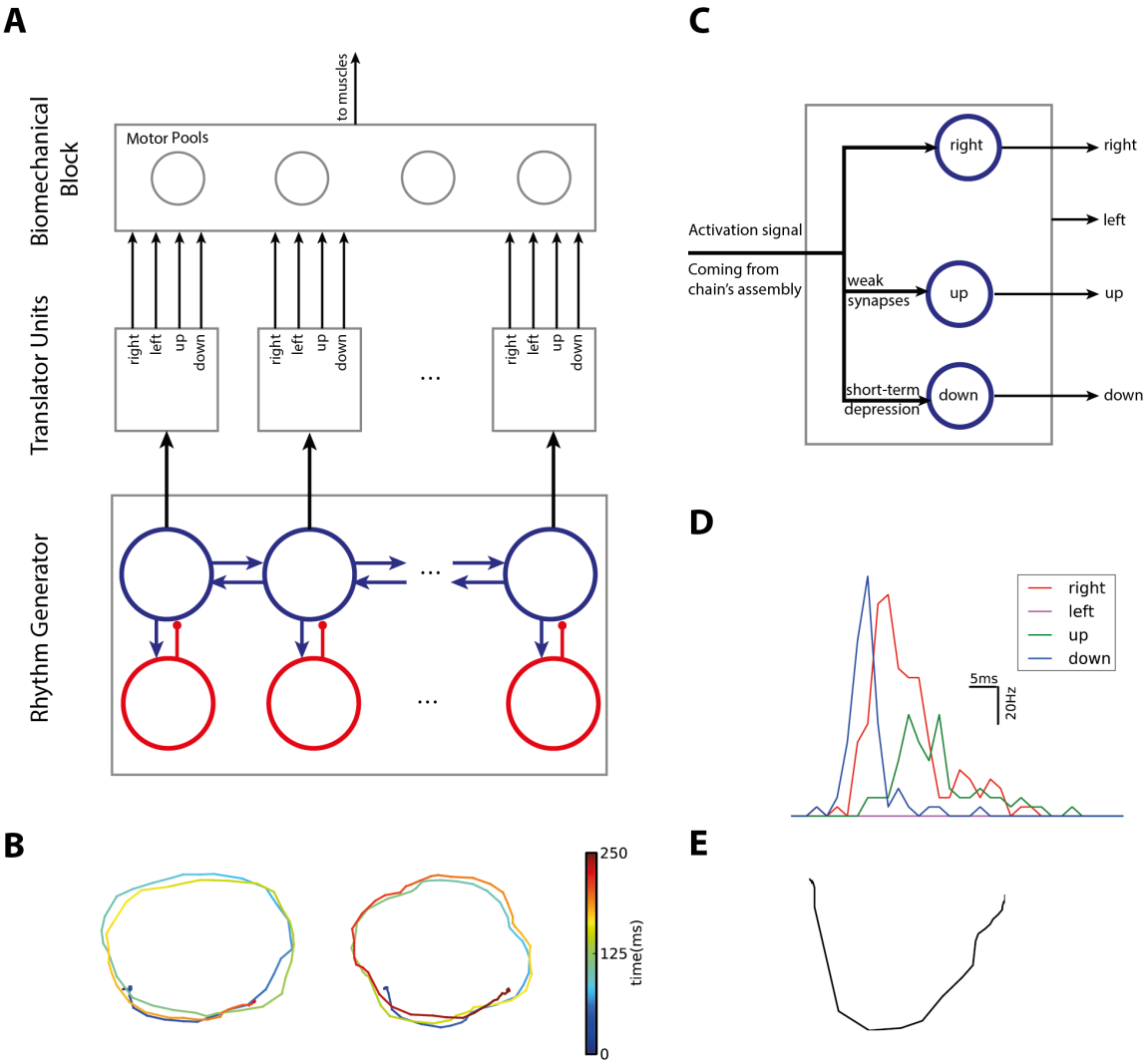

Figure A.1: Neuronal circuit model for reproducing monkey scribbling. **A**) The circuit consists of a rhythm generator (which is implemented by the excitation chain), a neuronal translator units and a biomechanical block which employs muscles to produce movements by using four direction signals. **B**) Trajectories made by the system are composed of several parabolas, several example trajectories are shown. The left trajectory (ends at $t = 190$ms) is drawn faster than the right one (ends at $t = 250$ms) because of the different propagation speeds of the excitation chains ($w_{\text{exc}} = 0.6$mV, $w_{\text{inh}} = 0.25$mV for the left one and $w_{\text{exc}} = 0.4$mV, $w_{\text{inh}} = 0.25$mV for the right one) **C**) Schematic of a neuronal translator unit. It receives the activation signal from an assembly of the chain and produces a parabolic motor command signal, from top-left to top-right. **D**) The population-averaged rates (with 2ms bin size) of directional neural populations of the translator unit are considered as the direction signals sent out from the unit shown in (C). The right signal is present throughout the activation period, while the down and up signals, respectively, show up at the beginning and end of the period. Since this particular parabola is sketched by moving from left to right, the left signal is always off. This translator unit draws a trajectory from left to right which approximates a parabola with horizontal symmetry and the concavity to up (**E**).

	CP	τ_{syn} (ms)	Synaptic weight	
			PSP amplitude(mV)	w_{ij} (pA)
assembly→'right' pop.	15%	7.7	0.45	10
assembly→'up' pop.	15%	7.7	0.23	5
assembly→'down' pop.*	15%	7.7	0.95	21

* Expresses short-term depression ($U = 0.7,\ \tau_{rec} = 800$ms)

Table A.1: Parameters of neuronal translator unit. Each direction population contains 100 neurons. (CP: Connection Probability, PSP: Postsynaptic Potential, pop.: population)

Bibliography

Abeles M. Role of the cortical neuron: integrator or coincidence detector? *Isr. J. Med. Sci.*, 18 (1):83–92, 1982.

Abeles M. *Corticonics: Neural circuits of the cerebral cortex*. Cambridge University Press, 1991.

Achermann P and AABorbely. Low-frequency (< 1hz) oscillations in the human sleep electroencephalogram. *Neuroscience*, 81(1):213–222, 1997.

Amit DJ and Brunel N. Model of global spontaneous activity and local structured activity during delay periods in the cerebral cortex. *Cereb. Cortex*, 7(3):237–252, 1997.

Arieli A, Sterkin A, Grinvald A, and Aertsen A. Dynamics of ongoing activity: explanation of the large variability in evoked cortical responses. *Science*, 273(5283):1868, 1996.

Avermann M, Tomm C, Mateo C, Gerstner W, and Petersen CCH. Microcircuits of excitatory and inhibitory neurons in layer 2/3 of mouse barrel cortex. *J. Neurophysiol.*, 107(11):3116–3134, 2012.

Barabási AL and Albert R. Emergence of scaling in random networks. *Science*, 286(5439): 509–512, 1999.

Barak O and Tsodyks M. Persistent activity in neural networks with dynamic synapses. *PLoS Comput. Biol.*, 3(2):e35, 2007.

Bazhenov M, Timofeev I, Steriade M, and Sejnowski TJ. Model of thalamocortical slow-wave sleep oscillations and transitions to activated states. *J. Neurosci.*, 22(19):8691–8704, 2002.

Beltramo R, D'Urso G, Maschio MD, Farisello P, Bovetti S, Clovis Y, Lassi G, Tucci V, Tonell DDP, and Fellin T. Layer-specific excitatory circuits differentially control recurrent network dynamics in the neocortex. *Nat. Neurosci.*, 16:227–234, 2013.

Bersagliere A and Achermann P. Slow oscillations in human non-rapid eye movement sleep electroencephalogram: effects of increased sleep pressure. *J. Sleep Res.*, 19(1p2):228–237, 2010.

Binzegger T, Douglas RJ, and Martin KA. A quantitative map of the circuit of cat primary visual cortex. *J. Neurosci.*, 24(39):8441–8453, 2004.

Bon-Jego ML and Yuste R. Persistently active, pacemaker-like neurons in neocortex. *Front. Neurosci.*, 1(1), 2007.

Bonifazi P, Goldin M, Picardo MA, Jorquera I, Cattani A, Bianconi G, Represa A, Ben-Ari Y, and Cossart R. Gabaergic hub neurons orchestrate synchrony in developing hippocampal networks. *Science*, 326(5958):1419–1424, 2009.

Borbély AA, Baumann F, Brandeis D, Strauch I, and Lehmann D. Sleep deprivation: effect on sleep stages and eeg power density in man. *Electroencephalogr. Clin. Neurophysiol.*, 51(5): 483–493, 1981.

Borbély AA, Tobler I, and Hanagasioglu M. Effect of sleep deprivation on sleep and eeg power spectra in the rat. *Behav. Brain Res.*, 14(3):171–182, 1984.

Boucsein C, Nawrot M, Schnepel P, and Aertsen A. Beyond the cortical column: abundance and physiology of horizontal connections imply a strong role for inputs from the surround. *Front. Neurosci.*, 5:32, 2011.

Bressloff P. Synaptically generated wave propagation in excitable neural media. *Phys. Rev. Lett.*, 82(14):2979, 1999.

Brunel N. Dynamics of sparsely connected networks of excitatory and inhibitory spiking neurons. *J. Comput. Neurosci.*, 8(3):183–208, 2000.

Bullmore E and Sporns O. Complex brain networks: graph theoretical analysis of structural and functional systems. *Nat. Rev. Neurosci.*, 10(3):186–198, 2009.

Buonomano DV and Maass W. State-dependent computations: spatiotemporal processing in cortical networks. *Nat. Rev. Neurosci.*, 10(2):113, 2009.

Chapeton J, Fares T, LaSota D, and Stepanyants A. Efficient associative memory storage in cortical circuits of inhibitory and excitatory neurons. *Proc Natl Acad Sci USA*, 109(51): E3614–E3622, 2012.

Chauvette S, Volgushev M, and Timofeev I. Origin of active states in local neocortical networks during slow sleep oscillation. *Cereb. Cortex*, 20(11):2660–2674, 2010.

Chiappalone M, Bove M, Vato A, Tedesco M, and Martinoia S. Dissociated cortical networks show spontaneously correlated activity patterns during in vitro development. *Brain Res.*, 1093 (1):41–53, 2006.

Chiappalone M, Vato A, Berdondini L, Koudelka-Hep M, and Martinoia S. Network dynamics and synchronous activity in cultured cortical neurons. *Int. J. Neural Syst.*, 17(02):87–103, 2007.

Cirelli C and Giulio. Is sleep essential? *PLoS Biol.*, 6(8):e216, 2008.

Civillico EF and Contreras D. Integration of evoked responses in supragranular cortex studied with optical recordings in vivo. *J. Neurophysiol.*, 96(1):336–351, 2006.

Colombi I, Tinarelli F, Pasquale V, Tucci V, and Chiappalone M. A simplified in vitro experimental model encompasses the essential features of sleep. *Front. Neurosci.*, 10, 2016.

Compte A, Brunel N, Goldman-Rakic PS, and Wang XJ. Synaptic mechanisms and network dynamics underlying spatial working memory in a cortical network model. *Cereb. Cortex*, 10 (9):910–923, 2000.

Compte A, Sanchez-Vives MV, McCormick DA, and Wang XJ. Cellular and network mechanisms of slow oscillatory activity ($<$ 1 hz) and wave propagations in a cortical network model. *J. Neurophysiol.*, 89(5):2707–2725, 2003.

Contreras D and Steriade M. Cellular basis of eeg slow rhythms: a study of dynamic corticothalamic relationships. *J. Neurosci.*, 15(1):604–622, 1995.

Coombes S. Waves, bumps, and patterns in neural field theories. *Biol. Cybern.*, 93(2):91–108, 2005.

Coombes S. Neural fields. *Scholarpedia*, 1(6):1373, 2006.

Corner MA, Baker RE, and van Pelt J. Physiological consequences of selective suppression of synaptic transmission in developing cerebral cortical networks in vitro: differential effects on intrinsically generated bioelectric discharges in a living ÔmodelÕsystem for slow-wave sleep activity. *Neuroscience & Biobehavioral Reviews*, 32(8):1569–1600, 2008.

Cossart R, Aronov D, and Yuste R. Attractor dynamics of network up states in the neocortex. *Nature*, 423(6937):283–288, 2003.

Cowan RL and Wilson CJ. Spontaneous firing patterns and axonal projections of single corticostriatal neurons in the rat medial agranular cortex. *J. Neurophysiol.*, 71(1):17–32, 1994.

Cowley BR, Kaufman MT, Butler ZS, Churchland MM, Ryu SI, Shenoy KV, and Byron MY. Datahigh: graphical user interface for visualizing and interacting with high-dimensional neural activity. *J. Neural Eng.*, 10(6):066012, 2013.

de Kock CP and Sakmann B. Spiking in primary somatosensory cortex during natural whisking in awake head-restrained rats is cell-type specific. *Proc Natl Acad Sci USA*, 106(38):16446–16450, 2009.

Deco G, Jirsa VK, Robinson PA, Breakspear M, and Friston K. The dynamic brain: from spiking neurons to neural masses and cortical fields. *PLoS Comput. Biol.*, 4(8):e1000092, 2008.

Deco G, Jirsa V, McIntosh AR, Sporns O, and Kötter R. Key role of coupling, delay, and noise in resting brain fluctuations. *Proc Natl Acad Sci USA*, 106(25):10302–10307, 2009.

Deco G, Jirsa VK, and McIntosh AR. Emerging concepts for the dynamical organization of resting-state activity in the brain. *Nat. Rev. Neurosci.*, 12(1):43–56, 2011.

Deger M, Schwalger T, Naud R, and Wulfram. Fluctuations and information filtering in coupled populations of spiking neurons with adaptation. *Phys. Rev. E*, 90(6):062704, 2014.

Diesmann M, Gewaltig MO, and Aertsen A. Stable propagation of synchronous spiking in cortical neural networks. *Nature*, 402(6761):529–533, 1999.

Ding F, OÕDonnell J, Xu Q, Kang N, Goldman N, and Nedergaard M. Changes in the composition of brain interstitial ions control the sleep-wake cycle. *Science*, 352(6285):550–555, 2016.

Doiron B and Litwin-Kumar A. Balanced neural architecture and the idling brain. *Fron. Comput. neurosci.*, 8:56, 2014.

Ecker AS, Berens P, Keliris GA, Bethge M, Logothetis NK, and Tolias AS. Decorrelated neuronal firing in cortical microcircuits. *Science*, 327(5965):584–587, 2010.

Erdös P and Rényi A. On random graphs, i. *Publicationes Mathematicae (Debrecen)*, 6:290–297, 1959.

Esser SK, Hill SL, and Tononi G. Sleep homeostasis and cortical synchronization: I. modeling the effects of synaptic strength on sleep slow waves. *Sleep*, 30(12):1617–1630, 2007.

Feldmeyer D, Egger V, Lübke J, and Sakmann B. Reliable synaptic connections between pairs of excitatory layer 4 neurones within a single ÔbarrelÕof developing rat somatosensory cortex. *J. Physiol.*, 521(1):169–190, 1999.

Feldmeyer D, Lübke J, Silver RA, and Sakmann B. Synaptic connections between layer 4 spiny neurone-layer 2/3 pyramidal cell pairs in juvenile rat barrel cortex: physiology and anatomy of interlaminar signalling within a cortical column. *J. Physiol.*, 538(3):803–822, 2002.

Feldmeyer D, Lübke J, and Sakmann B. Efficacy and connectivity of intracolumnar pairs of layer 2/3 pyramidal cells in the barrel cortex of juvenile rats. *J. Physiol.*, 575(2):583–602, 2006.

Feldt S, Bonifazi P, and Cossart R. Dissecting functional connectivity of neuronal microcircuits: experimental and theoretical insights. *Trends Neurosci.*, 34(5):225–236, 2011.

Ferezou I, Bolea S, and Petersen CC. Visualizing the cortical representation of whisker touch: voltage-sensitive dye imaging in freely moving mice. *Neuron*, 50(4):617–629, 2006.

Ferezou I, Haiss F, Gentet LJ, Aronoff R, Weber B, and CH C. Spatiotemporal dynamics of cortical sensorimotor integration in behaving mice. *Neuron*, 56(5):907–923, 2007.

Fino E and Yuste R. Dense inhibitory connectivity in neocortex. *Neuron*, 69(6):1188–1203, 2011.

Fino E, Packer AM, and Yuste R. The logic of inhibitory connectivity in the neocortex. *The Neuroscientist*, 19(3):228–237, 2013.

Fourcaud-Trocmé N, Hansel D, Vreeswijk CV, and Brunel N. How spike generation mechanisms determine the neuronal response to fluctuating inputs. *J. Neurosci.*, 23(37):11628–11640, 2003.

Frick A, Feldmeyer D, Helmstaedter M, and Sakmann B. Monosynaptic connections between pairs of l5a pyramidal neurons in columns of juvenile rat somatosensory cortex. *Cereb. Cortex*, 18(2):397–406, 2008.

Fucke T, Suchanek D, Nawrot MP, Seamari Y, Heck DH, Aertsen A, and Boucsein C. Stereotypical spatiotemporal activity patterns during slow-wave activity in the neocortex. *J. Neurophysiol.*, 106(6):3035–3044, 2011.

Garis HD, Shuo C, Goertzel B, and Ruiting L. A world survey of artificial brain projects, part i: Large-scale brain simulations. *Neurocomputing*, 74(1):3–29, 2010.

Gentet LJ, Kremer Y, Taniguchi H, Huang ZJ, Staiger JF, and Petersen CC. Unique functional properties of somatostatin-expressing gabaergic neurons in mouse barrel cortex. *Nat. Neurosci.*, 15(4):607–612, 2012.

Gerstner W. Population dynamics of spiking neurons: fast transients, asynchronous states, and locking. *Neural Comput.*, 12(1):43–89, 2000.

Gerstner W, Ritz R, and Hemmen JLV. A biologically motivated and analytically soluble model of collective oscillations in the cortex. *Biol. Cybern.*, 68(4):363–374, 1993.

Gerstner W, Kistler WM, Naud R, and Paninski L. *Neuronal dynamics: From single neurons to networks and models of cognition*. Cambridge University Press, 2014.

Gewaltig MO. *Evolution of synchronous spike volleys in cortical Networks: Network simulations and continuous probabilistic models*. Shaker, 2000.

Gewaltig MO and Diesmann M. Nest (neural simulation tool). *Scholarpedia*, 2(4):1430, 2007.

Ghorbani M, Mehta M, Bruinsma R, and Levine AJ. Nonlinear-dynamics theory of up-down transitions in neocortical neural networks. *Phys. Rev. E*, 85(2):021908, 2012.

Ghosh A, Rho Y, McIntosh AR, Kötter R, and Jirsa VK. Noise during rest enables the exploration of the brain's dynamic repertoire. *PLoS Comput. Biol.*, 4(10):e1000196, 2008.

Gilson M, Moreno-Bote R, Ponce-Alvarez A, Ritter P, and Deco G. Estimation of directed effective connectivity from fmri functional connectivity hints at asymmetries of cortical connectome. *PLoS Comput. Biol.*, 12(3):e1004762, 2016.

Giszter SF. Motor primitivesÑnew data and future questions. *Curr. Opin. Neurobiol.*, 33: 156–165, 2015.

Giugliano M, Darbon P, Arsiero M, Lüscher HR, and Streit J. Single-neuron discharge properties and network activity in dissociated cultures of neocortex. *J. Neurophysiol.*, 92(2):977–996, 2004.

Giugliano M, Camera GL, Fusi S, and Senn W. The response of cortical neurons to in vivo-like input current: theory and experiment: Ii. time-varying and spatially distributed inputs. *Biol. Cybern.*, 99(4-5):303–318, 2008.

Goedeke S and Diesmann M. The mechanism of synchronization in feed-forward neuronal networks. *New J. Phys.*, 10(1):015007, 2008.

Goodman D and Brette R. Brian: A simulator for spiking neural networks in python. *Front. Neuroinform.*, 2, 2008.

Greenberg DS, Houweling AR, and Kerr JN. Population imaging of ongoing neuronal activity in the visual cortex of awake rats. *Nat. Neurosci.*, 11(7):749–751, 2008.

Grinvald A, Anglister L, Freeman J, Hildesheim R, and Manker A. Real-time optical imaging of naturally evoked electrical activity in intact frog brain. *Nature*, 1984.

Hahnloser RH, Kozhevnikov AA, and Fee MS. An ultra-sparse code underliesthe generation of neural sequences in a songbird. *Nature*, 419(6902):65–70, 2002.

Hanuschkin A, Diesmann M, and Morrison A. A reafferent and feed-forward model of song syntax generation in the bengalese finch. *J. Comput. Neurosci.*, 31(3):509–532, 2011a.

Hanuschkin A, Herrmann JM, Morrison A, and Diesmann M. Compositionality of arm movements can be realized by propagating synchrony. *J. Comput. Neurosci.*, 30(3):675–697, 2011b.

Hebb DO. *The organisation of behaviour: a neuropsychological theory.* Wiley, 1949.

Helias M, Deger M, Rotter S, and Diesmann M. Instantaneous non-linear processing by pulse-coupled threshold units. *PLoS Comput Biol*, 6(9):e1000929, 2010.

Hengen KB, Pacheco AT, McGregor JN, Hooser SDV, and Turrigiano GG. Neuronal firing rate homeostasis is inhibited by sleep and promoted by wake. *Cell*, 165(1):180–191, 2016.

Hertäg L, Durstewitz D, and Brunel N. Analytical approximations of the firing rate of an adaptive exponential integrate-and-fire neuron in the presence of synaptic noise. *Front. Comput. Neurosci.*, 8, 2014.

Hill S and Tononi G. Modeling sleep and wakefulness in the thalamocortical system. *J. Neurophysiol.*, 93(3):1671–1698, 2005.

Hinard V, Mikhail C, Pradervand S, Curie T, Houtkooper RH, Auwerx J, Franken P, and Tafti M. Key electrophysiological, molecular, and metabolic signatures of sleep and wakefulness revealed in primary cortical cultures. *J. Neurosci.*, 32(36):12506–12517, 2012.

Hodgkin AL and Huxley AF. A quantitative description of membrane current and its application to conduction and excitation in nerve. *J. Physiol.*, 117(4):500–544, 1952.

Hogan N. An organizing principle for a class of voluntary movements. *J. Neurosci.*, 4(11): 2745–2754, 1984.

Hogan N and Sternad D. Dynamic primitives of motor behavior. *Biol. Cybern.*, pages 1–13, 2012.

Holcman D and Tsodyks M. The emergence of up and down states in cortical networks. *PLoS Comput. Biol.*, 2(3):e23, 2006.

Honey CJ, Kötter R, Breakspear M, and Sporns O. Network structure of cerebral cortex shapes functional connectivity on multiple time scales. *Proc Natl Acad Sci USA*, 104(24):10240–10245, 2007.

Hopfield JJ. Neurons with graded response have collective computational properties like those of two-state neurons. *Proc Natl Acad Sci USA*, 81(10):3088–3092, 1984.

Hopfield JJ. Neural networks and physical systems with emergent collective computational abilities. In *Spin Glass Theory and Beyond: An Introduction to the Replica Method and Its Applications*, pages 411–415. World Scientific, 1987.

Hromádka T, DeWeese MR, and Zador AM. Sparse representation of sounds in the unanesthetized auditory cortex. *PLoS Biol.*, 6(1):e16, 2008.

Hu Y, Trousdale J, Josić K, and Shea-Brown E. Motif statistics and spike correlations in neuronal networks. *J. Stat. Mech. Theor. Exp.*, 03(03):P03012, 2013.

Hu Y, Trousdale J, Josić K, and Shea-Brown E. Local paths to global coherence: Cutting networks down to size. *Phys. Rev. E*, 89(3):032802, 2014.

Ito D, Tamate H, Nagayama M, Uchida T, Kudoh S, and Gohara K. Minimum neuron density for synchronized bursts in a rat cortical culture on multi-electrode arrays. *Neuroscience*, 171 (1):50–61, 2010.

Iyer R, Menon V, Buice M, Koch C, and Mihalas S. The influence of synaptic weight distribution on neuronal population dynamics. *PLoS Comput. Biol.*, 9(10):e1003248, 2013.

Izhikevich EM. Simple model of spiking neurons. *IEEE Trans. Neural Netw*, 14(6):1569–1572, 2003.

Izhikevich EM. Polychronization: computation with spikes. *Neural Comput.*, 18(2):245–282, 2006.

Izhikevich EM and Edelman GM. Large-scale model of mammalian thalamocortical systems. *Proc Natl Acad Sci USA*, 105(9):3593–3598, 2008.

Jahnke S, Memmesheimer RM, and Timme M. Hub-activated signal transmission in complex networks. *Phys. Rev. E*, 89(3), 2014.

Jewett KA, Taishi P, Sengupta P, Roy S, Davis CJ, and Krueger JM. Tumor necrosis factor enhances the sleep-like state and electrical stimulation induces a wake-like state in co-cultures of neurons and glia. *Eur. J. Neurosci.*, 42(4):2078–2090, 2015.

Ji D and A M. Coordinated memory replay in the visual cortex and hippocampus during sleep. *Nat. Neurosci.*, 10(1):100, 2007.

Jirsa VK and Haken H. A derivation of a macroscopic field theory of the brain from the quasi-microscopic neural dynamics. *Physica D: Nonlinear Phenomena*, 99(4):503–526, 1997.

Jolivet R, Rauch A, Lüscher HR, and Gerstner W. Predicting spike timing of neocortical pyramidal neurons by simple threshold models. *J. Comput. Neurosci.*, 21(1):35–49, 2006.

Kamioka H, Maeda E, Jimbo Y, Robinson HP, and Kawana A. Spontaneous periodic synchronized bursting during formation of mature patterns of connections in cortical cultures. *Neurosci. Lett.*, 206(2):109–112, 1996.

Kampa BM, Letzkus JJ, and Stuart GJ. Cortical feed-forward networks for binding different streams of sensory information. *Nat. Neurosci.*, 9(12):1472–1473, 2006.

Kattler H, Dijk DJ, and Borbely AA. Effect of unilateral somatosensory stimulation prior to sleep on the sleep eeg in humans. *J. Sleep Res.*, 3(3):159–164, 1994.

Kaufman M, Reinartz S, and E N. Adaptation to prolonged neuromodulation in cortical cultures: an invariable return to network synchrony. *BMC Biol.*, 12(1):83, 2014.

Kenet T, Bibitchkov D, Tsodyks M, Grinvald A, and Arieli A. Spontaneously emerging cortical representations of visual attributes. *Nature*, 425(6961):954–956, 2003.

Kistler WM and Gerstner W. Stable propagation of activity pulses in populations of spiking neurons. *Neural Comput.*, 14(5):987–997, 2002.

Kistler WM, Seitz R, and Hemmen JLV. Modeling collective excitations in cortical tissue. *Physica D: Nonlinear Phenomena*, 114(3-4):273–295, 1998.

Klinshov VV, nosuke Teramae J, Nekorkin VI, and Fukai T. Dense neuron clustering explains connectivity statistics in cortical microcircuits. *PloS one*, 9(4):e94292, 2014.

Ko H, Hofer SB, Pichler B, Buchanan KA, Sjöström PJ, and Mrsic-Flogel TD. Functional specificity of local synaptic connections in neocortical networks. *Nature*, 473(7345):87–91, 2011.

Koulakov AA, Hromadka T, and Zador AM. Correlated connectivity and the distribution of firing rates in the neocortex. *J. Neurosci.*, 29(12):3685–3694, 2009.

Krishnamurthy P, Silberberg G, and Lansner A. A cortical attractor network with martinotti cells driven by facilitating synapses. *PloS one*, 7(4):e30752, 2012.

Krueger JM, Rector DM, Roy S, Dongen HPV, Belenky G, and Panksepp J. Sleep as a fundamental property of neuronal assemblies. *Nat. Rev. Neurosci.*, 9(12):910, 2008.

Kumar A, Rotter S, and Aertsen A. Conditions for propagating synchronous spiking and asynchronous firing rates in a cortical network model. *J. Neurosci.*, 28(20):5268–5280, 2008.

Kumar A, Rotter S, and Aertsen A. Spiking activity propagation in neuronal networks: reconciling different perspectives on neural coding. *Nat. Rev. Neurosci.*, 11(9):615–627, 2010.

La Camera G, Rauch A, Lüscher HR, Senn W, and Fusi S. Minimal models of adapted neuronal response to in vivo-like input currents. *Neural Comput.*, 16(10):2101–2124, 2004.

Laing CR and Chow CC. A spiking neuron model for binocular rivalry. *J. Comput. Neurosci.*, 12(1):39–53, 2002.

Lampl I, Reichova I, and Ferster D. Synchronous membrane potential fluctuations in neurons of the cat visual cortex. *Neuron*, 22:361–374, 1999.

Lawn N, Lieblich S, Lee J, and Dunne J. Are seizures in the setting of sleep deprivation provoked? *Epilepsy & Behavior*, 33:122–125, 2014.

Lefort S, Tomm C, Sarria JCF, and Petersen CC. The excitatory neuronal network of the c2 barrel column in mouse primary somatosensory cortex. *Neuron*, 61(2):301-316, 2009.

Lemieux M, Chen JY, Lonjers P, Bazhenov M, and Timofeev I. The impact of cortical deafferentation on the neocortical slow oscillation. *J. Neurosci.*, 34(16):5689–5703, 2014.

Litwin-Kumar A and Brent. Formation and maintenance of neuronal assemblies through synaptic plasticity. *Nat. Commun.*, 5:5319, 2014.

Litwin-Kumar A and Doiron B. Slow dynamics and high variability in balanced cortical networks with clustered connections. *Nat. Neurosci.*, 15(11):1498–1505, 2012.

Lonardoni D, Marco SD, Amin H, Maccione A, Berdondini L, and Nieus T. High-density mea recordings unveil the dynamics of bursting events in cell cultures. In *Engineering in Medicine and Biology Society (EMBC), 2015 37th Annual International Conference of the IEEE*, pages 3763–3766. IEEE, 2015.

Luccioli S, Ben-Jacob E, Barzilai A, Bonifazi P, and Torcini A. Clique of functional hubs orchestrates population bursts in developmentally regulated neural networks. *PLoS Comput Biol*, 10(9):e1003823, 2014.

Lustig BR, Friedman RM, Winberry JE, Ebner FF, and Roe AW. Voltage-sensitive dye imaging reveals shifting spatiotemporal spread of whisker-induced activity in rat barrel cortex. *J. Neurophysiol.*, 109(9):2382–2392, 2013.

Maeda E, Robinson H, and Kawana A. The mechanisms of generation and propagation of synchronized bursting in developing networks of cortical neurons. *J. Neurosci.*, 15(10):6834–6845, 1995.

Maret S, Dorsaz S, Gurcel L, Pradervand S, Petit B, Pfister C, Hagenbuchle O, O'Hara BF, Franken P, and Mehdi. Homer1a is a core brain molecular correlate of sleep loss. *Proc Natl Acad Sci USA*, 104(50):20090–20095, 2007.

Markram H, Lübke J, Frotscher M, Roth A, and Sakmann B. Physiology and anatomy of synaptic connections between thick tufted pyramidal neurones in the developing rat neocortex. *J. Physiol.*, 500(Pt 2):409, 1997.

Markram H, Toledo-Rodriguez M, Wang Y, Gupta A, Silberberg G, and Caizhi W. Interneurons of the neocortical inhibitory system. *Nat. Rev. Neurosci.*, 5(10):793–807, 2004.

Markram H, Muller E, Ramaswamy S, Reimann MW, Abdellah M, Sanchez CA, Ailamaki A, Alonso-Nanclares L, Antille N, Arsever S, et al. Reconstruction and simulation of neocortical microcircuitry. *Cell*, 163(2):456–492, 2015.

Mazzucato L, Fontanini A, and La Camera G. Dynamics of multistable states during ongoing and evoked cortical activity. *J. Neurosci.*, 35(21):8214–8231, 2015.

Mazzucato L, Fontanini A, and La Camera G. Stimuli reduce the dimensionality of cortical activity. *Front. Syst. Neurosci.*, 2016.

McDonnell M and Ward L. Small modifications to network topology can induce stochastic bistable spiking dynamics in a balanced cortical model. *PloS one*, 9(4):e88254, 2014.

McNaughton BL, Battaglia FP, Jensen O, Moser EI, and Moser MB. Path integration and the neural basis of the'cognitive map'. *Nat. Rev. Neurosci.*, 7(8):663–678, 2006.

Melamed O, Barak O, Silberberg G, Markram H, and Tsodyks M. Slow oscillations in neural networks with facilitating synapses. *J. Comput. Neurosci.*, 25(2):308–316, 2008.

Mensi S, Naud R, Pozzorini C, Avermann M, Petersen CC, and Gerstner W. Parameter extraction and classification of three cortical neuron types reveals two distinct adaptation mechanisms. *J. Neurophysiol.*, 107(6):1756–1775, 2012.

Merolla PA, Arthur JV, Alvarez-Icaza R, Cassidy AS, Sawada J, Akopyan F, Jackson BL, Imam N, Guo C, Nakamura Y, et al. A million spiking-neuron integrated circuit with a scalable communication network and interface. *Science*, 345(6197):668–673, 2014.

Mikhail C, Vaucher A, Jimenez S, and Tafti M. Erk signaling pathway regulates sleep duration through activity-induced gene expression during wakefulness. *Sci. Signal.*, 10(463):eaai9219, 2017.

Mok S, Nadasdy Z, Lim Y, and Goh S. Ultra-slow oscillations in cortical networks in vitro. *Neuroscience*, 206:17–24, 2012.

Mongillo G, Barak O, and Tsodyks M. Synaptic theory of working memory. *Science*, 319(5869): 1543–1546, 2008.

Moreno-Bote R, Rinzel J, and Rubin N. Noise-induced alternations in an attractor network model of perceptual bistability. *J. Neurophysiol.*, 98(3):1125–1139, 2007.

Mukai Y, Shiina T, and Jimbo Y. Continuous monitoring of developmental activity changes in cultured cortical networks. *Electrical Engineering in Japan*, 145(4):28–37, 2003.

Murray JD. *Mathematical Biology. II Spatial Models and Biomedical Applications {Interdisciplinary Applied Mathematics V. 18}*. Springer-Verlag New York Incorporated, 2001.

Naud R and Gerstner W. Coding and decoding with adapting neurons: a population approach to the peri-stimulus time histogram. *PLoS Comput. Biol.*, 8(10):e1002711, 2012a.

Naud R and Gerstner W. The performance (and limits) of simple neuron models: generalizations of the leaky integrate-and-fire model. In *Computational Systems Neurobiology*, pages 163–192. Springer, 2012b.

Novellino A, Scelfo B, Palosaari T, Price A, Sobanski T, Shafer TJ, Johnstone AF, Gross GW, Gramowski A, Schroeder O, et al. Development of micro-electrode array based tests for neurotoxicity: assessment of interlaboratory reproducibility with neuroactive chemicals. *Front Neuroeng*, 4, 2011.

Okun M, Steinmetz N, Cossell L, Iacaruso M, Ko H, Barthó P, Moore T, Hofer S, Mrsic-Flogel T, Carandini M, et al. Diverse coupling of neurons to populations in sensory cortex. *Nature*, 521(7553):511–515, 2015.

Oram M, Wiener M, Lestienne R, and Richmond B. Stochastic nature of precisely timed spike patterns in visual system neuronal responses. *J. Neurophysiol.*, 81(6):3021–3033, 1999.

Palm G. *Neural assemblies: An alternative approach to artificial intelligence*. Springer-Verlag, Inc., Secaucus, NJ, 1982.

Parga N and Abbott LF. Network model of spontaneous activity exhibiting synchronous transitions between up and down states. *Front. Neurosci.*, 1(1):57, 2007.

Perin R, Berger TK, and Markram H. A synaptic organizing principle for cortical neuronal groups. *Proc Natl Acad Sci USA*, 108(13):5419–5424, 2011.

Pernice V, Deger M, Cardanobile S, and Rotterf S. The relevance of network micro-structure for neural dynamics. *Front. Comput. Neurosci.*, 7, 2013.

Petersen CC. The functional organization of the barrel cortex. *Neuron*, 56(2):339–355, 2007.

Petersen CC, Grinvald A, and Sakmann B. Spatiotemporal dynamics of sensory responses in layer 2/3 of rat barrel cortex measured in vivo by voltage-sensitive dye imaging combined with whole-cell voltage recordings and neuron reconstructions. *J. Neurosci.*, 23(4):1298–1309, 2003a.

Petersen CC, Hahn TT, Mehta M, Grinvald A, and Sakmann B. Interaction of sensory responses with spontaneous depolarization in layer 2/3 barrel cortex. *Proc Natl Acad Sci USA*, 100(23): 13638–13643, 2003b.

Pfeffer CK, Xue M, He M, Josh Z, and Scanziani M. Inhibition of inhibition in visual cortex: the logic of connections between molecularly distinct interneurons. *Nat. Neurosci.*, 16(8): 1068–1076, 2013.

Pillow JW, Shlens J, Paninski L, Sher A, Litke AM, Chichilnisky E, and Simoncelli EP. Spatio-temporal correlations and visual signalling in a complete neuronal population. *Nature*, 454 (7207):995–999, 2008.

Poli D, Pastore VP, and Massobrio P. Functional connectivity in in vitro neuronal assemblies. *Front Neural Circuit*, 9, 2015.

Polyakov F, Drori R, Ben-Shaul Y, Abeles M, and Flash T. A compact representation of drawing movements with sequences of parabolic primitives. *PLoS Comput. Biol.*, 5(7):e1000427–e1000427, 2009.

Potjans TC and Diesmann M. The cell-type specific cortical microcircuit: relating structure and activity in a full-scale spiking network model. *Cereb. Cortex*, 24(3):785–806, 2014.

Poulet JF, Fernandez LM, Crochet S, and Petersen CC. Thalamic control of cortical states. *Nat. Neurosci.*, 15(3):370–372, 2012.

Pozzorini C, Naud R, Mensi S, and Gerstner W. Temporal whitening by power-law adaptation in neocortical neurons. *Nat. Neurosci.*, 16(7):942–948, 2013.

Pozzorini C, Mensi S, Hagens O, Naud R, Koch C, and Gerstner W. Automated high-throughput characterization of single neurons by means of simplified spiking models. *PLoS Comput Biol*, 11(6):e1004275, 2015.

Prettejohn BJ, Berryman MJ, and McDonnell MD. Methods for generating complex networks with selected structural properties for simulations: a review and tutorial for neuroscientists. *Front. Comput. Neurosci.*, 5, 2011.

Rector DM, Topchiy IA, Carter KM, and Rojas MJ. Local functional state differences between rat cortical columns. *Brain Res.*, 1047(1):45–55, 2005.

Rector DM, Schei JL, Dongen HV, Belenky G, and Krueger JM. Physiological markers of local sleep. *Eur. J. Neurosci.*, 29(9):1771–1778, 2009.

Reich DS, Mechler F, and Victor JD. Independent and redundant information in nearby cortical neurons. *Science*, 294(5551):2566–2568, 2001.

Richardson MJ. Firing-rate response of linear and nonlinear integrate-and-fire neurons to modulated current-based and conductance-based synaptic drive. *Phys. Rev. E*, 76(2):021919, 2007.

Richardson MJ. Dynamics of populations and networks of neurons with voltage-activated and calcium-activated currents. *Phys. Rev. E*, 80(2):021928, 2009.

Riedner BA, Vyazovskiy VV, Huber R, Massimini M, Esser S, Murphy M, and Tononi G. Sleep homeostasis and cortical synchronization: Iii. a high-density eeg study of sleep slow waves in humans. *Sleep*, 30(12):1643–1657, 2007.

Rocha JDL, Doiron B, Shea-Brown E, Josic K, and Reyes A. Correlation between neural spike trains increases with firing rate. *Nature*, 448(7155):802, 2007.

Rodriguez AV, Funk CM, Vyazovskiy VV, Nir Y, Tononi G, and Cirelli C. Why does sleep slow-wave activity increase after extended wake? assessing the effects of increased cortical firing during wake and sleep. *J. Neurosci.*, 36(49):12436–12447, 2016.

Roxin A. The role of degree distribution in shaping the dynamics in networks of sparsely connected spiking neurons. *Front. Comput. Neurosci.*, 5, 2011.

Roxin A, Riecke H, and Solla SA. Self-sustained activity in a small-world network of excitable neurons. *Phys. Rev. Lett.*, 92(19):198101, 2004.

Roxin A, Brunel N, Hansel D, Mongillo G, and van Vreeswijk C. On the distribution of firing rates in networks of cortical neurons. *J. Neurosci.*, 31(45):16217–16226, 2011.

Rudolph-Lilith M and Muller LE. Aspects of randomness in neural graph structures. *Biol. Cybern.*, 108(4):381–396, 2014.

Rudy B, Fishell G, Lee S, and Hjerling-Leffler J. Three groups of interneurons account for nearly 100% of neocortical gabaergic neurons. *Dev. Neurobiol.*, 71(1):45–61, 2011.

Runyan CA, Piasini E, Panzeri S, and Harvey CD. Distinct timescales of population coding across cortex. *Nature*, 548(7665):92–96, 2017.

Sakata S and Harris KD. Laminar structure of spontaneous and sensory-evoked population activity in auditory cortex. *Neuron*, 64(3):404–418, 2009.

Samsonovich A and McNaughton BL. Path integration and cognitive mapping in a continuous attractor neural network model. *J. Neurosci.*, 17(15):5900–5920, 1997.

Sanchez-Vives MV and McCormick DA. Cellular and network mechanisms of rhythmic recurrent activity in neocortex. *Nat. Neurosci.*, 3(10):1027–1034, 2000.

Sanchez-Vives MV, Nowak LG, and McCormick DA. Membrane mechanisms underlying contrast adaptation in cat area 17 in vivo. *J. Neurosci.*, 20(11):4267–4285, 2000.

Schrader S, Grün S, Diesmann M, and Gerstein GL. Detecting synfire chain activity using massively parallel spike train recording. *J. Neurophysiol.*, 100(4):2165–2176, 2008.

Schwalger T, Deger M, and Gerstner W. Towards a theory of cortical columns: From spiking neurons to interacting neural populations of finite size. *PLoS Comput. Biol.*, 13(4):e1005507, 2017.

Setareh H, Deger M, and Gerstner W. The role of interconnected hub neurons in cortical dynamics. *BMC Neurosci.*, 15(Suppl 1):P158, 2014.

Setareh H, Deger M, and Gerstner W. Synaptic efficacy tunes speed of activity propagation through chains of bistable neural assemblies. In *COSYNE 2015*, number EPFL-POSTER-206999, 2015.

Setareh H, Deger M, Petersen CCH, and Gerstner W. Cortical dynamics in presence of assemblies of densely connected weight-hub neurons. *Front. Comput. Neurosci.*, 11:52, 2017.

Shpiro A, Moreno-Bote R, Rubin N, and Rinzel J. Balance between noise and adaptation in competition models of perceptual bistability. *J. Comput. Neurosci.*, 27(1):37–54, 2009.

Sirota A and Buzsáki G. Interaction between neocortical and hippocampal networks via slow oscillations. *Thalamus & related systems*, 3(4):245–259, 2005.

Slomowitz E, Styr B, Vertkin I, Milshtein-Parush H, Nelken I, Slutsky M, and Slutsky I. Interplay between population firing stability and single neuron dynamics in hippocampal networks. *Elife*, 4(4), 2015.

Smetters D, Majewska A, and Yuste R. Detecting action potentials in neuronal populations with calcium imaging. *Methods*, 18(2):215–221, 1999.

Song S, Sjostrom PJ, Reigl M, Nelson S, and Chklovskii DB. Highly nonrandom features of synaptic connectivity in local cortical circuits. *PLoS Biol.*, 3.3:68, 2005.

Steriade M. Grouping of brain rhythms in corticothalamic systems. *Neuroscience*, 137(4): 1087–1106, 2006.

Steriade M, Nuñez A, and Amzica F. Intracellular analysis of relations between the slow ($<$ 1 hz) neocortical oscillation and other sleep rhythms of the electroencephalogram. *J. Neurosci.*, 13(8):3266–3283, 1993a.

Steriade M, Nuñez A, and Amzica F. A novel slow ($<$ 1 hz) oscillation of neocortical neurons in vivo: depolarizing and hyperpolarizing components. *J. Neurosci.*, 13(8):3252–3265, 1993b.

Stern EA, Kincaid AE, and Wilson CJ. Spontaneous subthreshold membrane potential fluctuations and action potential variability of rat corticostriatal and striatal neurons in vivo. *J. Neurophysiol.*, 77(4):1697–1715, 1997.

Thomson AM, West DC, Wang Y, and Bannister AP. Synaptic connections and small circuits involving excitatory and inhibitory neurons in layers 2–5 of adult rat and cat neocortex: triple intracellular recordings and biocytin labelling in vitro. *Cereb. Cortex*, 12(9):936–953, 2002.

Timofeev I, Grenier F, Bazhenov M, Sejnowski TJ, and Steriade. M. Origin of slow cortical oscillations in deafferented cortical slabs. *Cereb. Cortex*, 10(12):1185–1199, 2000.

Timofeev I, Grenier F, and Steriade M. Disfacilitation and active inhibition in the neocortex during the natural sleep-wake cycle: an intracellular study. *Proc Natl Acad Sci USA*, 98(4): 1924–1929, 2001.

Tomm C. *Analysing Neuronal Network Architectures: From Weight Distributions to Structure and Back*. PhD thesis, Ecole Polytechnique Federale de Lausanne, 2011.

Tomm C, Avermann M, Petersen CC, Gerstner W, and Vogels TP. Connection-type specific biases make random network models consistent with cortical recordings. *J. Neurophysiol.*, 112 (8):1801–1814, 2014.

Tononi G and Chiara. Sleep and the price of plasticity: from synaptic and cellular homeostasis to memory consolidation and integration. *Neuron*, 81(1):12–34, 2014.

Torre E, Canova C, Denker M, Gerstein G, Helias M, and Grün S. Asset: analysis of sequences of synchronous events in massively parallel spike trains. *PLoS Comput. Biol.*, 12(7):e1004939, 2016.

Trengove C, van Leeuwen C, and Diesmann M. High-capacity embedding of synfire chains in a cortical network model. *J. Comput. Neurosci.*, 34(2):185–209, 2013.

Trengove C, Diesmann M, and Leeuwen CV. Dynamic effective connectivity in cortically embedded systems of recurrently coupled synfire chains. *J. Comput. Neurosci.*, 40(1):1–26, 2016.

Tsodyks M. Attractor neural network models of spatial maps in hippocampus. *Hippocampus*, 9 (4):481–489, 1999.

Tsodyks M, Pawelzik K, and Markram H. Neural networks with dynamic synapses. *Neural Comput.*, 10(4):821–835, 1998.

Tsodyks MV and Markram H. The neural code between neocortical pyramidal neurons depends on neurotransmitter release probability. *Proc Natl Acad Sci USA*, 94(2):719–723, 1997.

van Rossum MC, Turrigiano GG, and Nelson SB. Fast propagation of firing rates through layered networks of noisy neurons. *J. Neurosci.*, 22(5):1956–1966, 2002.

Vasquez J, Houweling A, and Tiesinga P. Simultaneous stability and sensitivity in model cortical networks is achieved through anti-correlations between the in-and out-degree of connectivity. *Front. Comput. Neurosci.*, 7, 2013.

Vijayan S, Hale GJ, Moore CI, Brown EN, and Wilson M. Activity in the barrel cortex during active behavior and sleep. *J. Neurophysiol.*, 103(4):2074–2084, 2010.

Vogels T and Abbott L. Signal propagation and logic gating in networks of integrate-and-fire neurons. *J. Neurosci.*, 25(46):10786–10795, 2005.

Vyazovskiy VV and D K. Sleep and the single neuron: the role of global slow oscillations in individual cell rest. *Nat. Rev. Neurosci.*, 14(6):443, 2013.

Vyazovskiy VV, Riedner BA, Cirelli C, and Tononi G. Sleep homeostasis and cortical synchronization: Ii. a local field potential study of sleep slow waves in the rat. *Sleep*, 30(12): 1631–1642, 2007.

Vyazovskiy VV, Olcese U, Lazimy YM, Faraguna U, Esser SK, Williams JC, Cirelli C, and Tononi G. Cortical firing and sleep homeostasis. *Neuron*, 63(6):865–878, 2009.

Vyazovskiy VV, Cirelli C, and Tononi G. Electrophysiological correlates of sleep homeostasis in freely behaving rats. *Prog. Brain Res.*, 193:17, 2011a.

Vyazovskiy VV, Olcese U, Hanlon EC, Nir Y, Cirelli C, and Tononi G. Local sleep in awake rats. *Nature*, 472(7344):443–447, 2011b.

Wagenaar DA, Pine J, and Potter SM. An extremely rich repertoire of bursting patterns during the development of cortical cultures. *BMC Neurosci.*, 7(1):11, 2006.

Wang M, Yang Y, Wang CJ, Gamo NJ, Jin LE, Mazer JA, Morrison JH, Wang XJ, and Arnsten AF. Nmda receptors subserve persistent neuronal firing during working memory in dorsolateral prefrontal cortex. *Neuron*, 77(4):736–749, 2013.

Watts DJ and Strogatz SH. Collective dynamics of small-world networks. *Nature*, 393(6684): 440–442, 1998.

Wennekers T and Palm G. Controlling the speed of synfire chains. *Artificial Neural Networks - ICANN*, pages 451–456, 1996.

Wilson HR and Cowan JD. Excitatory and inhibitory interactions in localized populations of model neurons. *Biophys. J.*, 12(1):1–24, 1972.

Wilson HR and Cowan JD. A mathematical theory of the functional dynamics of cortical and thalamic nervous tissue. *Biol. Cybern.*, 13(2):55–80, 1973.

Yassin L, Benedetti BL, Jouhanneau JS, Wen JA, Poulet JF, and Barth AL. An embedded subnetwork of highly active neurons in the neocortex. *Neuron*, 68(6):1043–1050, 2010.

Yoshimura Y, Dantzker JL, and Callaway EM. Excitatory cortical neurons form fine-scale functional networks. *Nature*, 433(7028):868–873, 2005.

Zenke F, Agnes EJ, and Gerstner W. Diverse synaptic plasticity mechanisms orchestrated to form and retrieve memories in spiking neural networks. *Nat. Commun.*, 6, 2015.

Hesam SETAREH

PhD, Data Scientist/ Software Engineer

Route de la Plaine 16, 1022 - Chavannes-pres-Renens, Switzerland
hesam.setareh@epfl.ch
http://www.linkedin.com/in/hsetareh

- Double academic profile: **Data Scientist** and **Software Engineer**
- Expert in **Machine Learning** and Artificial Intelligence
- Have done many projects in data analysis and modeling during PhD and Master studies
- 9 years experiences in advanced computer programming and software development

Education

*PhD in **Computer and Information Sciences*** 2012- 2017
École Polytechnique Federale de Lausanne (EPFL), Switzerland,
Laboratory of computational neuroscience

- Applying machine learning techniques for extracting patterns and models from real datasets
- Designing and developing softwares and frameworks for analyzing the experimental data

*M.Sc. in **Computer Sciences*** 2010- 2012
École Polytechnique Federale de Lausanne (EPFL), Switzerland

- Implemented intelligent softwares for pattern recognitions and information retrieval
- Implemented very early models in nascent field of deep learning in 2011
- Passed many computer sciences courses (advanced algorithms, distributed algorithms, information coding, machine learning, ...)

*B.Sc. in **Computer Engineering (Software)*** 2006- 2010
Sharif University of Technology, Iran

- Implemented dozens of programming projects ranging from compiler constructions to kernel programming and programming for networks

Experiences

Research assistant in Computational Neuroscience Lab. (2012-present)
Analyzing data (Neural data, voltages, LFP signals, ...) extracted from experiments on brain. Modeling neuronal networks of different areas of brain based on the data, Simulating brain activities using computer programming (Python and Matlab).

Member of NEural Simulator Technology (NEST) development team (2013-present)
Implementing modules (using C++) for neuron models in a spiking neural network simulator. This simulator received scientific recognitions from many laboratories and used for numerous researches published in scientific journals.

Summer intern at Logitech International S.A. summer 2011
Worked on developing applications for Android tablets at Logitech Innovation Center. Developed a tool (using Java) to capture statistics on different ways of inputs (touchscreen, keyboard, mouse, ...) in order to improve next generation of products.

Significant projects

Modeling Oscillations in neural networks and cell cultures
Modeled and simulated the dynamics of neurons in brain. Built a theoretical framework and simulation software for reproducing oscillations in the brain of mice and cell cultures

Library for analyzing brain's experimental data
Developed a library (using Python) for analyzing the data extracted from experiments on brain. The library includes different machine learning and pattern recognition technics (clustering, classification, ...), data reconstruction and modeling.

Deep Time Restricted Boltzmann Machine
Built a machine learning system (using C++) which can model sequential patterns using artificial neural network. It learns and reproduces patterns using stochastic methods and probability.

LANTERN, an interactive awareness tool
Member of the development team. Programmed the chip of LANTERN (using C) and implemented a software as the server which controls many LANTERNs and interactions between them.

Reinforcement Learning-based Dialogue Manager
Member of the research team. Implemented a Persian spoken dialogue system (using Java) which can refine itself by reinforcement learning methods.

Publications

H. Setareh, M. Deger, C. Petersen, and W. Gerstner. "Cortical dynamics in presence of assemblies of densely connected weight-hub neurons." *Frontiers in Computational Neuroscience,* 2017.

H. Setareh, M. Deger, and W. Gerstner. "Synaptic efficacy tunes speed of activity propagation through chains of bistable neural assemblies." *COSYNE. Salt lake city, UT, USA, 2015.*

H. Setareh, M. Deger, and W. Gerstner. "The role of interconnected hub neurons in cortical dynamics." *Computational Neuroscience Meeting, Quebec City, Canada, 2014.*

M. Habibi, H. Sameti, and **H. Setareh**. "On-line learning of a Persian spoken dialogue system using real training data." In *Information Sciences Signal Processing and their Applications (ISSPA), 2010 10th International Conference on*. IEEE, 2010.

Technical skills

Programming: Proficient in: Java, C/C++, Python
Matlab, CUDA platform (GPU), Verilog HDL
Tools: Hadoop, Spark, TensorFlow, NEST, Brian, NEURON
Mathematics: Statistics, Probabilities, Differential equations, Dynamical systems
Web development: Javascript, PHP, Spring, Symfony

Languages

English: Fluent, C2 equivalent
German: Basic proficiency, A2 equivalent
Persian: Mother tongue

References

Prof. Wulfram Gerstner, Head of Computational Neuroscience Laboratory, EPFL,
Email: wulfram.gerstner@epfl.ch

Prof. Carl Petersen, Head of Sensory Processing Laboratory, EPFL,
Email: carl.petersen@epfl.ch